Structure and catalytic properties of gallium promoted zeolites in light alkane conversion

Koji Nishi

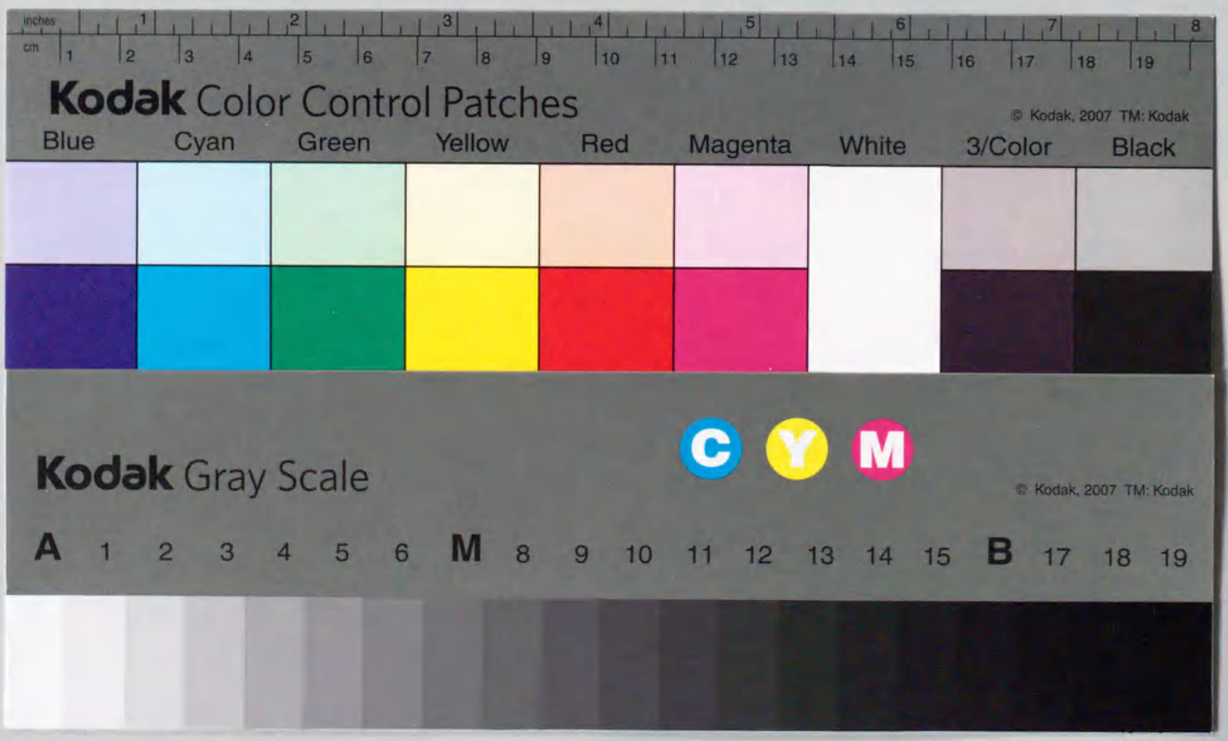

Structure and catalyic properties of gallium promoted zeolites in light alkane conversion

Koji Nishi

Department of Applied Chemistry
Graduate School of Engineering
Nagoya University

1998

Chief-Referee: Professor Tadashi Hattori
Co-Referee: Professor Yusuke Izumi
Professor Kosuke Shobatake
Associate Professor Kazuo Urabe
Assistant Professor Kyoichi Sawabe

Preface

This thesis presents the studies on **structure and catalytic properties of gallium promoted zeolites in light alkane** which details with the elucidation of the relationships among structural, chemical and catalytic properties of gallosilicate MFI-type zeolites.

The studies have been carried out under the direction of Professor Tadashi Hattori at Department of Applied Chemistry, Graduate School of Engineering, Nagoya University during 1992 - 1998.

Without the help and criticism of many researchers, this work could have been possible. The author wishes to express his sincere gratitude to Professor Tadashi Hattori for his kind and fruitful suggestions and encouragement throughout the course of this work. The author would like to make a grateful acknowledgment to Honorary Professor Yuichi Murakami for his helpful and constructive suggestions.

The author extends his faithful gratefulness to Professor Yusuke Izumi for his fruitful advice especially for understanding the reaction mechanisms. The author also express his grateful acknowledgment for Professor Kosuke Shobatake for the kind comments from the view point of physical chemists. Faithful thanks are also expressed for Associate Professor Kazuo Urabe and Assistant Professor Kyoichi Sawabe for their constructive discussion and helpful suggestions.

The author would like to make an acknowledgment to Assistant Professor Atsushi Satsuma for careful advice and fruitful suggestions. Hearty thanks are made to Dr. Hisao Yoshida for his instructive advice and helpful suggestions.

The author wishes to make an acknowledgment to Professor Satohiro Yoshida and Associate Professor Tsunehiro Tanaka in Kyoto University for their helpful suggestions for XAFS analyses. The author is grateful to Dr. Masaharu Nomura for his advice in recording XAFS spectra and also to the staffs of Photon Factory at KEK for making the beam available. Herthy thanks are made to Associate Professor Masao Kamada, Associate Professor Toyohiko Kinoshita, Messrs. Osamu Matsudo and Jun-ichiro Yamazaki and the staffs of UVSOR for assistance in XAFS measurements. Acknowledgment is made to Mr. Masayoshi Hirano at Chubu Electric Power Co. for XRD measurement.

The author sincerely thanks Mr. Masato Endo, Mr. Takeshi Shimizu, Mr. Ken-ichi Shimizu, Mr. Mikio Takamatsu, Mr. Kazumi Inagaki, Mr. Akihiro Gon-no and Mr. Kenji Kawai for their collaboration in Nagoya University. The author extends a grateful acknowledgment to Mr. Shin-ichi Komai for his helpfulness in Nagoya University.

The author thanks all the members in Laboratory of Professor Hattori for their valuable cooperation. Finally, the author wishes to express an acknowledgment to his family for their supports and understandings, without which this work would not be possible.

Koji Nishi

Nagoya
January, 1998

Contents

Chapter 1

General Introduction

Light alkane conversion

Alkanes presently play a major role in many areas of human activity. In energy they still represent the principal source, even if their relative importance has been reduced during the last decade. In chemical industry, they represent 95% of the raw materials, after having slowly displaced coal in the 1950s. However, even though modern industrial chemicals are derived from oil, they are not usually obtained directly from alkanes but, through cracking, from alkenes; the main reason is that alkanes have little reactivity. In fact, chemical reactions of alkanes, including large scale industrial syntheses, like cracking, oxidation or chlorination, are well known, however, these reactions take place usually at high temperatures, and they involve in most cases free radical intermediates; in other words their regioselectivity is poor.

C_2-C_4 alkanes are present in significant amounts in natural gas or in crude oil or are formed by refining processes: FCC, hydrocracking, *etc*. Butanes can be used as components of gasoline, as LPG (liquid petroleum gas) or as a feedstock to various refinery processes. Isobutane has its greatest value when used in alkylation units for production of high octane C_7-C_8 isoalkane compounds. A significant amount of isobutane (part of which results from n-butane isomerization) is converted to isobutene which reacts with methanol to produce methyl-t-buthylether (MTBE). Ethane and propane can be used as a feedstock to steam cracking for production of light olefins or benzenics. Various processes: Cyclar from UOP and BP, Aroforming from Salutec, Z-forming from Mitsubishi and Chiyoda have recently been developed for C_3-C_4 alkane aromatization [1].

Acid catalyzed transformation of hydrocarbons, such as cracking, isomerization and alkylation. Acid catalyzed reactions play a significant role in the processes of light alkane transformations, *e.g.*, sulfuric acid and hydrofluoric acid are used in commercial isobutane alkylation processes [2], isobutane isomerization is generally catalyzed by platinum chlorinated alumina and doped HZSM-5 zeolite catalysts are used for light alkane aromatization [3-7]. In the near future, due to a worldwide trend toward more severe environmental legislation, liquid acids such as sulfuric acid and hydrofluoric acid should be progressively replaced by strong solid acids or supported acids that are easier to recover and regenerate. For this reason a strong research effort is reflected in the past decade by a large number of papers [8, 9] describing preparation and characterization of solid acids and superacid, as well as mechanistic aspects of acid-catalyzed alkane conversion.

Although carbocations are believed to be intermediates in alkane reactions over solid acid catalysts, their mechanism of formation is still unclear. One of the problems associated with the study of the mechanism of alkane activation over solid acid is the high temperatures usually used (ca. 673-773 K), which cannot totally prevent the involvement of radical species

[10, 11]. On the other hand, the mechanism of alkane activation in liquid superacid is well studied at low to moderate temperatures, evidencing the involvement of pentacoordinated carbonium ions [12, 13].

In order to clarify the mechanism of activation of alkanes on solid acid catalysts, the H-D exchange between catalysts and alkanes has been investigated [14-24]. It was shown that the involvement of pentacoordinated carbonium ions is not completely clear [20-22]. The exchange on zeolites is similar to exchange in sulfuric acid [23, 24], which has been attributed to involve carbenium ions and olefins. Sommer et al. proposed the dehydrogenation on conjugated Lewis acid and basic sites or formation of a short-lived pentacoordinated carbonium ion, which decomposes to carbenium ion and hydrogen, as possible pathways for mechanism of alkane activation on zeolites [20, 21]. Nevertheless, the mechanism of alkane activation is still open for discussion.

Aromatization of light alkanes

BTX hydrocarbons (benzene, toluene and xylene) have two main industrial uses: (1) because of their high octane number, they constitute a significant part of the gasoline pool (about 30%), (2) they are also an important source of petrochemicals: aromatic chemicals represent about 30% of the total of some 8 million known organic compounds. BTX are now obtained by catalytic reforming of naphthas. However light hydrocarbons, in particular light alkanes, are becoming an attractive feed for the production of aromatics. Indeed in many cases production regions of light alkanes are far away from consumption centers with consequently a high cost for transportation. This is why various firms have looked for ways of converting light alkanes more valuable products.

There has been continued interest in the design of catalysts for the effective utilization of light alkanes as chemical feedstocks. This interest is due to the wide availability of these alkanes either from natural gas, or as a refinery by-product. Since 1984, most effort has been devoted to the activation of methane, but as yet no success has been achieved that is of commercial significance [25, 26]. It was noted that vanadium phosphate catalysts could activate butane under oxidizing conditions to give high yields of maleic anhydride. Subsequently this has led to the commercialization of this catalyst which is utilized in many production units around the world at present time [27-29]. Both of the research approaches adopted for the activation of the C_1 and the C_4 hydrocarbons involved the use of oxygen as a

co-reactant since oxygenates were the desired products and also the formation of water as a by-product overcomes the severe thermodynamic limitations that exist for non-oxidative activation of light alkanes.

However, it was known for some time that C_3-C_4 alkanes could be activated in the absence of oxygen as co-reactant. If hydrocarbons, rather than oxygenates, are desired product then the use of non-oxidizing conditions could be preferred, since carbon loss as carbon dioxide cannot occur. The selective conversion of light alkanes to alkenes, aromatics, and hydrogen via non-oxidative routes significantly expands the range of feedstocks available to form these useful petrochemicals and fuels. Early work in this area by Csiscery [30-33] showed that alkanes could be dehydrocyclodimerized using bifunctional Pt/Al_2O_3 catalysts. Coke formation with these catalysts resulted in their rapid deactivation and significant quantities of methane and ethane were produced as by-products. Zeolites were found to be active for alkane activation: the disproportion of alkanes using mordenite and the conversion of alkanes to aromatics using ZSM-5.

Since these initial reports, many studies have focused on the use of medium-pore pentasil zeolites. H-ZSM-5 catalyzes the conversion of light alkanes to aromatics with low selectivity because of fast cracking side reactions [34-38]. H-ZSM-5 catalysts are uniquely resistant to deactivation at the high temperature and low hydrogen concentration required for favorable dehydrocyclodimerization thermodynamics. H-ZSM-5 catalysts also provide the basis for the M-forming catalytic reforming process reported by Mobil, a process that uses the alkene products of cracking reactions to alkylate benzene and toluene to higher octane aromatics [39].

The introduction of Ga[40-58], Zn [59-63], and Pt [64-68] species into H-ZSM-5 increases the rate and selectivity of aromatization reactions and inhibits cracking side reactions that lead to loss of carbon to undesirable products. These cations, however, also decrease the unique stability of H-ZSM-5 and lead to significantly faster rates of catalyst deactivation during alkane dehydrocyclodimerization [52]. This undesired side effect of the promotion of H-ZSM-5 with Ga, Zn and Pt has led to the recent use of these materials in moving-bed reactors in the Cyclar process jointly developed by British Petroleum and UOP.

In recent years there has been considerable academic interest in the mechanism of propane activation with zeolite catalysts and most workers consider that the activation involves a synergistic interaction between a gallium species and the zeolite. It is generally accepted that the reaction sequence involves the initial formation of propylene via dehydrogenation. The propylene is then oligomerized and aromatized; in addition, there is a competing pathway of acid catalyzed propane cracking to give methane and ethane [69] which can be major by-products. A major problem concerning any mechanistic study of this system is that the initial dehydrogenation of propane to propylene is slow relative to secondary oligomerization and aromatization reactions. A similar situation is found in the conversion

of methanol to hydrocarbons over zeolite catalysts when the rapid secondary reactions are a complicating factor in unraveling the reaction mechanism [70].

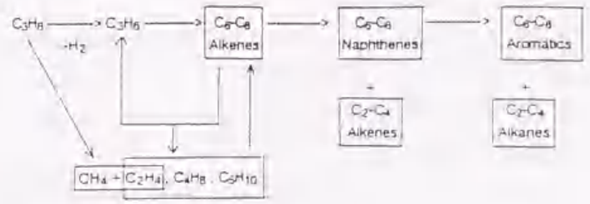

Aromatization of propane on H-ZSM-5, reaction pathway [4]

The catalytic role and structure and location of metal cations in light alkane aromatization remains the subject of intense controversy even after significant emphasis and numerous publications. Ono and co-workers [40, 60] have proposed that metal cations catalyze the selective conversion of alkenes to aromatics, but do not participate in the activation of the light alkane reactants. Their proposal is based on the observed increase in aromatic synthesis rate and selectivity as well as the decrease in the concentration of intermediate alkenes when Ga is added. Guisnet *et al.* [4, 42, 43, 49] suggest on the basis of the higher initial rate of propylene formation when Ga is added, that metal cations are exclusively involved in propane dehydrogenation and naphthene dehydrogenation steps, while the remaining required reaction steps occur via conventional acid catalysis on intrazeolitic Brønsted acid sites.

Mole *et al.* [59] proposed that Zn cations in H-ZSM-5 catalyze the desorption of H-atoms formed during C-H bond activation steps as H_2, while the remaining required steps occur on zeolitic acid sites. This proposal is consistent with kinetic and isotopic tracer studies for propane reactions on Zn- and Ga-promoted H-ZSM-5 by Inui *et al.* [64], Le Van Mao *et al.* [44, 46, 63] and Iglesia *et al.* [47, 53, 54]. These studies suggests synergistic requirement for both acid sites, in order to dispose of the resulting H-atoms.

Development in gasoline reformulation

The growing concern about the environment has led to a drastic reduction of emissions from the transport sector. Taking 1968 as a base level for gasoline fueled cars, the European commission standards for nitrogen oxides (NO_x) and hydrocarbons have both decreased by 90%. In the USA, and particularly in California, even more severe standards are being introduced. Between 1970 and 1990 emissions were reduced by the introduction of exhaust catalysts which required unleaded gasoline. However, air quality is still not acceptable in many cities so further measures are needed. The new "Clean Air Act Amendments" of 1990 require both lower vehicle emission limits and the introduction of so-called "reformulated

gasoline" in major cities. In Europe there is an ongoing "Tripartite" debate under the leadership of the European Commission and involving the Oil and Motor industries. Its intention is to establish new optimized vehicle emission limits and fuel specifications for the year 2000 in order to improve air quality.

In recent years, the continuing refinement of engine management and emission control system has made a significant contribution to lowering tail pipe emissions from gasoline fueled cars. In the USA, the penetration of cars with catalyst converters is effectively complete. In Europe penetration is around 20% as only recently there has been a requirement for all new cars to be equipped with an exhaust gas catalyst system. Despite these improvements, there is still pressure for further reductions in exhaust emissions. This will require further improvements to vehicles and emission control systems, but attention is also being focused on how changes in the composition and properties of fuels can contribute.

In the USA the new 1990 Clean Air Act Amendments require both reduced vehicle emission limits and the introduction of so-called "reformulated gasoline" in cities which do not meet atmospheric ozone targets. The expected trends in transportation fuel composition are given in Table 1. While gasoline octane requirements will remain quite high, lead, sulfur and benzene levels will all significantly decrease. The isoalkane and oxygenate contents will increase to provide octane quality. In the coming years, the reformulation of gasoline mandated in USA by the Clean Air Act will require a decrease in the utilization of olefins and aromatics and an increase in the demand for highly branched paraffinic molecules, such as trimethylpentanes [71, 72].

Table 1 Expected trends in transportation fuel composition [71]

Fuel	Characteristic	Change	Comment
Gasoline	Lead content	↓	Reduced lead emissions; Prerequisite for use of exhaust catalysts
	Benzene content	↓	Reduced toxic benzene emissions
	Sulfur content	↓	Reduced sulfur inhibition of exhaust catalytic activity and the rist of H_2S emission
	Vapor pressure	↓	Reduced evaporative hydrocarbon emissions
	Isoalkanes content	↑	Increase octane quality
	Oxygenate content	↑	Reduced exhaust emissions of CO but increased those of aldehydes
Diesel	Sulfur content	↓	Reduced exhaust particulate emissions
	Aromatics content	↓	Increased cetane number
	Volatility	↑	Reduced exhaust emissions

Promotion of light alkane conversion by the introduction of carbon dioxide

Because the dehydrogenation of light alkane is thermodynamically restricted, the aromatization of light alkane is highly endothermic and requires significant energy input. This reaction is consequently significant only at high temperature. Since the highly branched aliphatics, such as trimethylpentanes, are thermodynamically more unstable than aromatics, the synthesis of environmentally acceptable gasoline from light alkane would be difficult. The introduction of carbon dioxide could be expected to thermodynamically and/or kinetically promote the reaction, because hydrogen is consumed through the reverse water-gas shift (RWGS) reaction (1).

$$CO_2 + H_2 \rightarrow CO + H_2O \quad (1)$$

The solid line A in Fig. 1 stands for the equilibrium conversion of butane in the reaction (2) under atmospheric pressure, and it indicates that the reaction is thermodynamically restricted under the present condition. The dotted line B stands for the conversion of butane in the combined reaction (3) in equilibrium. In the combined reaction (3), carbon dioxide reacts with butane directly and thermodynamically and kinetically promotes the conversion of butane. As shown, the combined reaction is slightly advantageous from thermodynamic viewpoint in comparison with the simple reaction (2). The broken line C is the conversion on the assumption that both the reactions (1) and (2) are in equilibrium. In the reactions (1) and (2), the reaction (2) is improved by thermodynamic effect through the consumption of hydrogen generated on a catalyst surface with the RWGS reaction (1). As shown, the introduction of carbon dioxide clearly promotes the conversion, and the effect is larger than the combined reaction (3). The effect is, however, not so large because of large equilibrium restriction of the RWGS reaction.

$$2\,C_4H_{10} \rightarrow \textit{iso}\text{-}C_8H_{18} + H_2 \quad (2)$$

$$2\,C_4H_{10} + CO_2 \rightarrow \textit{iso}\text{-}C_8H_{18} + CO + H_2O \quad (3)$$

It was reported that the introduction of carbon dioxide has some another favorable effects. The introduction of carbon dioxide was found to suppress the formation of ethane and the deposition of coke on aromatization of propane [73]. In the dehydrogenation of ethylbenzene to styrene over Na_2O/Al_2O_3 catalyst, it has been suggested that carbon dioxide is activated by the strong basic site and reacts easily with hydrogen generated on catalyst surface [74]. In contrast, in the case of the lithium ferrite catalyst, it has been suggested that carbon dioxide oxidizes oxygen defects and participate in a redox cycle of iron oxide in lithium ferrite catalyst [75].

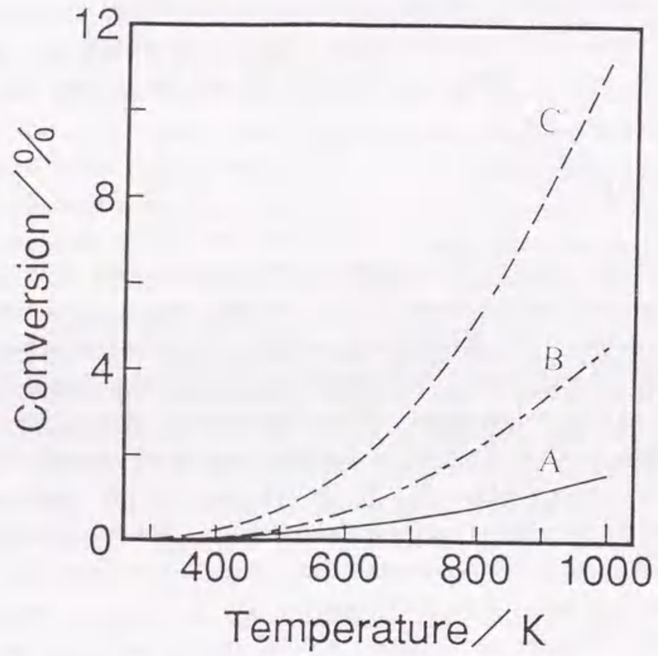

Fig. 1 Equilibrium conversions of C_4H_{10} in (A) reaction (1), (B) reaction (3) and (C) reaction (1) + (2): C_4H_{10}/N_2=0.5/0.5 (atom); C_4H_{10}/CO_2=0.5/0.5 (atom).

Property and structure of gallium promoted zeolites

Zeolite catalysts

Zeolites are tridimensional crystalline aluminosilicates with the following formula in the as-synthesized form: $xM_{2/n}O{\cdot}xAl_2O_3{\cdot}ySiO_2{\cdot}wH_2O$ where M is a cation which can belong to the group Ⅰ A or Ⅱ A or can be an organic cation, while n is the cation valence, and *w* represents water contained in zeolite voids. Crystalline structures of the zeolite type but containing tetrahedrally coordinated Si, Al, P, as well as transition metals and many group elements with the valence ranging from Ⅰ to Ⅴ such as, B, Ga, Fe, Cr, Ti, V, Mn, Co, Zn, Cu, *etc.*, have also been synthesized with the generic name of zeotypes, including AlPO, SAPO, MeAPO and MeAPSO type molecular sieves [76-82].

The main characteristic of the zeolites and zeotypes is that the tetrahedral primary building blocks are linked through oxygens producing a three-dimensional network containing channels and cavities of molecular dimensions. Considering the channel size they are conventionally defined as ultralarge (>12-), large (12-), medium (10-) or small (8-membered ring) pore materials depending on the smallest number of O or T atoms that limits the pore aperture of their largest channel, and whose diameter varies between 5 and 20 Å. A summary of zeolites and zeotypes with different pore size is given in Table 2 [83]. The system of channels of these molecular sieves produces solids with very high surface area and pore volume, which are capable of adsorbing great amounts of hydrocarbons. This fact combined with the possibility to generate active sites inside of the channels and cavities of zeolites and zeotypes produces a very unique type of catalyst, which by itself can be considered as a catalytic microreactor.

In catalytic reaction the reactant follows a sequence of events before it becomes a desorbed product. In the case of a zeolite, the sequence is diffusion of reactant through the zeolite micropores to reach an active site, adsorption of reactant on the active site, chemical reaction to give the adsorbed product, desorption of the product and, finally, diffusion of the product through the zeolite channels.

Zeolites can be considered to be constructed of tetrahedra, with oxygen atoms as apices and cations in their center. The tetrahedra form a three-dimensional system by sharing of one oxygen atom between each two tetrahedra. With Si^{4+} cations the zeolitic framework is a polymorph of quartz and has SiO_2 stoichiometry. Brønsted acid sites are developed when lattice Si^{4+} cation is isomorphically substituted by a trivalent metal cation, for instance Al^{3+}, and a negative charge is created in the lattice, which is compensated by a proton. The proton is attached to the oxygen atom connected to neighbor silicon and aluminum atoms, resulting in so-called bridged hydroxyl group which is the site responsible for the Brønsted acid property of zeolites [84].

Table 2 Zeolites and zeotypes and their ring size for the major channel [83]

molecular sieve type	framework struct.type (IUPAC CODE)	type species	window size
ultralarge pore	CLO	cloverite	20
		JDF-20	20
	UFI	VPI-5, MCM-9, $AlPO_4$-54	18
	AET	$AlPO_4$-8, MCM-37	14
large pore	FAU, EMZ	cubic and hexagonal faujasite, SAPO-37	12
	BEA	beta	12
	MOR	mordenite	12
	OFF	offretite	12
	MAZ	mazzite, omega, ZSM-4	12
	LTL	Linde Tpe L	12
	MTW	ZSM-12 MCM-22 SSZ-26, SSZ-23	12
	AFI	$AlPO_4$-5, $SAPO_4$-5	12
	ATO	$AlPO_4$-31, SAPO-31	12
	AFR	SAPO-40	12
	AFS	MAPSO-46	12
	AFY	COAPO-50	12
	ATS	MAPO-36	12
medium pore	MFI	ZSM-5, silicate	10
	MEL	ZSM-11	10
	FER	ferrierite ZSM-48	10
	MTT	ZSM-23	10
	TON	ZSM-222, theta 1	10
	HEU	clinoptilolite	10
	AEL	$AlPO_4$-11, SAPO-11	10
	AFO	$AlPO_4$-41	10
small pore	LTA	A	8
	ERI	erionite, $AlPO_4$-17	8
	CHA	chabazite	8
	KFI	ZK-5	8
	RHO	RhO, BeAsPO-RHO	8
	AEI	$AlPO_4$-18	8
	AFT	$AlPO_4$-52	8
	ANA	$AlPO_4$-24	8
	APC	$AlPO_4$-C, $AlPO_4$-H_3, MCM-1	8
	APD	$AlPO_4$-D	8
	ATT	$AlPO_4$-33, $AlPO_4$-12-TAMU	8
	ATV	$AlPO_4$-25	8
	AWW	$AlPO_4$-22	8
		$AlPO_4$-12	8
		$AlPO_4$-14	8
		$AlPO_4$-14A	8
		$AlPO_4$-15	8
		$AlPO_4$-21	8
	ATN	MAPO-39	8
	CHA	SAPO-34, COAPO-44, COAPO-47, ZYT-6	8
	GIS	MAPSO-43	
	LTA	SAPO-42	

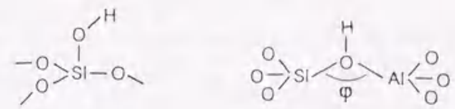

Schematic representations of silanol and zeolitic Brønsted hydroxyl [84]

Gallium promoted zeolites

The beneficial effect of Ga on alkane aromatization rates and selectivity has been observed whether Ga ions are introduced by impregnation [41, 50, 52, 53, 57] or ion exchange techniques [40, 43, 47, 48, 55]. These effects are even observed when catalyst precursors consist of Ga_2O_3/H-ZSM-5 physical mixtures [42, 44-46, 48, 58] or gallosilicates containing Ga species within framework positions in the pentasil structure [85-87]. Ion exchange procedures lead to the preferential deposition of Ga^{3+} species on the outer surface of zeolite crystals [45, 48, 50]. It appears that hydrated Ga^{3+} cations cannot enter the (5.5×5.7Å) elliptical channels in ZSM-5 during impregnation or ion-exchange [88]. During calcination, these extracrystslline Ga species convert to Ga_2O_3 crystals [45, 48, 50]. It was suggested that the activation under reducing conditions appears to lead to the reduction of Ga_2O_3 crystals and to their migration from extracrystalline positions to zeolite channels [45, 50].

The presence of cationic Ga species within zeolite channels may displace protons and thus reduce the number of sites available for acid-catalyzed reactions. Several titration and probe reaction studies on H-ZSM-5 and Ga/H-ZSM-5, however, suggest that the density of acid sites does not decrease as metal loading increases within H-ZSM-5 channels. For example, measurement of ammonia adsorption [40, 41, 43], n-alkane cracking rates [40, 43, 55] and m-xylene, cyclohexene and 2-methyl-2-pentene isomerization rates [43, 50, 55] support this conclusion. One possible reason is that Ga species have not exchange during synthesis and remain as extracrystalline Ga_2O_3.

Most literature reports suggest that propane dehydrocyclodimerization proceeds via a bifunctional route requiring the metal and acid sites to catalyze specific and distinct steps within the reaction sequence. The functions are C-C bond cleavage and formation, C-H bond activation and hydrogen disposal. On HZSM-5, hydrogen disposal proceeds by hydrogen transfer to hydrocarbon fragments, a process that leads to high cracking selectivities. On Ga/H-ZSM-5, hydrogen disposal proceeds predominantly through the recombinative desorption of H-atoms to form H_2.

It was confirmed that the Ga species also increase markedly the rate of propane

conversion to propylene. As shown in Fig. 2, the rate of propane conversion increased by a factor of 7, while the rate of propylene conversion increased by a factor of 4 when Ga was added to H-ZSM-5. These results are consistent with a hydrogen desorption function provided by Ga species and do not require the proposal of Ga-catalyzed cyclization reaction. In effect, the conversion of propylene to aromatics also requires a sequence of several additional dehydrogenation steps that are limited by the disposal of H-atoms in recombinative desorption or hydrogen transfer reactions.

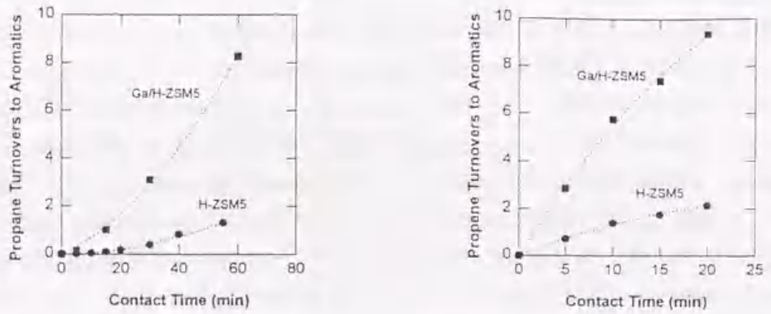

Fig. 2 (a) Propane (26.6 kPa) and (b) propene (0.67 kPa) conversion turnovers to aromatics versus contact time in recirculating batch reactor on H-ZSM-5 and 2.1 wt% Ga/H-ZSM-5 (773 K, balance He, turnover rates given by slope) [6].

Meriaudeau *et al.* [49] and Guisnet *et al.* [4, 42, 43, 67] have suggested that Ga species provide a propane and naphthene dehydrogenation function, while all subsequent reactions of propylene proceed exclusively and rapidly on protonic acid sites via conventional acid catalysis. Guisnet *et al.* [42] stated that Ga_2O_3 shows "great activity" for propane dehydrogenation to propylene. Meriaudeau and Naccache [89] and Buckles and Hutchings [58] have also examined the dehydrogenation activity of Ga_2O_3. Dehydrogenation turnover rates on Ga_2O_3 and Ga/H-ZSM-5 were calculated from the reported literature. Ga_2O_3 catalyzes propane dehydrogenation, but the dehydrogenation turnover rate on Ga/H-ZSM-5 is more than 10 times greater than the observed reactions rates on Ga_2O_3. The low dehydrogenation rates on Ga_2O_3 catalyst suggested that propane activation does not occur solely on monofunctional Ga sites at typical propane dehydrocyclodimerization conditions.

It is of interest to mention that Ga_2O_3 can selectively dehydrogenate alkanes into the corresponding olefins [90, 91]. From this study, it appears that Ga_2O_3 has, for the

dehydrogenation of alkanes, properties similar to that of ZnO. It has also been shown [92] that reduced Ga_2O_3 is able to dissociate H_2 into H^+ and H^-; those two entities are observed by IR spectroscopy (formation of OH at 3640 cm^{-1} and of Ga^{x+}-H^- at 2020 cm^{-1}) and the assignments of these species have been confirmed by replacing hydrogen with deuterium. By analogy with the previously proposed mechanism for the activation of propane over ZnO, one can assume for Ga_2O_3 the following scheme:

$$Ga_2O_3 + C_3H_8 \rightarrow \overset{H^-\quad G_3H_7^+}{Ga - O - Ga} \rightarrow \overset{H^-\quad H^+}{Ga - O - Ga} + C_3H_6 \rightarrow Ga_2O_3 + H_2 + C_3H_6$$

The addition of gallium to an acid H-ZSM-5 has a beneficial effect on both activity and selectivity for short alkanes cyclization. It was suggested the active site for the propane activation is a dual site composed of Ga^{x+} ion and of a proton and by analogy with the activation of propane over Ga_2O_3. On Ga_2O_3/H-ZSM-5 the following equations were proposed [93, 94]:

$$Ga_2O_3 + C_3H_8 + HZ \rightarrow \overset{H^-\quad G_3H_7^+}{Ga - O - Ga} + HZ \rightarrow \overset{H^-\quad H^+}{Ga - O - Ga} + C_3H_7^+Z$$
$$\rightarrow Ga_2O_3 + HZ + H_2 + C_3H_6$$

In this scheme, the ionic state of Ga is not known but could be either Ga^{3+} or Ga^{1+} since both states exist for this compound; indeed, if the Ga ion is in an exchange position the reaction scheme should be the same.

Modification of the acid properties of zeolite catalysts through the isomorphous substitution of trivalent species into tetrahedral positions in the zeolite framework has generated a great deal of interest recently [95-101]. The catalytic properties of the gallosilicates with MFI structure, in particular, have been the subject of many studies. These zeolites act as acid catalysts for several reactions such as hydrocarbon cracking [86, 102], methanol conversion [103], alkylation [104] and especially for the aromatization of light alkanes [42, 85, 105-109] In earlier studies, gallosilicate has been found to be more effective than Ga-ion exchanged H-ZSM-5 in aromatization of light alkanes [107]. In the aromatization of n-hexane, gallosilicate showed much higher activity than Ga-ion exchanged H-ZSM-5 or Ga_2O_3/H-ZSM-5 zeolite [105]. The high selectivity of gallosilicate in the aromatization of alkanes is due to the unusual acid properties of this material: the medium strength of Brønsted acid sites of bridging OH groups in the framework connected with the optimum Lewis acid of the available extraframework gallium species [110]. Usually, during the hydrothermal synthesis of gallosilicates, only a part of the gallium in the synthesis gel undergoes isomorphous substitution with framework silicon atoms. The remaining part is

localized within the micropores of the structure and/or outside the crystallites and it has been suggested that this phase may itself exhibit catalytic activity [43, 111]. Therefore, it is important to determine where gallium is in the gallosilicate. Although the incorporation of gallium has been characterized by many experimental techniques, such as solid state magic angle spinning nuclear magnetic resonance (MAS NMR) and X-ray diffraction [54, 112-114], there is still lack of chemical and structural data concerning this material.

Structure-activity relationship

Structure sensitivity in catalysis by supported metals

Metals are among the most important catalysts, being used on a large scale for refining of petroleum, conversion of automobile exhaust, hydrogenation of carbon monoxide, hydrogenation of fats and many other processes. The metal is often expensive and may constitute only about 1 wt% of the catalytic material, being applied in a finely dispersed form as particles on a high-area porous metal oxide support [115-119]. The smaller the metal particles, the larger the fraction of the metal atoms that are exposed at surfaces, where they are accessible to reactant molecules and available for catalysis.

In the 1960s and early 1970s several hydrocarbon reactions over platinum catalysts were studied as a function of the catalyst particle size. It was found that reactions like alkane hydrogenolysis [120] and isomerization [121] were strongly dependent on the particle size, while reactions like cyclopropane ring opening [122] and olefin hydrogenation [123] were independent of the particle size. In a review article in 1969 [119], Boudart classified the first type of reaction as structure sensitive and the second as structure insensitive. Thermal desorption studies using single-crystal surfaces revealed increasingly the structure sensitivity of the surface chemical bond [124]. Since the relative concentrations of terraces, steps and kinks change with catalyst particle size, it was reasonable to suggest that variations of adsorbate bond strengths due to changes in local atomic structure are responsible for the modification of reaction rates.

Boudart classified supported metals into three categories according to particle size [118], as follows:

(1) Metal particles larger than about 5 nm, which have surface structures resembling those of chunks of the bulk metal. These particles expose a number of different crystal faces with a distribution that is more or less independent of the particle size.

(2) Supported metal particles in the size range 1-5 nm, which, at least until recently, have been regarded as the ones of most interest because changes in properties for many catalytic reactions [125].

(3) Supported metal particles with diameters <1 nm, which are henceforth referred to as

clusters to distinguish them from the larger particles.

Because of this change in structure and property of metal particles with the particle size, the areal rate of the reaction or its turnover frequency (TOF) varies when the particle size is varied in the critical range between 1 and 10 nm.

Structure sensitivity in catalysis by metal oxides

Although a number of structure-sensitive and structure-insensitive reactions have been established for metal catalysts, the structure sensitivity has been barely investigated for metal oxide catalysts. As for the metal oxide catalysts, the catalysis, in particular mild oxidation catalysis, have been discussed in molecular order only in few cases [126, 127]. Volta *et al.* discussed the catalysis of the specific crystallographic planes of MoO_3 crystals having various exposure of plane [128-130]. Other cases of structure sensitivity have been reported: oxidation of methanol on V_2O_5 [131], o-xylene on V_2O_5 [132], propylene on WO_3 [133], propylene and o-xylene on brannerite type vanadates M-V-Mo-O [134, 135]. Differences of catalytic properties between polymorphic varieties of the same oxide such as hexagonal and orthorhombic MoO_3 [136] and rutile and anatase TiO_2 [137], are also a proof of structure sensitivity.

For dehydrogenation of alkanes on oxide catalysts, such as chromium oxide on different supports [138-143], numerous papers have been published in the literature regarding the characterization of these catalysts. Many works have dealt with the use of a specific technique, e.g., UV-Vis diffuse reflectance spectroscopy, laser Raman spectroscopy, X-ray photoelectron spectroscopy, to characterize supported-chromium oxide catalysts. The effects of the type of support and of some preparation parameters (calcination temperature, chromium oxide loading) on the nature of the chromium species have been the object of most of these investigations. However, complete characterization of these catalysts using a combination of several techniques which could give a better picture of such systems and a thorough examination of the relationships between activity in dehydrogenation of alkanes and chromium species in an industrial-like catalyst have not yet been reported. This seems to be due to the lack of a well-established method for determining the surface structure of these industrial-like metal oxide catalysts, especially the number of active sites.

Objective and scope

As mentioned previously, in recent years the growing concern about the environment has led to the reformulation of gasoline required a decrease in the utilization of olefins and aromatics and an increase in the demand for highly branched aliphatics, such as trimethylpentanes. If demanding highly branched aliphatics can be formed from light

alkanes, the reaction will be attractive from the view point of the utilization of light alkanes as carbon resources as well as the emission control.

Gallium promoted zeolite catalysts are known to be active for the conversion of light alkanes into aromatics. The loading of extraframework gallium species by conventional methods (ion-exchange and/or impregnation), or their generation by degalliation of gallosilicate MFI-type zeolites, produces an increase in the activity for light alkane aromatization, and in the selectivity toward aromatics. The catalytic role and the structure and location of gallium species in light alkane aromatization remains the subject of intense controversy even after significant emphasis and numerous publications.

The main objectives of this thesis are to evaluate the possibility of the light alkane conversion into highly branched aliphatics, and finally to design the catalyst for the effective conversion of light alkanes. On the basis of the background shown in previous sections, the author clarifies the relationships among structural, chemical and catalytic properties of gallosilicate MFI-type zeolites.

In Chapter 2, in order to clarify the influence of the structure of the framework and extraframework gallium species on the dehydrogenation activity, the reaction of propane and cyclohexane was carried out using gallosilicate catalysts calcined at various temperatures. The structure of gallium species was investigated through temperature programmed desorption of ammonia (NH_3-TPD) and transmission electron microscopy (TEM).

The gallosilicate catalysts would contain both framework and extraframework gallium species. The fractions of these gallium species vary with the preparation parameters. It is difficult to determine the effects of specific structures or species on catalysis, because of the complexity of the structure of gallosilicate catalysts prepared by various conditions. In order to overcome the complexity of the catalyst structures, the well-defined model Ga_2O_3 catalysts are prepared, and relation of the structures with the catalysis are discussed in the light of atomic scale in Chapter 3. Ga_2O_3 catalysts are prepared by various methods, in order to obtain the catalysts having various particle sizes, crystal phases and crystallinities. These catalysts were applied to the propane dehydrogenation, and the relationship between catalytic activity and particle size. The atomic scale structures, *i.e.*, the coordination state around gallium atom and the surface density of [Ga-O] sites, were investigated through X-ray absorption spectroscopy (XAFS) and benzaldehyde-ammonia titration (BAT) method, respectively. These local structures determining catalytic activity of Ga_2O_3 were clarified.

Chapter 4 deals with the local structures, such as the coordination state around gallium atom and location of gallium atom in gallosilicate catalysts. In order to clarify the effects of specific structures and species on catalysis, the fractions of framework and extraframework gallium species were quantitatively investigated. The effects of these local structures of gallosilicate on propane dehydrogenation activity were also discussed.

Because of large thermodynamic and equilibrium restrictions, the formation of highly

branched aliphatics, such as *iso*-octane, from light alkanes would be difficult. The introduction of carbon dioxide could be expected to thermodynamically and/or kinetically promote the reaction through the consumption of hydrogen. In Chapter 5, for the improvement of the activity of carbon dioxide reduction, metal oxide components were screened through catalytic tests of reverse water-gas shift reaction and cracking of propane in carbon dioxide atmosphere. It was examined that the possibility to improve the activity for carbon dioxide reduction by using a composite catalysts containing an oxide component for carbon dioxide reduction and Ga-HZSM-5 which is known to aromatize propane selectively. In Chapter 6, it was examined if carbon dioxide improves aromatization activity of zeolite catalysts. The aromatization of ethane which is less active than propane was conducted in the presence and absence of carbon dioxide over Ga-, Zn- and Pt-HZSM-5 catalysts. Through the test reactions, the mechanism of promotion of aromatization by the introduction of carbon dioxide was discussed.

In order to form a highly branched aliphatics, large pore zeolites would be more attractive. Because the highly branched aliphatics are bulky. In Chapter 7, the influences of zeolite pore structure, dealumination and Na ion exchange on the product distribution were examined, in order to explore the possibility of selective formation of highly branched aliphatics, such as iso-octane, in methanol conversion.

Chapter 8 summarizes the findings obtained by this study, and shows the future prospects.

References

[1] M. Guisnet and N. S. Gnep, *Appl. Catal. A*, **146** (1996) 33.

[2] A. Corma and A. Martinez, *Catal. Rev. Sci. Eng.*, **35** (1993) 483.

[3] Y. Ono, *Catal. Rev. Sci. Eng.*, **34** (1992) 179.

[4] M. Guisnet, N. S. Gnep and F. Alario, *Appl. Catal.*, **89** (1992) 1.

[5] G. Giannetto, R. Monque and R. Galiasso, *Catal. Rev. Sci. Eng.*, **34** (1994) 271.

[6] J. A. Biscardi and E. Iglesia, *Catal. Today*, **31** (1996) 207.

[7] G. J. Buckles and G. J. Hutchings, *Catal. Today*, **31** (1996) 233.

[8] A. Corma, *Chem. Rev.*, **95** (1995) 559.

[9] W. E. Farneth and G. J. Gorte, *Chem. Rev.*, **95** (1995) 615.

[10] G. B. McVicker, G. M. Kramer and J. J. Ziemiak, *J. Catal.*, **83** (1983) 286.

[11] G. M. Kramer and G. B. McVicker, *J. Catal.*, **115** (1989) 608.

[12] G. A. Olah and R. H. Schlosberg, *J. Am. Chem. Soc.*, **90** (1968) 2726.

[13] G. A. Olah, Y. Halpern, J. Shen and Y. K. Mo, *J. Am. Chem. Soc.*, **95** (1973) 4960.

[14] C. J. A. Mota, S. C. Menezes, L. Nogueria and W. B. Kover, *Appl. Catal. A*, **146** (1996) 181.

[15] J. Sommer, D. Habermacher, M. Hachoumy, R. Jost and A. Reynaud, *Appl. Catal. A*, **146** (1996) 193.

[16] C. J. A. Mota and R. L. Martins, *J. Chem. Soc. Chem. Commun.*, (1991) 171.

[17] C. J. A. Mota, R. L. Martins, L. Nogueria and W. B. Kover, *J. Chem. Soc. Faraday Trans.*, **90** (1994) 2297.

[18] C. J. A. Mota, L. Nogueria and W. B. Kover, *J. Am. Chem. Soc.*, **114** (1992) 1121.

[19] C. J. A. Mota, L. Nogueria, S. C. Menezes, V. Alekstich, R. C. L. Pereira and W. B. Kover, *Stud. Surf. Sci. Catal.*, **75** (1993) 463.

[20] J. Sommer, M. Hauchomy, F. Garin and D. Barthomeuf, *J. Am. Chem. Soc.*, **116** (1994) 5491.

[21] J. Sommer, M. Hauchomy, F. Garin, D. Barthomeuf and J. C. Vedrine, *J. Am. Chem. Soc.*, **117** (1995) 1135.

[22] J. Engelhardt and W. K. Hall, *J. Catal.*, **151** (1995) 1.

[23] J. W. Otvos, D. P. Stevenson, C. D. Wagner and O. Breek, *J. Am. Chem. Soc.*, **73** (1951) 5741.

[24] D. P. Stevenson, C. D. Wagner and J. W. Otvos, *J. Am. Chem. Soc.*, **70** (1952) 3269.

[25] G. J. Hutchings, M. S. Scurrell and J. R. Woodhouse, *Chem. Soc. Rev.*, **18** (1989) 251.

[26] N. D. Parkyns, C. I. Warburton and J. D. Wilson, *Catal. Today*, **18** (1993) 385.

[27] G. Centi, F. Trifiro, J. R. Ebner and V. M. Franchetti, *Chem. Rev.*, **88** (1988) 55.

[28] G. J. Hutchings, *Appl. Catal.*, **72** (1992) 1.

[29] G. Centi, *Catal. Today*, **16** (1993).

[30] S. M. Csiscery, *J. Catal.*, **17** (1970) 205.

[31] S. M. Csiscery, *J. Catal.*, **17** (1970) 216.

[32] S. M. Csiscery, *J. Catal.*, **17** (1970) 315.

[33] S. M. Csiscery, *J. Catal.*, **17** (1970) 323.

[34] J. R. Anderson, K. Foger, T. Mole, R. A. Rajadhyaksha and J. V. Sanders, *J. Catal.*, **58** (1979) 144.

[35] D. V. Dass and A. L. Odell, *J. Catal.*, **113** (1988) 259.

[36] R. Shigeishi, A. Garforth, I. Harris and J. Dwyer, *J. Catal.*, **130** (1991)423.

[37] Y. Ono and K. Kanae, *J. Chem. Soc. Faraday Trans.*, **87** (1991) 663.

[38] M. Guisnet, N. S. Gnep, D. Aittaleb and J. Y. Doyemet, *Appl. Catal.*, **87** (1992) 255.

[39] N. Y. Chen, W. E. Garwood and R. H. Heck, *Ind. Eng. Chem. Res.*, **26** (1987) 706.

[40] H. Kitagawa, Y. Sendoda and Y. Ono, *J. Catal.*, **101** (1986) 12.

[41] T. Yashima, T. Sasaki, K. Takahashi, S. Watanabe and S. Namba, *Sekiyu Gakkaishi*, **31** (1988) 154.

[42] N. S. Gnep, J. Y. Doyemet and M Guisnet, *J. Mol. Catal.*, **45** (1988) 281.

[43] N. S. Gnep, J. Y. Doyemet, A. M. Seco, F. R. Ribeiro and M. Guisnet, *Appl. Catal.*, **43** (1988) 155.

[44] J. Yao, R. Le Van Mao and L. Dufresne, *Appl. Catal.*, **65** (1990) 175.

[45] G. L. Price and V. Kanazirev, *J. Catal.*, **126** (1990) 267.

[46] R. Le Van Mao, R. Carli, J. Yao and V. Ragaini, *Catal. Lett.*, **16** (1992) 43.

[47] E. Iglesia, J. E. Baumgartner and G. L. Price, *J. Catal.*, **134** (1992) 549.

[48] K. M. Dooley, C. Chang and G. L. Price, *Appl. Catal.*, **84** (1992) 17.

[49] P. Meriaudeau, S. B. Abdul Hamid and C. Naccache, *J. Catal.*, **139** (1993) 683.

[50] G. D. Meitzner, E. Iglesia, J. E. Baumgartner and E. S. Huang, *J. Catal.*, **140** (1993) 209.

[51] B. S. Kwak and W. H. M. Sachtler, *J. Catal.*, **141** (1993) 729.

[52] E. Iglesia and J. E. Baumgartner, *Catal. Lett.*, **21** (1993) 55.

[53] E. Iglesia, J. E. Baumgnartner and G. D. Metzner, *Proc. 10th Int. Congr. Catal.*, Elsevier, Amsterdam, 1992, p. 2353.

[54] B. S. Kwak and W. H. M. Sachtler, *J. Catal.*, **145** (1994) 456.

[55] M. Barre, N. S. Gnep, P. Magnoux, S. Sansare, V. R. Choudhary and M. Guisnet, *Catal. Lett.*, **21** (1993) 275.

[56] P. Meriaudeau, G. Sapaly, G. Wicker and C. Naccache, *Catal. Lett.*, **27** (1994) 143.

[57] E. G. Derouane, S. B. Abdl Hamid, I. I. Ivanova, N. Blom and P. E. Hojlund-Nielsen, *J. Mol. Catal.*, **86** (1994) 371.

[58] G. Buckles and G. J. Hutchings, *Catal. Lett.*, **27** (1994) 361.

[59] T. Mole, J. R. Anderson and G. Creer, *Appl. Catal.*, **17** (1985) 141.

[60] M. Shibata, H. Kitagawa, Y. Sendoda and Y. Ono, *Proc. 7th Int. Zeolite Conf.*, 1986, p. 717.

[61] M. S. Scurrell, *Appl. Catal.*, **41** (1988) 89.
[62] Y. Ono and K. Kanae, *J. Chem. Soc. Faraday Trans.*, **87** (1991) 669.
[63] L. A. Dufresne and R. Le Van Mao, *Catal. Lett.*, **25** (1994) 371.
[64] T. Inui and F. Okazumi, *J. Catal.*, **90** (1984) 366.
[65] C. W. R. Engelen, J. P. Wolthuizen and J. H. C. van Hooff, *Appl. Catal.*, **19** (1985) 153.
[66] C. W. R. Engelen, J. P. Wolthuizen, J. H. C. van Hooff and H. W. Zandbergen, *Stud. Surf. Sci. Catal.*, **28** (1986) 709.
[67] N. S. Gnep, J. Y. Doyemet, A. M. Seco, F. R. Ribeiro and M. Guisnet, *Appl. Catal.*, **35** (1987) 93.
[68] B. S. Kwak, W. M. H. Sachtler and W. O. Haag, *J. Catal.*, **149** (1994) 465.
[69] D. Seddon, *Catal. Today*, **6** (1990) 351.
[70] G. J. Hutchings and R. Hunter, *Catal. Today*, **6** (1990) 279.
[71] I. E. Maxwell, J. E. Naber and K. P. de Jong, *Appl. Catal. A*, **113** (1994) 153.
[72] K. P. de Jong, W. Bosch and J. D. B. Morgan, *Stud. Surf. Sci. Catal.*, **96** (1995) 15.
[73] S. Yamauchi, A. Satsuma, T. Hattori and Y. Murakami, *Sekiyu Gakkaishi*, **37** (1994) 278.
[74] S. Sato, M. Ohhara, T. Sodesawa and F. Nozaki, *Appl. Catal.*, **37** (1988) 207.
[75] M. Sugino, H. Shimada, T. Turuda, H. Miura, N. Ikenaga and T. Suzuki, *Appl. Catal. A*, **121** (1995) 125.
[76] E. M. Flanigen, *Stud. Surf. Sci. Catal.*, **58** (1991) 1.
[77] S. T. Wilson, B. M. Lok, C. A. Masina, T. R. Cannan and E. M. Flanigen, *J. Am. Chem. Soc.*, **104** (1982) 1146.
[78] B. M. Lok, C. A. Masina, R. L. Patton, R. T. Gajek, T. R. Cannan and E. M. Flanigen, *J. Am. Chem. Soc.*, **106** (1984) 6092.
[79] E. M. Flanigen, B. M. Lok, R. L. Patton and S. T. Wilson, *Proc. 7th Int. Zeolite Conf.*, Kodansha Elsevier, Tokyo, 1986, p. 103.
[80] M. E. Davis, C. Montes, P. E. Hathaway and J. M. Garces, *Stud. Surf. Sci. Catal.*, **49** (1989) 199.
[81] Q. Huo, R. Xu, S. Li, Z. Ma, J. M. Thomas, R. H. Jones and A. M. Chippendale, *J. Chem. Soc. Chem. Commun.*, (1992) 875.
[82] M. Estermann, L. B. McCusker, C. Baerlocher, A. Merrouche and H. Kessler, *Nature*, **352** (1991) 320.
[83] A. Corma, *Chem. Rev.*, **95** (1995) 559.
[84] R. A. van Santen and G. J. Kramer, *Chem. Rev.*, **95** (1995) 637.
[85] C. R. Bayense, A. J. H. P. van der Pol and J. H. C. van Hoof, *Appl. Catal.*, **72** (1991) 81.
[86] J. Bandiera and Y. Taarit, *Appl. Catal.*, **76** (1991) 199.
[87] G. Giannetto, A. Montes, N. S. Gnep, A. Florentino, P. Cartraud and M. Guisnet, *J. Catal.*, **145** (1993) 86.

[88] S. Kaliaguine, G. Lemay, A. Adnot, S. Burelle, R. Audet, G. Jean and J. A. Sawicki, *Zeolites*, 10 (1990) 559.
[89] P. Meriaudeau and C. Naccache, *J. Mol. Catal.*, **50** (1989) L7.
[90] P. Meriaudeau and C. Naccache, *Catal. Today*, **31** (1996) 265.
[91] P. Meriaudeau and C. Naccache, *J. Mol. Catal.*, **50** (1989) L10.
[92] P. Meriaudeau and C. Naccache, *J. Mol Catal.*, **61** (1990) 227.
[93] P. Meriaudeau and C. Naccache, *J. Mol Catal.*, **59** (1990) L31.
[94] P. Meriaudeau, G. Sapaly and C. Naccache, *Chemistry of microporous crystals*, Kodansha, Tokyo, 1990, p. 267.
[95] T. J. G. Kofke, R. J. Gorte and G. T. Kokotailo, *Appl. Catal.*, **54** (1989) 177.
[96] C. T. -W. Chu and C. D. Chang, *J. Phys. Chem.*, **89** (1985) 1569.
[97] G. Coudurier, A. Auroux, J. C. Vedrine, R. D. Farlee, L. Abrams and R. D. Shannon, *J. Catal.*, **108** (1987) 1.
[98] C. T.-W. Chu, G. H. Kuehl, R. M. Lago and C. D. Chang, *J. Catal.*, **93** (1985) 451.
[99] R. Szotak, V. Nair and T. L. Thomas, *J. Chem. Soc. Faraday Trans. 1*, **83** (1987) 487.
[100] S. Sivasanker, K. J. Waghmare, M. Reddy and P. Ratnasamy, *Proc. 9th Int. Congr. Catal.*, The Chemical Institute of Canada, Ottawa, 1988, p. 120.
[101] H. Kosslick, V. A. Tuan, B. Parlitz, R. Fricke, C. Peuker and W. Storek, *J. Chem. Soc. Faraday Trans.*, **89** (1993) 1131.
[102] D. K. Simmons, R. Szoatak, P. K. Agrawal and T. L. Thomas, *J. Catal.*, **106** (1987) 287.
[103] G. P. Handreck and T. D. Smith, *J. Catal.*, **123** (1990) 513.
[104] J. H. Kim, S. Namba and T. Yashima, *Zeolites*, **11** (1991) 59.
[105] J. Kanai and N. Kawata, *Appl. Catal.*, **55** (1989) 115.
[106] J. M. Thomas and X. Liu, *J. Phys. Chem.*, **90** (1986) 4843.
[107] T. Inui, A. Miyamoto, H. Matsuda, H. Nagata, Y. Makino, K. Fukuda and F. Okazumi, *Proc. 7th Int. Zeolite Conf.*, Elsevier, Amsterdam, 1986, p. 859.
[108] T. Inui, Y. Makino, F. Okazumi, S. Nagano and A. Miyamoto, *Ind. Eng. Chem. Res.*, **26** (1987) 647.
[109] V. I. Yarkerson, T. V. Vasina, L. I. Lafer, V. P. Sytnyk, G. L. Dykh, A. V. Mokhov, O. V. Bragin and Kh. M. Minachev, *Catal. Lett.*, **3** (1989) 339.
[110] A. Yu. Khodakov, L. M. Kustov, T. N. Bondarenko, A. A. Dergachev, V. B. Kazansky, Kh. M. Minachev, G. Borbely and H. K. Beyer, *Zeolites*, **10** (1990) 603.
[111] D. K. Simmons, R. Szoatak, P. K. Agrawal and T. L. Thomas, *J. Catal.*, **106** (1987) 287.
[112] E. S. Shipiro, D. P. Shevchenko, O. P. Tkachenko and R. V. Drmitriv, *Appl. Catal.*, **107** (1994) 147.

[113] S. B. Abdul Hamid, E. G. Derouane, G. Demortier, J. Riga and M. A. Yarmo, *Appl. Catal.*, **108** (1994) 85.
[114] R. B. Borade and A. Clearfield, *J. Phys. Chem.*, **96** (1992) 6729.
[115] G. A. Somorjai and J. Carrazza, *Ing. Eng. Chem. Fundam.*, **25** (1986) 63.
[116] B. C. Gates, *Chem. Rev.*, **95** (1995) 511.
[117] M. Boudart, *Chem. Rev.*, **95** (1995) 661.
[118] M. Boudart, *J. Mol. Catal.*, **20** (1985) 27.
[119] M. Boudart, *Adv. Catal.*, **20** (1969) 153.
[120] J. R. Anderson and Y. Shinmoyama, *Proc. 5th Int. Congr. Catal.*, 1973, p. 965.
[121] M. Boudart, A. W. Aldag, L. D. Ptak and J. E. Benson, *J. Catal.*, **11** (1968) 35.
[122] M. Boudart, A. W. Aldag, J. E. Benson, N. A. Dougharty and G. C. Harkins, *J. Catal.*, **6** (1966) 92.
[123] T. A. Dorling and R. L. Moss, *J. Catal.*, **5** (1966) 111.
[124] G. A. Somorjai, *Adv. Catal.*, **26** (1977) 1.
[125] M. Che and C. O. Bennett, *Adv. Catal.*, **36** (1989) 55.
[126] J. E. Germain, *Stud. Surf. Sci. Catal.*, **21** (1985) 355.
[127] J. C. Volta and J. L. Portefaix, *Appl. Catal.*, **18** (1985) 1.
[128] J. C. Volta, M. Forissier, F. Theobald nd T. P. Pham, *J. Chem. Soc. Faraday Disc.*, 72 (1981) 225.
[129] J. C. Volta and B. Moraweck, *J. Chem. Soc. Chem. Commun.*, (1980) 338.
[130] J. C. Volta, W. Desquesnes, B. Moraweck and J. M. Tatibouet, *Proc. 7th Int. Congr. Catal.*, Elsevier, Amsterdam, (1981) 1398.
[131] A. Miyamoto, Y. Yamazaki, M. Inomata and Y. Murakami, *J. Phys. Chem.*, **85** (1981) 2366.
[132] M. Inomata, A. Miyamoto and Y. Murakami, *J. Phys. Chem.*, **85** (1981) 2372.
[133] M. Inomata, K. Mori, A. Miyamoto, T. Ui and Y. Murakami, *J. Phys. Chem.*, **87** (1983) 754.
[134] M. Inomata, K. Mori, A. Miyamoto and Y. Murakami, *J. Phys. Chem.*, **87** (1983) 761.
[135] Y. Murakami, M. Inomata, K. Mori, T. Ui, K. Suzuki, A. Miyamoto and T. Hattori, *Stud. Surf. Sci. Catal.*, **16** (1983) 531.
[136] D. J. Cole, C. F. Cullis and D. J. Hucknall, *J. Chem. Soc. Faraday Trans. 1*, **71** (1976) 2945.
[137] A. Vejux and P. Courtine, *J. Solid State Chem.*, **23** (1978) 93.
[138] A. Iannibello, S. Marengo, P. Tittarelli, G. Morelli and A. Zecchina, *J. Chem. Soc. Faraday Trans. 1*, **80** (1984) 2209.
[139] H. J. Lugo and J. H. Lunsford, *J. Catal.*, **91** (1985) 155.
[140] M. A. Vuurman and I. E. Wachs, *J. Phys. Chem.*, **96** (1992) 5008.
[141] M. A. Vuurman, F. D. Hardcastle and I. E. Wachs, *J. Mol. Catal.*, **84** (1993).

[142] S. De Rossi, G. Ferraris, S. Fremiotti, V. Indovina and A. Cimino, *Appl. Catal. A*, **106** (1993) 125.
[143] F. Cavani, M. Koutyrev, F. Trifiro, A. Bartolini, D. Ghisletti, R. Iezzi, A. Santucci and G. Del Piero, *J. Catal.*, **158** (1996) 236.

Chapter 2

Dehydrogenation of Propane and Cyclohexane over Ga-MFI Catalysts

Synopsis

MFI-type gallosilicate (Ga-MFI) catalysts with different Ga content (Si/Ga=12.5, 20, 40 and 80) were calcined at different temperatures (823-993 K). From the characterization of structure and physicochemical properties, the zeolitic strong acidity was decreased and the average diameter of extraframework Ga_2O_3 species was increased with increasing calcination temperature. Influence of the calcination temperature on the catalytic activity in reactions of propane and cyclohexane was investigated. The catalytic activity is found to be strongly influenced by the calcination temperature. This can be attributed to the extraction of gallium from zeolite framework and the formation of the extraframework Ga_2O_3 species.

Introduction

The transformation of light alkanes into aromatics has been extensively investigated with various acid and bifunctional zeolite catalysts, in particular HZSM-5 and MFI-type zeolites modified by gallium species [1-4]. Gallium species are saaid to be effective in various forms: incorporated into framework [5-8], impregnated [9, 10], ion exchanged [11-13], or even when they are in the form of physical mixtures of HZSM-5 and Ga_2O_3 [14]. Nevertheless, with the aluminosilicates a bifunctional reaction mechanism seems to be widely accepted. However, with the gallosilicates the catalytic role of framework and extraframework gallium is still a matter of serious controversy.

Kanai *et al.*[7] and Khodakov *et al.* [12] suggested that the active species is extraframework gallium, released from the framework or existing as an impurity in the preparation on gallosilicates. Simmons *et al.* showed that the activity can be strongly enhanced by steaming, a procedure of which transforms framework into extraframework gallium [5]. On the other hand, Bandiera and Ben Taarit [15] and Bayense *et al.* [8, 16] studied the active role of gallium species in the conversion of propane using gallosilicate zeolites. They concluded that the aromatization can be improved by framework gallium as well as extraframework gallium, according to a bifunctional mechanism widely accepted for H-ZSM-5 modified by gallium [17-20]. The bifunctional mechanism with a synergistic cooperation of framework and extraframework gallium was proposed by Minachev and Dergachev [21], too. In these mechanisms the general role of extraframework gallium is to provide Lewis sites, which abstract hydride ions [18]. The conversion of the carbocations takes place on the Brønsted sites provided by framework aluminum or gallium.

Recently, it was shown that the thermal treatments of Ga-MFI at 973-1073 K under dry air flow results in a significant increase in its selectivity in propane aromatization due to the formation of well dispersed extraframework gallium species [22, 23]. It is interesting to

study in details the influence of calcination temperature on structure and on activity of Ga-MFI in the reaction of propane.

In the present chapter, in order to clarify the influence of the structure of the framework and extraframework gallium species on the dehydrogenation activity, the reaction of propane and cyclohexane was carried out using gallosilicate catalysts calcined at various temperatures.

Experimental

Catalysts Preparation

The gallosilicates having MFI structure were synthesized with different gallium contents according to the literatures [8]. This includes the hydrothermal treatment of gels at 443 K under autogeneous pressure, having the following composition 15 Na_2O·x Ga_2O_3·100 SiO_2·13 TPABr·4400 H_2O. The samples with different Si/Ga ratio (Si/Ga=12.5, 20, 40, 80) were prepared under the same conditions, changing only the gallium content. The gels were prepared from sodium silicate (Kishida Chem.), gallium nitrate (Mitsuwa Chem.), sodium chloride, sulfuric acid, distilled water and tetrapropylammonium bromide (TPABr) was used as template. The crystallization time was 48 h. The as-synthesized products were calcined for 8 h at 803 K, ion exchanged three times with a 1 M NH_4NO_3 solution a 353 K for 24 h, and calcined for 4 h at various temperatures (823, 923 and 993 K) under dry air flow. All zeolites were pelleted without binder, crushed and sized to 28-48 mesh.

Characterization

Ga content and the degree of ion exchange were determined by inductively coupled plasma spectroscopy (ICP). X-ray diffraction (XRD) patterns were recorded on a Rigaku RINT 1200 equipment using Cu K α radiation. The acid amount and strength of zeolite samples were measured by temperature programmed desorption of ammonia (NH_3-TPD) in the same way as described previously [24-26]. The Ga_2O_3 particle size on Ga-MFI catalysts was measured by transmission electron microscopy (TEM, HITACHI H-800), and exposed Ga_2O_3 surface area was calculated from the particle size.

Catalytic test

The catalytic test was carried out by using a continuous flow reaction apparatus at atmospheric pressure. The catalyst (0.30 g) was placed in a quartz tube with an inner diameter of 10 mm. The catalyst was pretreated in flowing oxygen diluted with nitrogen (O_2/N_2=1/4) for 1 h at 823 K. Partial pressure of propane was 18 kPa with nitrogen balance, and total feed rate was 0.15 mol h^{-1}. On the other hand, cyclohexane (6.3 kPa) was fed with nitrogen gas (50 ml min^{-1}) over zeolite catalysts (0.05 g). The reaction temperature was

raised every 50 K from 673 to 873 K, and was kept constant at each temperature for 30 min at the end of which reaction products were analyzed on line by gas chromatography. The yield and selectivity were expressed in C% on the basis of propane and cyclohexane fed, and the selectivity was expressed in C% on the basis of total hydrocarbon products.

Results

Characterization of the structure

The MFI-type framework structure was confirmed by XRD. The XRD pattern, exhibiting the sharp and strong lines, revealed that the crystalline Ga-MFI was synthesied, and that the crystallinity of the catalysts remained even after calcination at 993 K. The extraframework Ga_2O_3 species, however, could not be detected by XRD, irrespective of Ga content and calcination temperature.

Typical electron micrograph are given in Fig. 1. The dark particles can be seen on substrate regions of constant optical density. These micrographs show the extraction of gallium species from zeolite framework and formation of Ga_2O_3 on the outer surface of zeolite crystals. For all catalysts examined, the size of particle observed appear to depend on the catalyst calcination. The particle size of Ga_2O_3 was increased with an increase of calcination temperature from 823 to 993 K. The particle size distributions for the Ga-MFI catalysts determined by electron micrographs are shown in Fig. 2. It can be seen that the width of distribution increases with increasing calcination temperature. Fig. 3 shows the effect of calcination temperature on the average diameters of the Ga_2O_3. On all catalysts, the particle size increased with increasing calcination temperature.

The total Ga contents of the Ga-MFI catalysts, determined by elemental analysis, were given in Table 1.

Acidity of Ga-MFI catalyst

The TPD profiles of NH_3 are characterized by the occurrence of low-temperature peak (*l*-peak) arising from the desorption of weakly bound ammonia and a high-temperature peak (*h*-peak) at about 600 K (Fig. 4). The *l*-peak increased with a increase of the calcination temperature. Therefore, the *l*-peak could be attributed to the desorption of ammonia bound to Ga_2O_3, which is responsible for Lewis acid sites. On the other hand, the *h*-peak is assigned to Brønsted acid sites arising from the incorporation of gallium into the crystal lattice. Its maximum temperature lies below that observed for HZSM-5 (650 K) [27, 28]. The amounts of total ammonia desorbed and strong acid sites, defined as the amount of ammonia desorbed above 520 K, are summarized in Table 1. From the amount of strong acid sites, the framework gallium content was determined assuming that each framework gallium atom

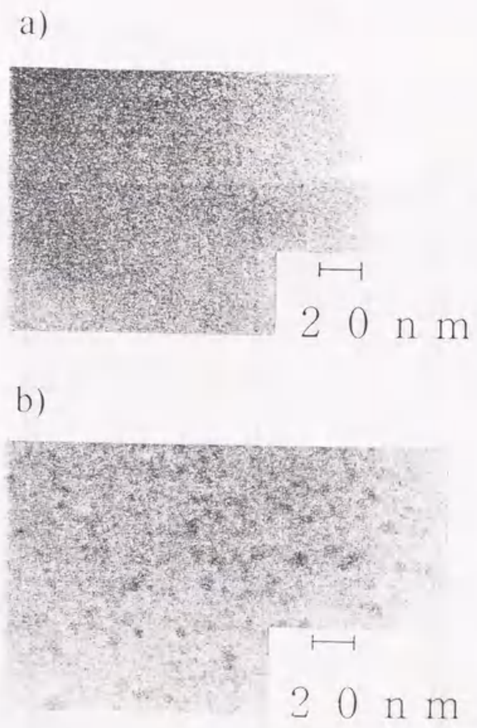

Fig. 1 Transmission electron micrograph of Ga-MFI catalysts (Si/Ga=40): calcined at (a) 823 K and (b) 993 K.

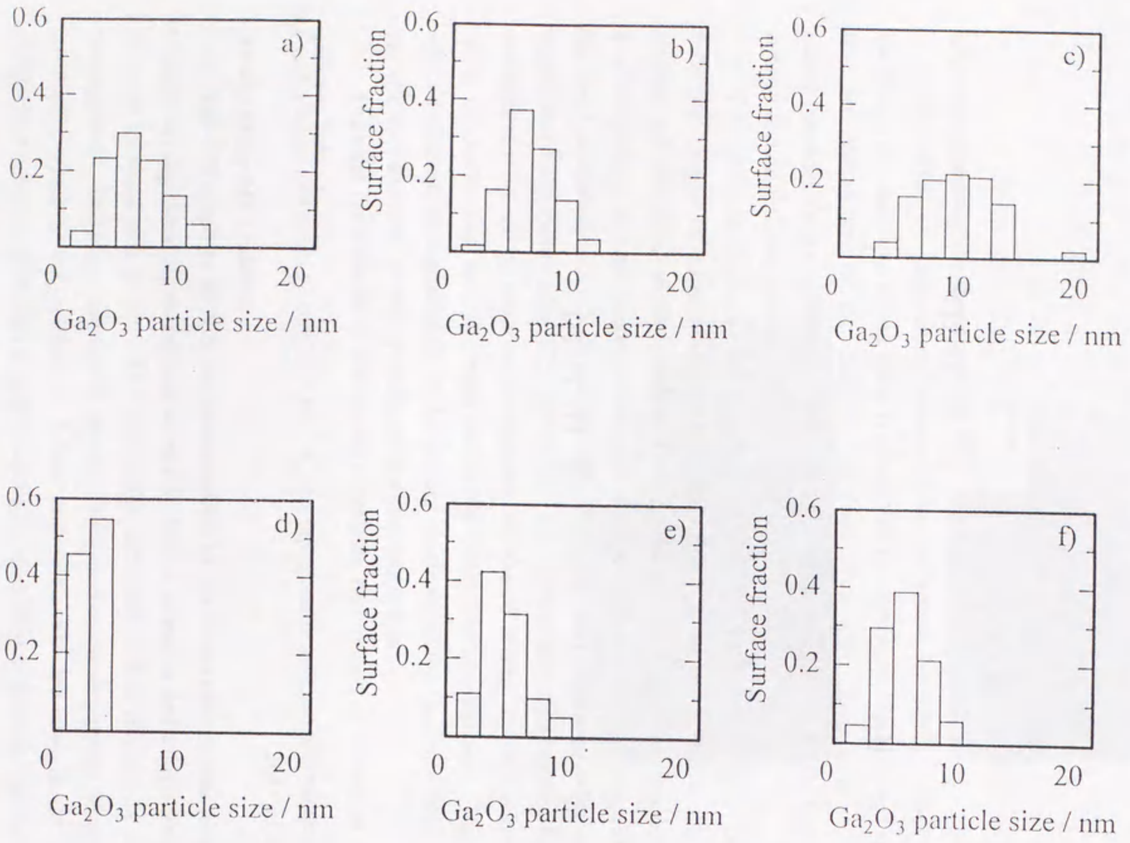

Fig. 2 Ga_2O_3 particle size distributions for Ga-MFI catalysts determined by electron microscopy: Si/Ga=12.5 calcined at (a) 823 K, (b) 923 K, (c) 993 K; Si/Ga=40 calcined at (d) 823 K, (e) 923 K, (f) 993 K.

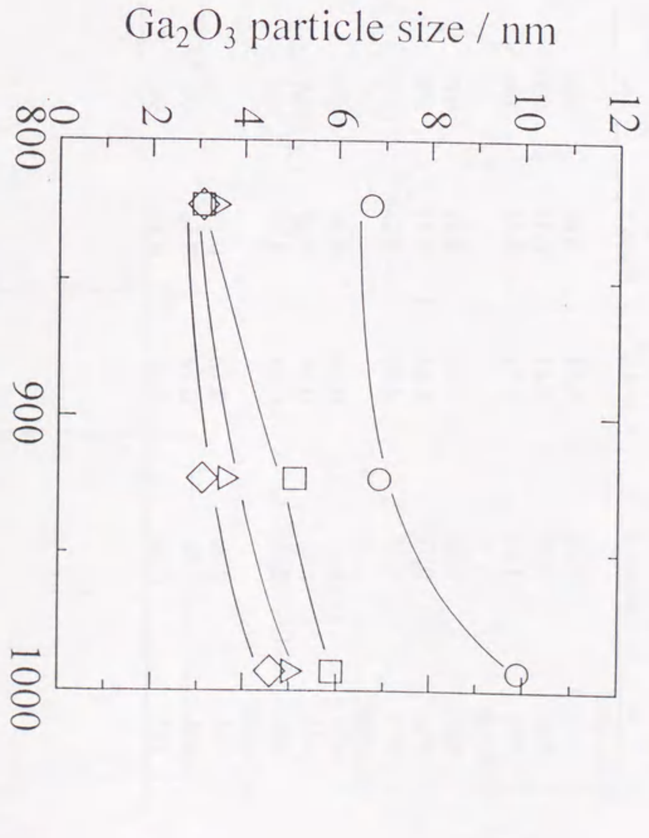

Fig. 3 Influence of calcination temperature on Ga_2O_3 particle size: Si/Ga= (○) 12.5, (△) 20, (□) 40 and (◇) 80.

Table 1 Composition and acid properties of Ga-MFI catalysts

calcination temperature K	Ga content mmol g^{-1}	NH_3 desorbed		
		total mmol g^{-1}	strong acid mmol g^{-1}	*h*-peak max. K
Si/Ga=12.5				
823	1.22	0.71	0.61	608
923	1.20	0.41	0.31	600
993	1.21	0.37	0.24	596
Si/Ga=20				
823	0.76	0.40	0.35	606
923	0.77	0.33	0.27	598
993	0.78	0.28	0.23	595
Si/Ga=40				
823	0.43	0.36	0.33	608
923	0.43	0.35	0.31	603
993	0.44	0.30	0.25	595
Si/Ga=80				
823	0.24	0.22	0.19	591
923	0.24	0.18	0.16	592
993	0.24	0.18	0.16	592

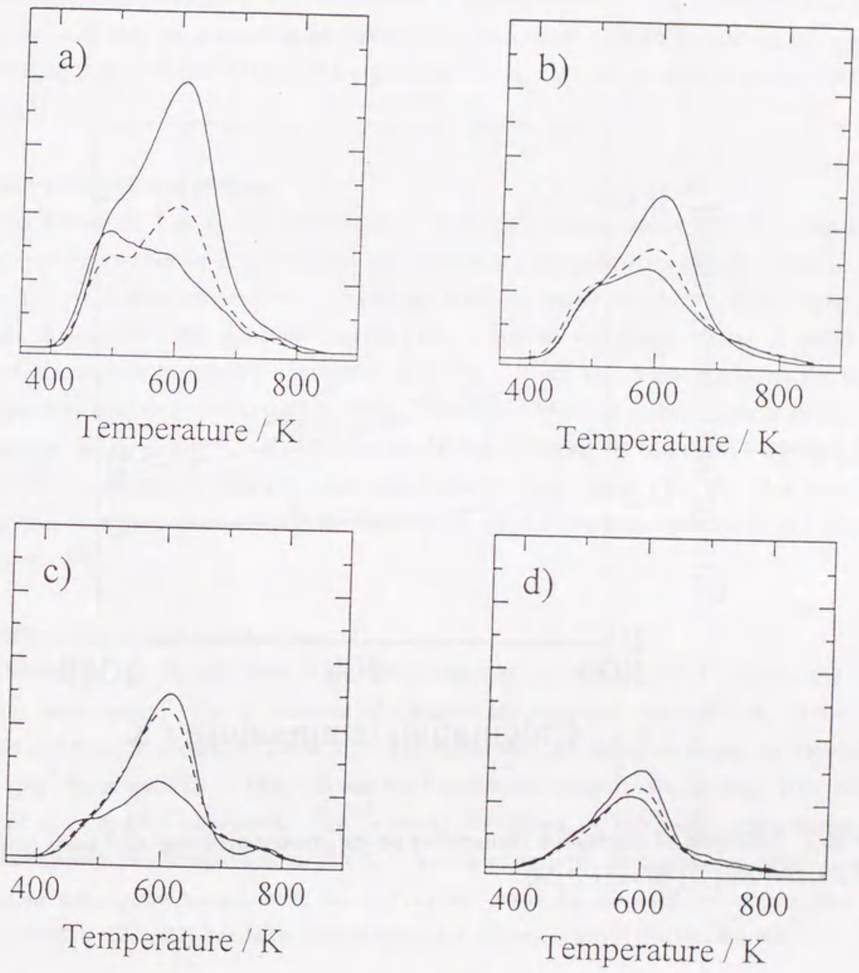

Fig. 4 TPD profiles of NH_3 on Ga-MFI catalysts: Si/Ga= (a) 12.5, (b) 20, (c) 40 and (d) 80; calcined at (——) 823, (– – -) 923 and (– · · –) 993 K.

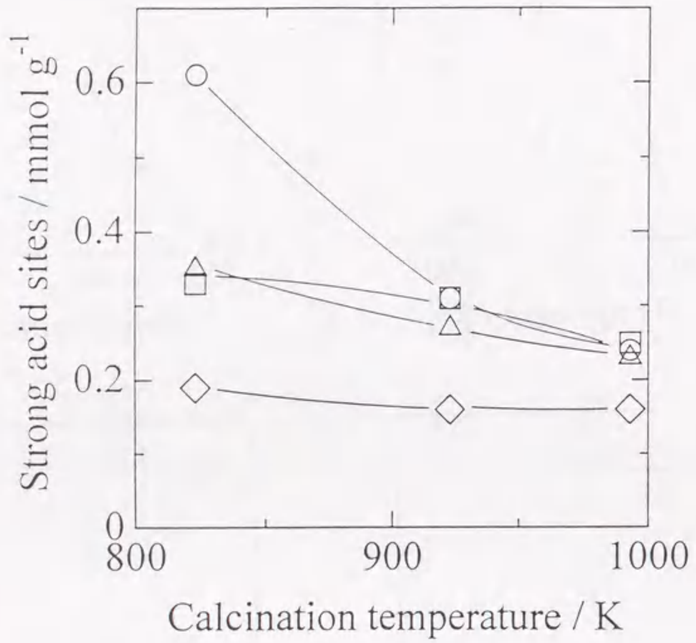

Fig. 5 Influence of calcination temperature on the amount of strong acid sites: Si/Ga= (○) 12.5, (△) 20, (□) 40 and (◇) 80.

desorbs one ammonia molecule, thus indicating one Brønsted site. The difference from the total number of gallium gives the extraframework gallium content. Fig. 5 shows the amount of strong acid sites as a function of calcination temperature. With increasing calcination temperature (from 823 to 993 K), the amount of strong cid sites decreased to less than 0.3 mmol g^{-1}.

Catalytic conversion of propane

As shown in Fig. 6, the conversion of propane occurred above 673 K. The main products were alkenes (mainly ethylene and propylene) and aromatics (mainly benzene and toluene). At lower temperatures, propylene was the major product. With increasing reaction temperature, the yield and selectivity of aromatics increased. Table 2 shows the product distribution in propane conversion at 773 K. It was found that the lower the Si/Ga the higher the selectivity of aromatics. Fig. 7 shows the effect of calcination temperature on the propane conversion at 773 K. On the catalysts with higher Ga content (Si/Ga=12.5, 20), the conversion decreased with a increase of calcination temperature. On the other hand, the conversion increased with calcination temperature on the catalysts with lower Ga content (Si/Ga=40, 80).

Catalytic conversion of cyclohexane

Shown in Fig. 8 and Table 3 are the changes in the conversion of cyclohexane with reaction temperature. The conversion of cyclohexane occurred above 673 K. From the product distribution shown in Table 3, it was found that the major products are aromatics. Especially, the selectivity of benzene was the highest and comprised more than 70% over a most of the catalysts examined. Fig. 9 shows the effect of calcination temperature on dehydrogenation of cyclohexane at 773 K. As shown in propane conversion (Fig. 7), with increasing calcination temperature, the activity increased on the catalysts with higher Ga content (Si/Ga=12.5, 20), while decreased when Ga content is lower (Si/Ga=40, 80).

Discussion

Table 4 summarizes the physicochemical properties and the catalytic activities of Ga-MFI catalysts. The physicochemical properties varied in a similar manner with calcination temperature, regardless of its Ga content. The change in the catalytic activity with calcination temperature, however, differ according to Ga content. The exposed Ga_2O_3 area was calculated from the Ga_2O_3 particle size and the amount of extraframework Ga, as follows:

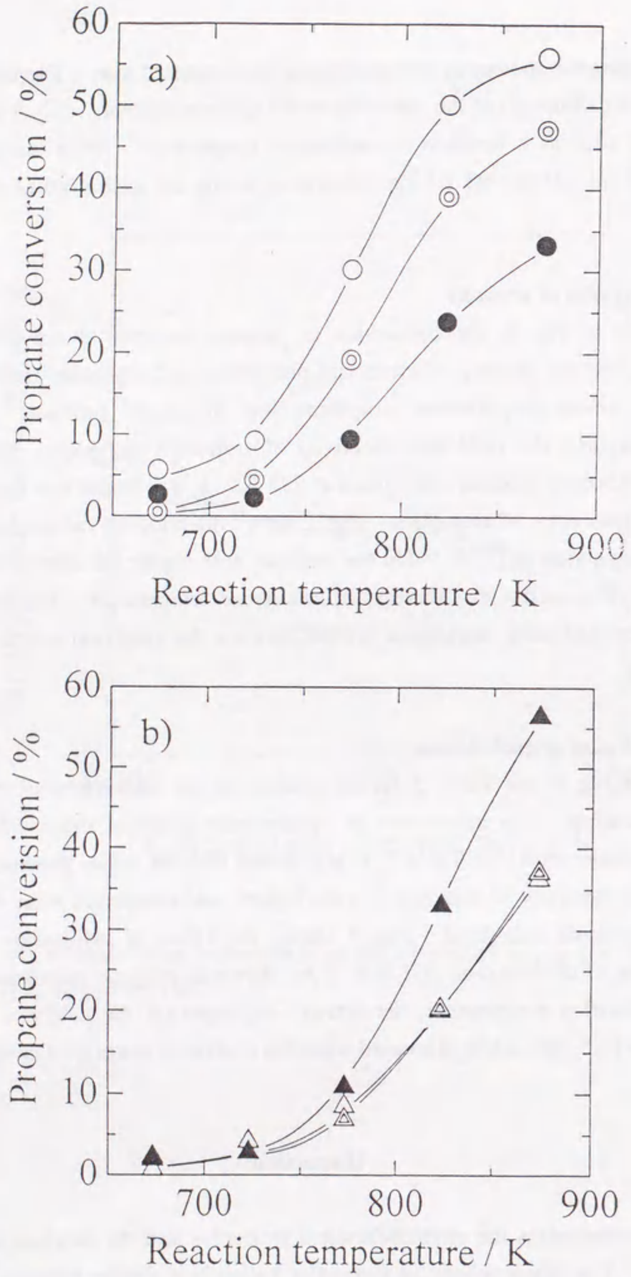

Fig. 6 Conversion in the reaction of propane on Ga-MFI catalysts: Si/Ga= (a) 12.5 and (b) 40; calcined at (○, △) 823, (◎, ◬) 923 and (●, ▲) 993 K.

Table 2 Product distribution in propane conversion over Ga-MFI catalysts at 773 K

Calcin.Temp.	Conversion	Selectivity / %					
K	%	CH_4	C_2H_6	C_2H_4	C_3H_6	C_{4+}	Aromatics
Si/Ga=12.5							
823	30.2	5.6	2.9	11.5	22.7	3.9	53.5
923	19.2	5.3	2.6	14.9	25.0	5.8	46.3
993	9.5	3.5	1.5	14.1	41.1	4.6	35.3
Si/Ga=20							
823	22.1	5.8	2.1	14.9	22.6	5.6	49.2
923	15.3	4.7	1.8	16.7	27.9	6.1	42.9
993	14.0	4.0	1.5	15.6	41.1	6.3	31.5
Si/Ga=40							
823	8.5	5.3	0.3	13.6	63.1	2.0	15.8
923	6.9	4.7	0.3	14.3	56.9	5.6	18.1
993	10.9	4.6	0.9	18.2	39.5	6.5	30.4
Si/Ga=80							
823	1.8	5.4	0.1	10.3	82.1	0.0	2.0
923	5.0	4.2	0.6	14.0	60.8	3.8	16.6
993	5.5	3.0	0.3	10.6	75.0	1.8	9.3

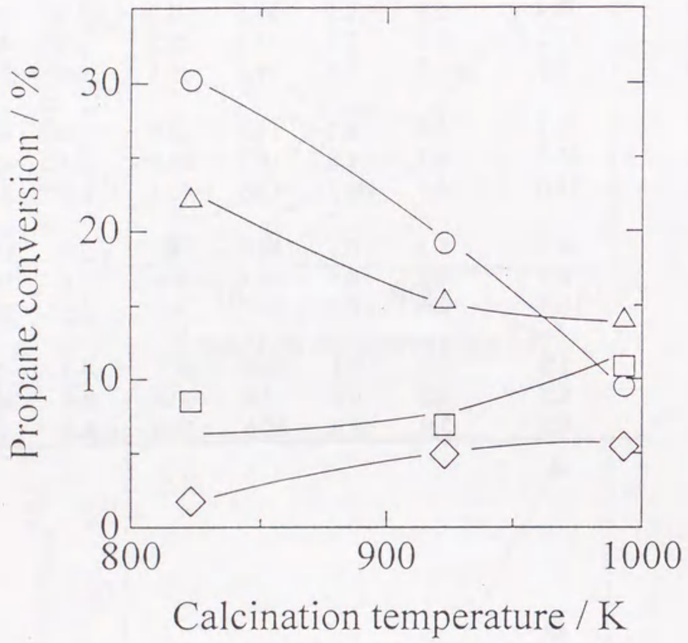

Fig. 7 Influence of calcination temperature on propane conversion over Ga-MFI catalysts at 773 K: Si/Ga= (○) 12.5, (△) 20, (□) 40 and (◇) 80.

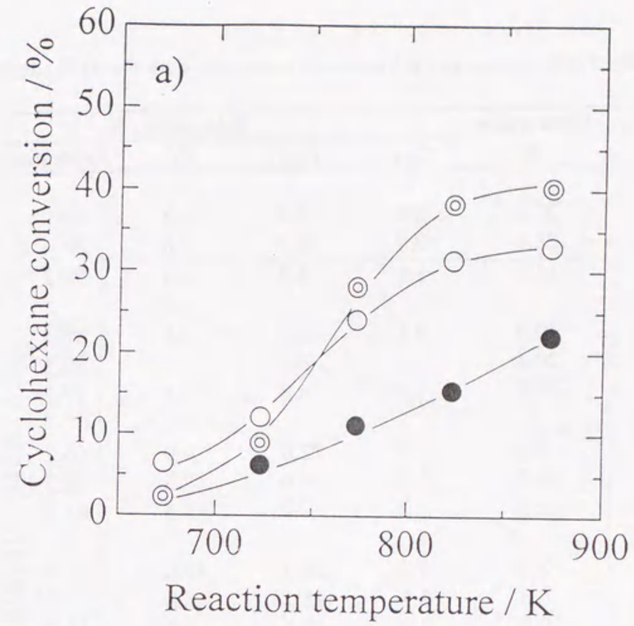

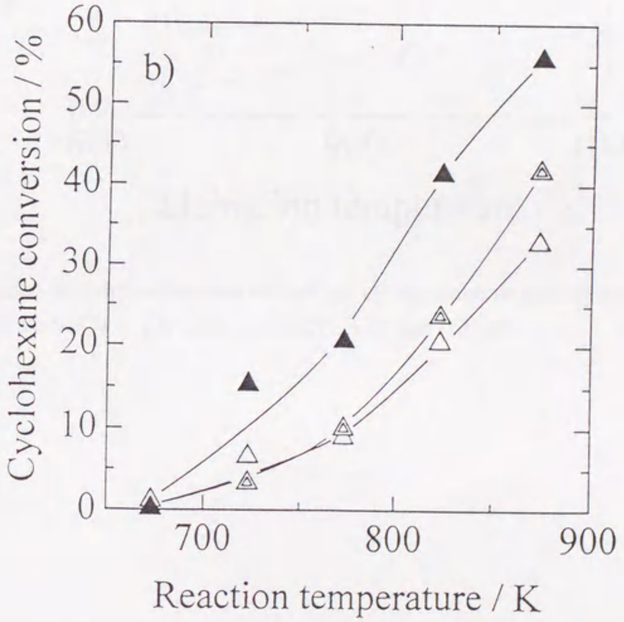

Fig. 8 Conversion in the reaction of cyclohexane on Ga-MFI catalysts: Si/Ga= (a) 12.5 and (b) 40; calcined at (○, △) 823, (◎, ◬) 923 and (●, ▲) 993 K.

Table 3 Product distribution in cyclohexane conversion over Ga-MFI catalysts at 773 K

Calcin.Temp.	Conversion	Selectivity / %				
K	%	C_{1-4}	$C_{2-4}^{=}$	C_{5+}	Aromatics	Benzene
Si/Ga=12.5						
823	27.1	2.0	4.6	2.5	90.9	84.8
923	28.1	2.7	6.1	2.8	88.4	83.3
993	11.1	1.4	4.3	4.1	90.2	88.0
Si/Ga=20						
823	40.9	4.1	8.3	2.1	85.5	78.9
923	29.4	3.2	6.8	2.6	87.5	82.8
993	27.5	2.8	6.8	3.3	87.2	83.6
Si/Ga=40						
823	9.0	2.9	22.0	9.0	66.2	53.2
923	10.1	2.2	16.6	7.5	73.7	66.3
993	20.6	3.2	7.9	3.3	85.7	82.0
Si/Ga=80						
823	2.9	1.8	26.3	19.0	52.9	44.9
923	6.0	3.1	15.1	8.8	73.0	70.5
993	10.9	2.7	13.5	7.4	76.4	74.3

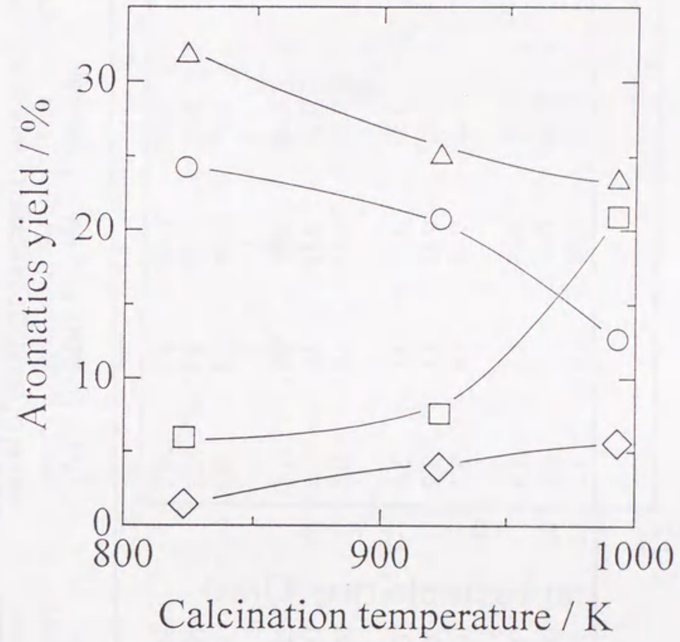

Fig. 9 Influence of calcination temperature on cyclohexane dehydrogenation over Ga-MFI catalysts at 773 K: Si/Ga= (○) 12.5, (△) 20, (□) 40 and (◇) 80.

Table 4 The physicochemical properties and catalytic activities of Ga-MFI catalysts

catalyst (calcin. temp.)	strong acid mmol g^{-1}	extra-framework Ga mmol g^{-1}	Ga_2O_3 particle size nm	Ga_2O_3 surface area $m^2\ g^{-1}$	Propane propane conversion %	Cyclohexane aromatics yield %
Si/Ga=12.5						
823 K	0.61	0.61	6.7	8.7	30.2	24.3
923	0.31	0.89	6.9	12.3	19.2	20.8
993	0.24	0.97	9.9	9.3	9.5	12.7
Si/Ga=20						
823 K	0.35	0.41	3.4	11.5	22.1	31.7
923	0.27	0.59	3.6	13.2	15.3	25.0
993	0.23	0.55	5.0	10.5	14.0	23.3
Si/Ga=40						
823 K	0.33	0.10	3.1	3.1	8.5	6.0
923	0.31	0.12	5.1	2.2	6.9	7.6
993	0.25	0.19	5.9	3.1	10.9	20.9
Si/Ga=80						
823 K	0.19	0.05	3.1	1.5	1.8	1.5
923	0.16	0.08	3.1	2.5	5.0	4.0
993	0.16	0.08	4.6	1.7	5.5	5.0

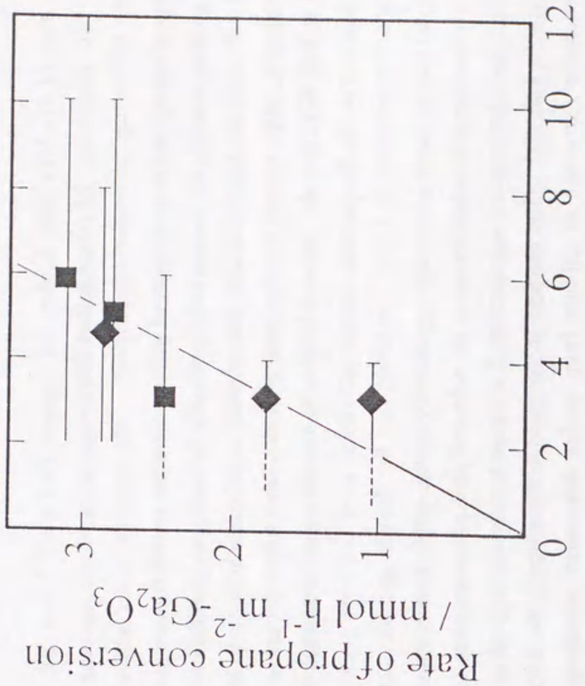

Fig. 10 Influence of Ga_2O_3 particle size on the conversion of propane at 773 K: Si/Ga= (■) 40 and (◆) 80.

$$Ga_2O_3 \text{ surface area} = \frac{3 \times (Ga_2O_3 \text{ formula weight}) \times (\text{extraframework Ga amount})}{(Ga_2O_3 \text{ particle size}) \times (Ga_2O_3 \text{ density})}$$

where the density of β-Ga_2O_3, calculated from the structural parameters [29], is 5.9×10^6 g m^{-3}.

In the case of Ga-MFI with higher Ga content (Si/Ga=12.5 and 20), the catalytic activities for both conversion of propane and dehydrogenation of cyclohexane were sharply decreased with increasing calcination temperature. The decrease in the activity is expected mostly because of the extensive extraction of gallium from the zeolite framework at the higher temperature, causing a large decrease in the framework Ga and consequently in zeolitic strong acidity. Choudhary *et al.* suggested that the propane conversion activity is almost linearly increased markedly with increasing the strong acidity measured in terms of pyridine chemisorbed at 673 K [23]. As shown in Table 4, the decrease in zeolitic strong acidity certainly corresponds to the decrease in catalytic activity.

The product distribution in Table 2 indicates that the dehydrogenation activity and the aromatization activity are also influenced appreciably by the calcination temperature. With the increase in the calcination temperature, the selectivity of propylene was increased very appreciably, and that of aromatics was decreased. These results are in good agreement with the reported results [22, 23]. The changes in the product distribution are expected mainly due to the extensive extraction of gallium from zeolite framework, resulting into a large decrease in the zeolitic acidity responsible for the oligomerization of propylene and the cyclization of the oligomers. In these catalysts, the amount of extraframework Ga was larger than that of framework Ga (Table 4). Consequently, it is suggested that the miner fraction of Ga species, the framework Ga in this case, controls the catalytic activity.

In the case of Ga-MFI with lower Ga content (Si/Ga=40 and 80), the catalytic activities for both conversion of propane and dehydrogenation of cyclohexane appear to be increased with increasing calcination temperature, while the zeolitic strong acidity was decreased (Table 4). The opposite feature was observed according to the Ga content. This result indicates that the catalytic activities for both reactions are influenced not only by the zeolitic acidity but also by the property of extraframework Ga_2O_3 species. The decrease in the dehydrogenation activity and the increase in the aromatization activity were shown in the product distribution (Table 2), regardless of the decrease in the zeolitic acidity. These results demonstrate the serious contribution of the structure of the extraframework Ga_2O_3 particle. As shown in Table 4, the larger the surface area and the particle size of Ga_2O_3, the higher the catalytic activity.

The influence of Ga_2O_3 particle size on the propane dehydrogenation rate per exposed Ga_2O_3 surface area is shown in Fig. 10. The dehydrogenation rate increased with increasing

Ga_2O_3 particle size. The feature of activity in dehydrogenation of cyclohexane is the same as that in propane conversion. These results indicate that the dehydrogenation on Ga-MFI catalysts is structure sensitive reaction demanding large Ga_2O_3 particle. It is suggested that the effect of the property of extraframework Ga_2O_3 species is significant when the change in the amount of strong acid sites is very little.

Conclusion

In order to clarify the influence of the framework and extraframework gallium species structure on the dehydrogenation activity, the reactions of propane and cyclohexane were investigated over gallosilicate catalysts calcined at various temperatures.

The calcination of Ga-MFI at high temperature caused a partial extraction of gallium from the framework and a decrease in acidity. The particle size of the extraframework gallium species extracted from the zeolite framework increased with increasing calcination temperature.

In the case of Ga-MFI catalyst with higher gallium content, in which the change in the amount of strong acid sites is large, the activity of Ga-MFI catalysts in the reactions of propane and cyclohexane was decreased by the calcination at higher temperature. This can be attributed to the decrease in the zeolitic strong acid sites, resulting from the extraction of gallium from zeolite framework.

In the case of Ga-MFI catalyst with lower gallium content, in which the change in the amount of strong acid sites is very little, the activity was increased with increasing calcination temperature. This can be attributed to the increase in the exposed surface area of extraframework Ga_2O_3 species. The reaction rate per exposed Ga_2O_3 surface area increased with increasing the Ga_2O_3 particle size, suggesting that conversion of propane and cyclohexane on Ga-MFI catalysts are structure sensitive reaction demanding large Ga_2O_3 particle. This feature becomes apparent when the change in the amount of strong acid sites is very little.

References

[1] M. Guisnet, N. S. Gnep and F. Alario, *Appl. Catal.*, **89** (1989) 1.

[2] Y. Ono, *Catal. Rev. Sci. Eng.*, **34** (1992) 189.

[3] J. A. Biscardi and E. Iglesia, *Catal. Today*, **31** (1996) 207.

[4] G. Giannetto, G. León, J. Papa, R. Monque, R. Galiasso and Z. Gabelica, *Catal. Today*, **31** (1996) 317.

[5] D. K. Simmons, R. Szostak, P. K. Agrawal and T. L. Thomas, *J. Catal.*, **106** (1987) 287.

[6] T. Inui, Y. Makino, F. Okazumi, S. Nagano and A. Miyamoto, *Ind. Eng. Chem. Res.*, **26** (1987) 647.

[7] I. Kanai and N. Kawata, *Appl. Catal.*, **55** (1989) 115.

[8] H. D. Lanh, V. A. Tuan, H. Kosslick, B. Parlitz, R. Fricke and J. Völter, *Appl. Catal. A*, **103** (1993) 205.

[9] C. R. Bayense, A. J. H. P. van der Pol and J. H. C. van Hoof, *Appl. Catal.*, **72** (1991) 81.

[10] P. Meriaudeau and C. Naccache, *J. Mol. Catal.*, **59** (1990) L31.

[11] N. S. Gnep, J. Y. Doyemet and M. Guisnet, *Stud. Surf. Sci. Catal.*, **46** (1989) 153.

[12] A. Yu. Khodakov, L. M. Kustov, T. N. Bondarenko, A. Dergachev, V. B. Kazansky, Kh. M. Minachev, G. Borbely and H. K. Beyer, *Zeolites*, **10** (1990) 603.

[13] Y. Ono, H. Nakatani, H. Kitagawa and E. Suzuki, *Stud. Surf. Sci. Catal.*, **44** (1989) 279.

[14] V. I. Yakerson, T. V. Vasina, L. I. Lafer, V. P. Sytnyk, G. L. Dylch, A. V. Mokhov, O. V. Bragin and Kh. M. Minachev, *Catal. Lett.*, **3** (1989) 339.

[15] J. Bandiera and Y. Ben Taarit, *Appl. Catal.*, **76** (1991) 199.

[16] C. R. Bayense and J. H. C. van Hooff, *Appl. Catal.*, **79** (1991) 127.

[17] E. Iglesia, J. E. Baumgartner and G. L. Price, *J. Catal.*, **134** (1992) 549.

[18] P. Meriaudeau, S. B. Abdul Hamid and C. Naccache, *J. Catal.*, **139** (1993) 679.

[19] C. Buckless, G. J. Hutchins and C. D. Williams, *Catal. Lett.*, **11** (1991) 89.

[20] R. Le Mao, J. Yao and R. Carli, *Appl. Catal. A*, **86** (1992) 127.

[21] Kh. M. Minachev and A. A. Degachev, *Catal. Today*, **13** (1992) 645.

[22] G. Giannetto, A. Montes, N. S. Gnep, A. Florentino, P. Cartrand and M. Guisnet, *J. Catal.*, **145** (1995) 86.

[23] V. R. Choudhary, C. Sivadinarayana, A. K. Kinage, P. Devadas and M. Guisnet, *Appl. Catal. A*, **136** (1996) 125.

[24] M. Niwa, M. Sawa and Y. Murakami, *Proc. 9th Intern. Cong. Catal.*, Chem. Inst. Canada, Ottawa, (1988) p. 380.

[25] M. Sawa, M. Niwa and Y. Murakami, *Appl. Catal.*, **53** (1989) 169.

[26] A. Satsuma, T. Ishikura, T. Shimizu, M. Niwa, T. Hattori and Y. Murakami, *Kagaku Kougaku Ronbubshu*, **21** (1995) 1120.

[27] C. V. Hidalgo, H. Itoh, T. Hattori, M. Niwa and Y. Murakami, *J. Catal.*, **85** (1984) 362.

[28] K. Nishi, T. Shimizu, H. Yoshida, A. Satsuma and T. Hattori, *Appl. Catal. A*, in press.

[29] S. Geller, *J. Chem. Phys.*, **33** (1960) 676.

Chapter 3

Dehydrogenation of propane on Gallium Oxide Catalysts

Synopsis

In order to clarify the structure-activity relationship in propane dehydrogenation on Ga_2O_3, the dehydrogenation of propane over supported and unsupported Ga_2O_3 catalysts was carried out. Ga_2O_3 catalysts were prepared by various methods, to obtain the catalysts having various particle sizes and crystal phases. On the whole, the reaction rate per surface Ga_2O_3 area of β-Ga_2O_3 was higher than those of α- and amorphous Ga_2O_3. In addition, the reaction rate per surface Ga_2O_3 area increased with increasing the Ga_2O_3 particle size up to 240 nm. These results indicate that this reaction is a structure sensitive reaction. The local structures of Ga_2O_3 catalysts were analyzed by X-ray absorption spectroscopy and benzaldehyde-ammonia titration method. Higher activity of large Ga_2O_3 particle can be attributed to high concentration of surface [Ga-O] sites. Higher activity of β-Ga_2O_3 of high crystallinity can be attributed to high concentration of [Ga-O] sites and coexistence of tetrahedrally and octahedrally coordinated Ga ions.

Introduction

The catalytic conversion of light alkane into higher hydrocarbons, such as aromatics and branched-chain aliphatics, attracts much attention as a possible technology for production of chemicals and fuels from less valuable light alkanes. And there has been continued interest in the design of catalysts for these reactions. The catalytic aromatization of light alkane over Ga-containing zeolites has been greatly studied in recent past [1-8]. As has been extensively discussed, it is unquestionable that gallium species are capable of significantly enhancing the production of aromatics, although substantial amount can be formed on acid form of zeolite ZSM-5 [9, 10]. It is widely accepted that their activity and selectivity result from bifunctional properties, whereby gallium species are responsible for their dehydrogenation activity and the Brønsted acid sites of zeolite provide the centers necessary for chain growth . This leads us to expect that the dispersion of gallium species would be the key factors controlling the catalytic activity. In the gallium promoted zeolites obtained by conventional method (ion exchange and/or impregnation), gallium species could be present as oxides and provide the dehydrogenation centers [11, 12]. Nevertheless, the structure and nature of gallium species is still a matter of controversy.

It is expected, and has been known, that the gallium ion closely resembles the aluminum ion and substitutes for it in several structures. Gallium oxide has been reported to have two structures, the trigonal α-Ga_2O_3 [13] and the monoclinic β-Ga_2O_3 [14]. The α-phase is isostructural with α-corundum, and therefore, the gallium ions are octahedrally coordinated. In the β-phase there are two kinds of coordination for gallium ions, namely one half in

tetrahedral sites and the other half in octahedral sites. Besides α- and β-Ga_2O_3, three polymorphs called γ-, δ- and ε-Ga_2O_3 have been found [15]. Alumina is one of the most widely used in heterogeneous catalysis and its properties have been extensively studied [16, 17]. While the use of gallium oxide in heterogeneous catalysis has been increasing in recent years, the surface properties were not well-known.

In this chapter, in order to clarify the structure-activity relationship in propane dehydrogenation on Ga_2O_3 catalysts, the effect of Ga_2O_3 particle size and local structure was investigated.

Experimental

Catalysts preparation

Unsupported and supported Ga_2O_3 catalysts, listed in Tables 1 and 2, were prepared in various ways to obtain a wide variety of Ga_2O_3. Unsupported Ga_2O_3 were prepared by calcining gallium hydroxide ($Ga_2O_3 \cdot nH_2O$) or gallium nitrate ($Ga(NO_3)_3 \cdot nH_2O$) at various temperatures in a dry air stream [15]. Five samples of gallium hydroxide were prepared in the following ways: (1) Initially, ammonia solution was added to gallium nitrate (Ga assay = 19%) solution. Then, under stirring, dodecyltrimethylammonium bromide (DTMABr), was obtained from Tokyo Kasei, was added as a templating agent, and the reaction mixture was heated at 343 K for 3 h. The pH of the mixture was adjusted to 9.0 with HNO_3 and heated at 343 K for 3 h. After cooling to room temperature, the resulting product was filtered, washed with water repeatedly, and air-dried to yield a gallium hydroxide. (2) The solution of gallium nitrate was added dropwise to dilute ammonia solution under stirring at room temperature. The precipitated product was filtered, washed with water, and air-dried to yield a gallium hydroxide. (3) The solution of ammonia solution was added to solution of gallium nitrate under stirring, and the product was filtered, washed with water, and air-dried to yield a gallium hydroxide. (4) Commercial reagent of gallium hydroxide (Mitsuwa Chemicals) was used without further purification. (5) Ammonia solution was added to the solution of gallium nitrate and the pH was adjusted at 8.5. After aging for 3 h at 333 K the product was filtered, washed with water and air-dried to yield gallium hydroxide. All unsupported Ga_2O_3 catalysts were pelleted without binder, crushed and sized to 28-48 mesh.

Supported Ga_2O_3 catalysts were prepared by impregnation of SiO_2 (reference catalyst, Catalysis Society of Japan, JRC-SIO-8) or SiO_2-Al_2O_3 (JRC-SAL-2, Al_2O_3 content is 13.8%) with an aqueous solution of gallium nitrate followed by evaporation-to-dryness and calcination in a dry air at 823 K for 4 h.

X-ray diffraction (XRD)

X-ray diffraction (XRD) patterns were recorded on a Rigaku RINT 1200 equipment using Cu K α radiation.

Ga_2O_3 surface area and particle size (nitrogen-adsorption, TEM)

The particle size of unsupported Ga_2O_3 was calculated from BET surface area measured by nitrogen-adsorption at 77 K with a flow-type apparatus. The Ga_2O_3 particle size of supported Ga_2O_3 catalysts was measured by transmission electron microscopy (TEM, JEOL JEM-2010), and exposed Ga_2O_3 surface area was calculated from the particle size.

Benzaldehyde-ammonia titration method (BAT)

The density of [Ga-O] site was calculated from the amount of benzoate adsorbed and the surface area. The amount of benzoate adsorbed was measured by benzaldehyde-ammonia titration (BAT) method proposed by Niwa *et al.* [18, 19] in the same way as previously reported. The Ga_2O_3 sample was oxidized at 673 K before measurements, and benzaldehyde was injected at 523 K until it eluted without reaction. Finally, ammonia was allowed to react at 673 K until benzonitrile was no longer produced. The amount of benzoate adsorbed was determined by the sum total of benzonitrile formed.

Ga K-edge X-ray absorption

X-ray absorption experiments were carried out at the beam line 10B (BL-10B) station at Photon Factory in National Laboratory for High Energy Physics (KEK-PF) with ring energy of 2.5 GeV and stored current of 250-350 mA. X-ray absorption spectra of Ga_2O_3 samples were collected in a transmission mode at room temperature with a Si(311) two-crystal monochromator. Sample powders were sealed with polypropylene film in a dry box to keep a dry state after evacuation at 773 K for 1 h. Normalization of X-ray absorption spectra and extraction of their EXAFS oscillations were performed as described elsewhere [20, 21].

Infrared spectroscopy

Infrared spectra were recorded on a Jasco FT/IR 300 spectrometer. An IR cell, which allowed the sample to be heated at controlled temperature *in situ*, was connected to a conventional high-vacuum system. The sample disk was evacuated at 773 K for 1h. Pyridine was adsorbed at room temperature for 1 h at the equilibrium pressure of 4.4 Torr (0.59 kPa), followed by evacuation at 373 K, and the spectrum of adsorbed pyridine was then measured at the same temperature.

Temperature-programmed desorption of carbon dioxide

Thermodesorption of carbon dioxide was carried out *in vacuo*. The quantity of desorbed carbon dioxide was measured by a mass spectrometer. Sample was pretreated at 773 K in the presence of 100 Torr oxygen for 1 h, followed by evacuation at the same temperature. Carbon dioxide (50 Torr) was adsorbed at room temperature. Remaining gaseous carbon dioxide was evacuated at room temperature, and the temperature of sample bed was then increased with constant heat rate of 2.5 K min^{-1}.

Propane dehydrogenation reaction

The catalytic test was carried out by using a continuous flow reaction apparatus at atmospheric pressure. The catalyst (0.167-0.50 g) was placed in a quartz tube with an inner diameter of 10 mm. The catalyst was pretreated in flowing oxygen diluted with nitrogen (O_2/N_2=1/4) for 1 h at 823 K. Partial pressure of propane were 18 kPa with nitrogen balance, and total feed rate was 0.15 mol h^{-1}. The reaction temperature was raised every 50 K from 673 to 873 K, and kept constant at each temperature for 30 min, at the end of which reaction products were analyzed with gas chromatography. The catalytic activity was evaluated under differential condition where conversion was less than 5%.

Results

Crystal Phase

The XRD patterns of unsupported Ga_2O_3 catalysts are shown in Figs. 1 and 2. The crystal phase confirmed by XRD is shown in Table 1. The unsupported catalysts prepared by calcining gallium hydroxide calcined below 923 K exhibited α-Ga_2O_3 phase. The samples H-1 and H-2 exhibited very broad bands owing to the poor intrinsic crystallization of the α-Ga_2O_3. The samples prepared by calcining starting substances above 923 K (H-7, N-3, 4, and 5) exhibit β-Ga_2O_3 phase, and this phase grew with an increase in the calcination temperature. The samples N-1 and N-2 exhibited shadowy peaks, and were confirmed as "X-ray amorphous". The commercially supplied sample N-6 exhibited very sharp lines of β-Ga_2O_3 phase. On the other hand, the crystal phase of Ga_2O_3 supported on SiO_2 and SiO_2-Al_2O_3 could not be identified, because the XRD patterns exhibited very shadowy peaks.

Ga_2O_3 particle size

The particle size of unsupported Ga_2O_3 catalysts is given in Table 1. The size of unsupported catalysts prepared by calcining commercially supplied gallium hydroxide (H-4, 5 and 7) increased from 19.6 to 41.7 nm with increase in calcination temperature. The Ga_2O_3 catalysts prepared by calcining gallium hydroxide obtained from precipitation (H-2 and 3)

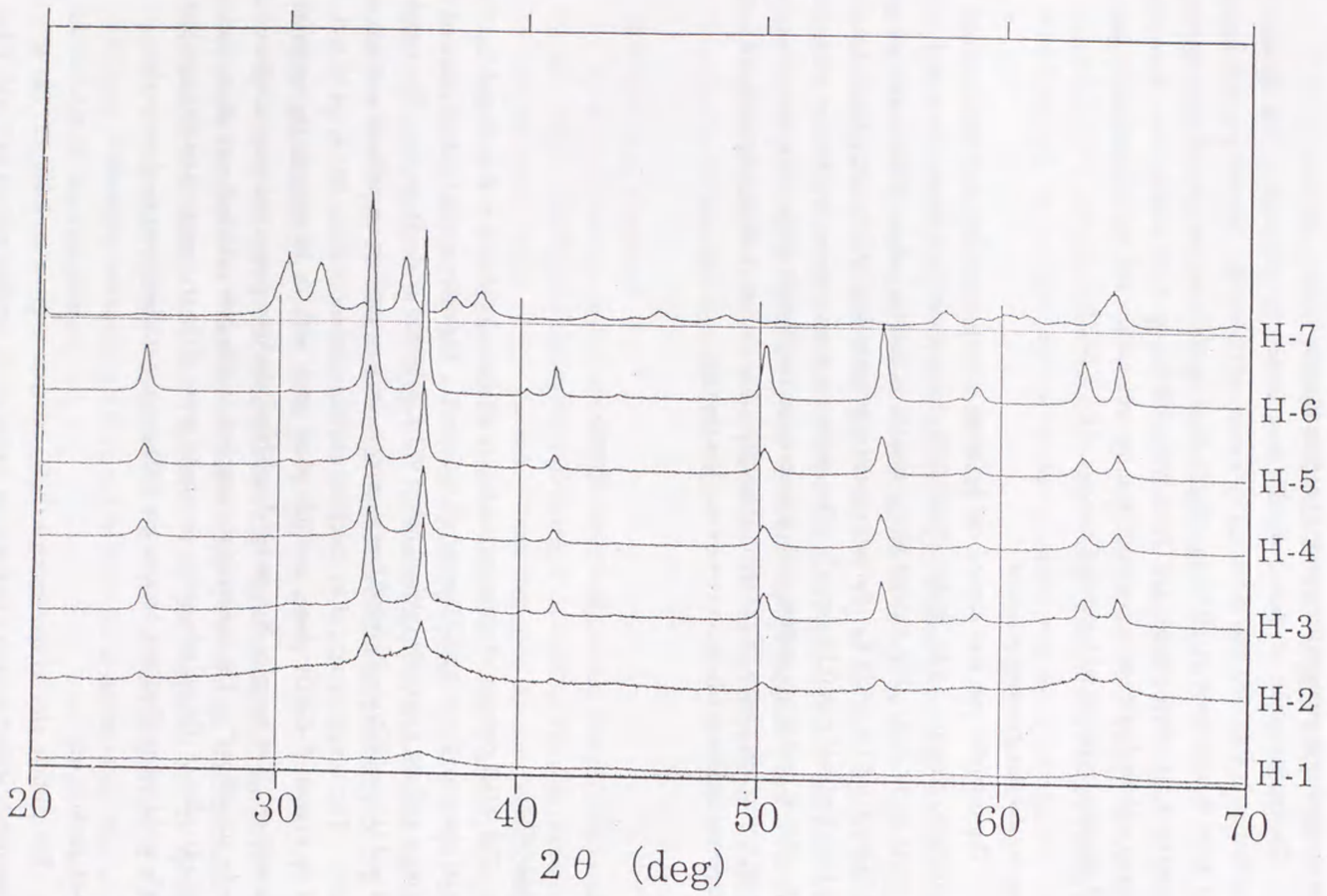

Fig. 1 X-ray diffraction patterns of unsupported Ga_2O_3 catalysts prepared by calcination of gallium hydroxide.

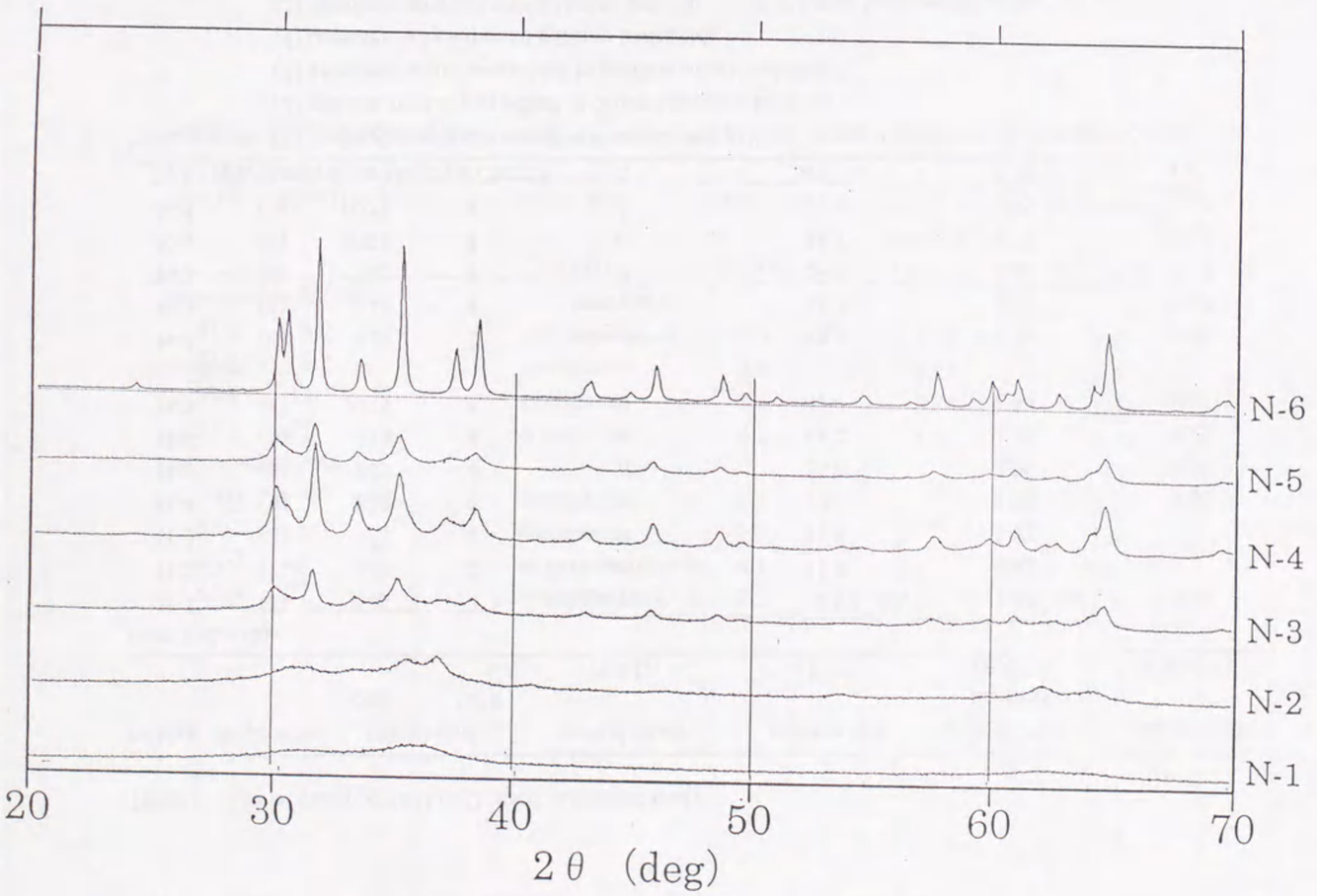

Fig. 2 X-ray diffraction patterns of unsupported Ga_2O_3 catalysts prepared by calcination of gallium nitrate.

Table 1 List of unsupported Ga_2O_3 used in present study

catalyst	preparation*	calcination temp.	calcination time	crystal phase (XRD)	particle size (BET)	[Ga-O] site density (BAT)	Ga(t)/Ga(o) (XANES)
from hydroxide							
H-1	(1)	823 K	2 h	amorphous + α	8.92 nm	1.48 nm^{-2}	0.48
H-2	(2)	823	2	α + amorphous	11.8	1.42	-
H-3	(3)	823	4	α	18.6	1.83	-
H-4	(4)	823	6	α	19.6	1.05	0.65
H-5	(4)	923	4	α	25.8	1.29	0.38
H-6	(5)	823	4	α	68.2	2.84	0.23
H-7	(4)	1073	4	β	41.7	1.84	0.85
from nitrate							
N-1	(6)	823	2	amorphous	13.5	1.57	0.60
N-2	(6)	823	4	amorphous	14.3	1.64	0.64
N-3	(6)	923	4	β	18.4	1.44	0.72
N-4	(6)	1073	4	β	44.1	1.79	0.80
N-5	(6)	1073	4	β	27.8	1.85	0.88
N-6	(purchased from Mitsuwa Chem.)			β	240	2.38	1.0

* preparation (1) dodecyltrimethylammonium bromide and gallium nitrate were added to ammonia solution
(2) gallium nitrate was added to dilute ammonia solution
(3) ammonia water was added to gallium nitrate solution
(4) commercially supplied gallium hydroxide
(5) ammonia solution was added to gallium nitrate solution followed by aging
(6) commercially supplied gallium nitrate

Table 2 List of supported Ga_2O_3 used in present study

catalyst	Ga_2O_3 content	crystal phase (XRD)	particle size (TEM)	[Ga-O] site density (BAT)	Ga(t)/Ga(o) (XANES)
supported on SIO-8					
SI-1	4.0 wt%	amorphous	2.0 nm	1.08 nm^{-2}	1.8
SI-2	6.7	amorphous	2.4	0.83	1.6
SI-3	13	amorphous	3.2	0.84	1.6
SI-4	27	amorphous	6.2	1.42	0.80
supported on SAL-2					
SA-1	4.0 wt%	amorphous	1.9	-	2.1
SA-2	6.7	amorphous	2.3	-	1.9
SA-3	13	amorphous	3.4	-	1.9
SA-4	27	amorphous	3.2	-	1.7

were smaller (11.8 and 18.6 nm) than that obtained from commercially supplied gallium hydroxide. The Ga_2O_3 catalyst prepared in the presence of the templating species (H-1) were found to be much smaller in size (8.92 nm). Aging the hydroxide gel (H-6) were found to increase the particle size to 68.2 nm. The particle size of Ga_2O_3 catalysts obtained from commercially supplied gallium nitrate ranged from 13.5 to 44.1 nm. For the Ga_2O_3 catalyst purchased from Mitsuwa Chem., the particle size was 240 nm.

Ga_2O_3 samples with smaller particle sizes were prepared by supporting Ga_2O_3 on SiO_2 and SiO_2-Al_2O_3. The particle sizes ranging between 1.9 and 6.2 nm were obtained by changing Ga_2O_3 content from 4.0 to 27 wt%. Table 2 shows the variation of Ga_2O_3 particle size with Ga_2O_3 content of the catalyst.

By varying the preparation method, Ga_2O_3 with different particle sizes ranging from 1.9 to 240 nm were obtained.

Benzaldehyde-ammonia titration method

The densities of [Ga-O] site on unsupported Ga_2O_3 catalysts are shown in Table 1. The density was as high as 1.05-2.84 nm^{-2}. These values are in good agreement with the reported results, the density of sites on Al_2O_3 is 2.2 ± 0.2 nm^{-2} [18].

Since the benzoate was hardly adsorbed on SiO_2, selective adsorption could be possible on Ga_2O_3/SiO_2. However, the BAT method was not applied to the SiO_2-Al_2O_3 supports, because the benzoate was adsorbed both on Ga_2O_3 and SiO_2-Al_2O_3. The density of surface [Ga-O] site on Ga_2O_3 supported on SiO_2 catalysts was measured by the BAT method, and the values are shown in Table 2. A low density of [Ga-O] site, 0.83-1.42 nm^{-2}, was observed on these catalysts.

Ga K-edge X-ray absorption

Figures 3 and 4 shows XANES spectra caused by excitation of electrons from core levels to empty valence levels or continuum. For the Ga K-edge shown here, the white line is assigned to 1s→4p electron transition [22], and its feature depends on the local arrangement of neighboring atoms.

In $Ga(acac)_3$ as reference sample, the six oxygen atoms of the three ligands form a nearly ideal octahedron around the Ga atom. On the other hand, the Ga ions occupy tetrahedral framework sites in the Ga-MFI. From the absorption spectra of $Ga(acac)_3$ and Ga-MFI, the prominent peaks found at 10376 and 10379 eV are assignable to Ga atom having tetrahedral and octahedral oxygen coordination, respectively. The positions of edge and peak maximum were shifted towards higher energies with increasing oxygen coordination number of Ga atom. This feature is consistent with the reported result reported that increasing the oxygen coordination number from 4 to 6 (sodalite to kyanite) shifts the edge further to a higher energy in Al K-edge XANES spectra.[23]

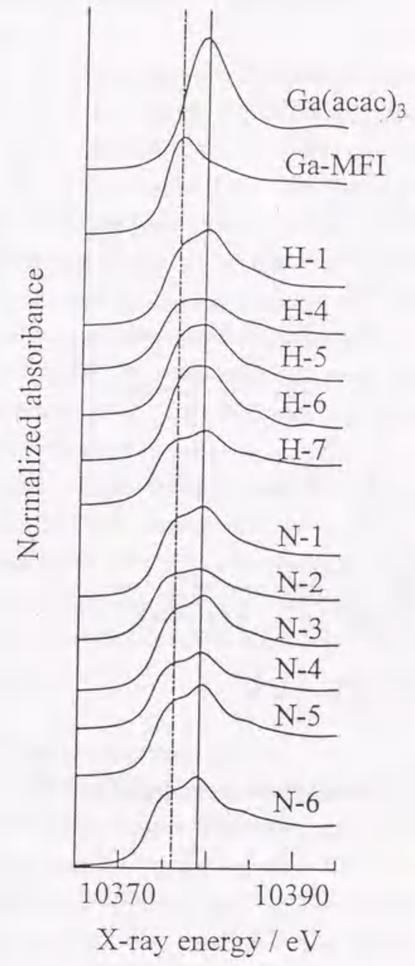

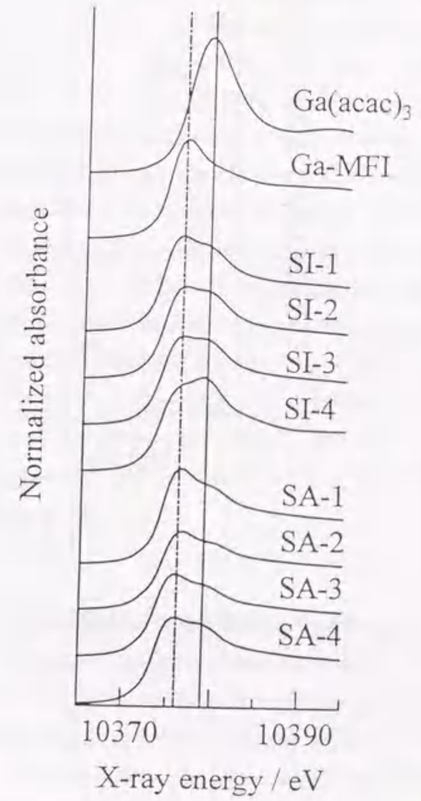

Fig. 3 (left) Ga K-edge XANES spectra of unsupported Ga_2O_3 catalysts.

Fig. 4 (right) Ga-K-edge XANES spectra of supported Ga_2O_3 catalysts.

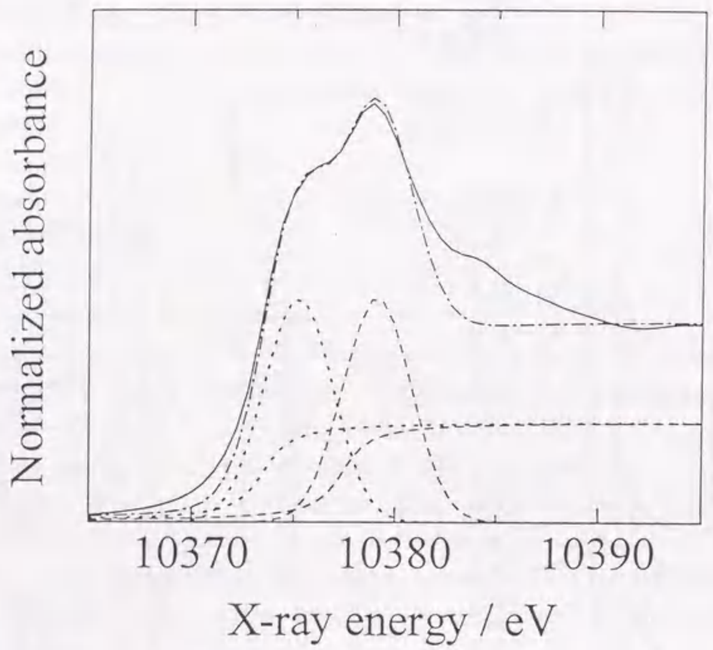

Fig. 5 Ga K-edge XANES and its deconvoluted spectrum of β-Ga_2O_3 (N-6).

Each Ga_2O_3 catalyst exhibited a broad absorption peak with various line shape. From a comparison with reference spectra, it was found that the catalysts contain two kinds of Ga species having different coordination, and the fraction of such species is different from each other.

In order to estimate the fraction of tetrahedrally and octahedrally coordinated Ga atoms (referred to as Ga(tet) and Ga(oct), respectively), deconvolution of XANES spectrum was carried out with two sets of curves of Gaussian for white line and arctangent function for continuum absorption [24]. The fraction of tetrahedrally and octahedrally coordinated Ga atoms were calculated from the area of deconvoluted spectra. Fig. 5 shows the deconvoluted spectrum of β-Ga_2O_3 (sample N-6) as an example. The ratio of integrated areas of the deconvoluted Ga(tet) and Ga(oct), *i.e.*, estimated Ga(tet)/Ga(oct), was 1.0 for this sample. Since theoretically, a half of Ga atoms are in tetrahedral sites and other half in octahedral sites in β-Ga_2O_3 [14], the estimated value of Ga(tet)/Ga(oct) is in good agreement with the theoretical value. This allows us to assume the ratio of areas corresponds directly to the ratio of Ga(tet) and Ga(oct), and to estimated the ratio of Ga(tet)/Ga(oct) by the deconvolution method. Table 1 and 2 show the ratio of Ga(tet)/Ga(oct) in unsupported and supported Ga_2O_3 catalysts, respectively. For unsupported catalysts, Ga(oct) was the major species in the catalysts defined as amorphous or α-phase by XRD. The ratios were evaluated to be 0.70-1.0 for the catalysts exhibited β-phase. On the other hand, the ratios of Ga(tet)/Ga(oct) in supported catalysts were 0.80-2.1, which indicates that Ga(tet) is the major species.

Infrared spectroscopy

The ring vibration mode 8a, according to the assignments of Kline and Turkevich [25], are the most sensitive vibrations with regard to the nature of intermolecular interactions via the nitrogen lone pair electrons. This mode is observed at 1580-1600 cm^{-1} for H-bonded pyridine, at 1600-1634 cm^{-1} for coordinated species (PyL) on Lewis acid sites and at around 1640 cm^{-1} for the pyridinium ion (PyH^+) on protonic sites. In this mode, increasing wavenumber indicates increasing coordination bond strength [26].

Figure 6 shows IR spectra, recorded after adsorption at room temperature followed by desorption at 373 K. All the spectra shows the ν 8a band at 1612-1620 cm^{-1}, which is ascribed to PyL. As generally stated in alumina [27], no band typical of PyH^+ was detected any of the samples. On α-Ga_2O_3 (sample H-6), the band was observed at 1613 cm^{-1}. β-Ga_2O_3 (N-6) presented a broad band having a maximum at 1612 cm^{-1} with a shoulder at 1618 cm^{-1}. It shows the presence of at least two types of Lewis acid sites. On supported catalyst 4.0 wt% Ga_2O_3/SiO_2 (SI-1), a sharp band at 1620 cm^{-1} was observed. Since the wavenumber could reflect the strength of acid sites, the order of the acid strength was 4.0 wt% Ga_2O_3/SiO_2 $>$ β-Ga_2O_3 $>$ α-Ga_2O_3.

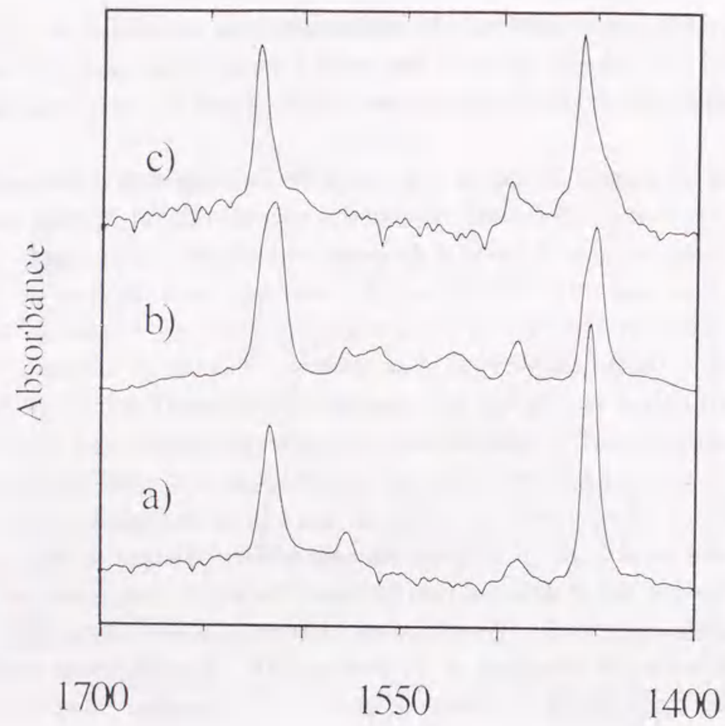

Fig. 6 IR spectra of pyridine adsorbed on Ga_2O_3 catalysts: (a) α-Ga_2O_3 (H-6); (b) β-Ga_2O_3 (N-6); (c) 4.0 wt% Ga_2O_3/SiO_2 (SI-1).

Temperature-programmed desorption of carbon dioxide

Figure 7 shows the profiles of CO_2-TPD on Ga_2O_3 catalysts. The profile on α-Ga_2O_3 (H-6) showed a broad peak at 400 K, which seems to resemble to the large desorption peak with maximum at about 400-410 K on some alumina samples [28]. β-Ga_2O_3 (N-6) showed two broad peaks: low temperature peak at 380 K with a long tailing part and high temperature peak at 900 K. In the case of 4.0 wt% Ga_2O_3/SiO_2 (SI-1), the profile showed only the very small peak at 350 K. It should be noted that the high temperature peak was observed only on β-Ga_2O_3. It is said that the strong chemisorption of carbon dioxide occurs through interaction with acid-base sites preferentially [26]. This suggests that the coexistence of Ga(tet) and Ga(oct) can provide the stronger acid-base pair sites.

Propane dehydrogenation reaction

The temperature dependence of propane conversion on unsupported Ga_2O_3 catalysts are shown in Fig. 8. The conversion above 823 K was decreased because of the catalyst deactivation due to coke deposition. Figure 9 shows the results of propane dehydrogenation on supported Ga_2O_3 catalysts. The conversion of propane increased with a rise in reaction temperature. In all cases, major product was propylene, and its selectivity exceeded 95% below 773 K.

Discussion

The effect of Ga_2O_3 particle size -structure sensitive reaction-

Fig. 10 shows the relation between the dehydrogenation rate at 773 K per exposed Ga_2O_3 surface area and Ga_2O_3 particle size. The dehydrogenation activity increased with increasing Ga_2O_3 particle size up to 240 nm. This result suggests that propane dehydrogenation on Ga_2O_3 catalyst is a structure sensitive reaction demanding large Ga_2O_3 particle. Since Boudart introduced the concept of structure sensitivity [29], the number of studies dealing with particle size effect have been made. In the case of supported metal catalysts, the catalytic activity depend on the surface structure, which varies when the particle size is varied in the critical range between 1 and 10 nm [30, 31]. As far as oxide catalysts are concerned, the role of the structure on the catalytic properties have been put forward referring to selective oxidation of hydrocarbons. The reactional specificity of crystalline faces has been demonstrated using a single-crystal sample [32, 33]. Consequently, it is noteworthy that the particle size effect was observed up to 240 nm of Ga_2O_3 particles in this study.

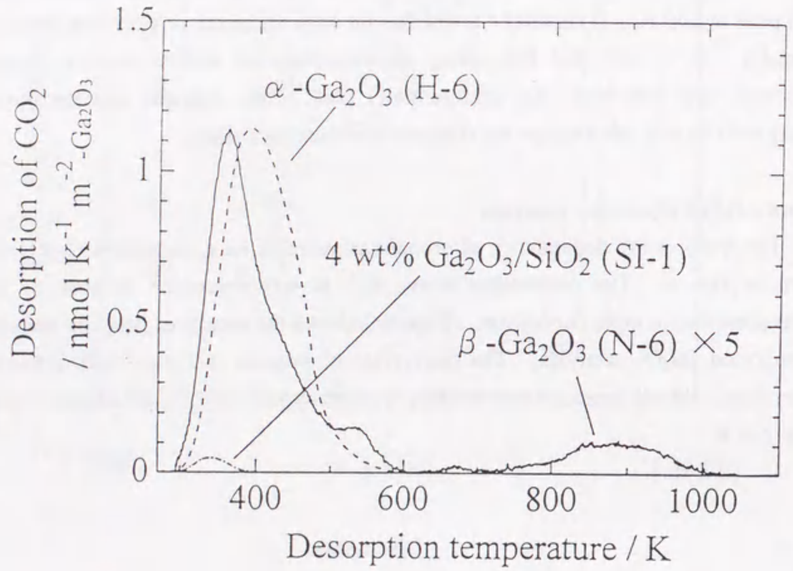

Fig. 7 CO_2-TPD profiles of Ga_2O_3 catalysts: (a) α -Ga_2O_3 (H-6); (b) β -Ga_2O_3 (N-6); (c) 4.0 wt% Ga_2O_3/SiO_2 (SI-1).

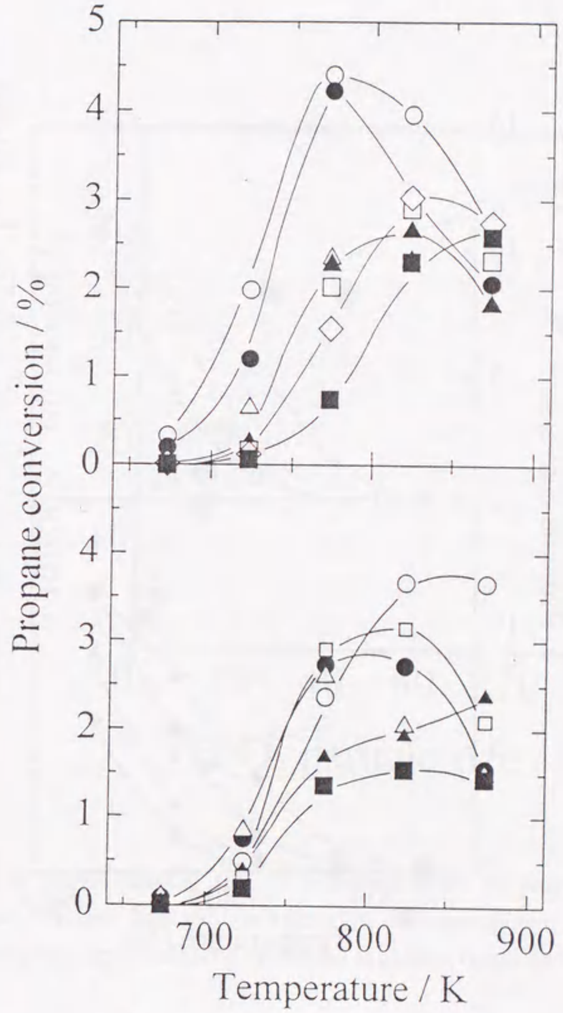

Fig. 8a Conversion in the reaction of propane dehydrogenation on unsupported Ga_2O_3 catalysts prepared by calcination of gallium hydroxide and (b) gallium nitrate: (○) H-1; (●) H-2; (△) H-3; (▲) H-4; (□) H-5; (■) H-6; (◇) H-7.

Fig. 8b Conversion in the reaction of propane dehydrogenation on unsupported Ga_2O_3 catalysts prepared by calcination of gallium nitrate: (○) N-1; (●) N-2; (△) N-3; (▲) N-4; (□) N-5; (■) N-6; (◇) N-7.

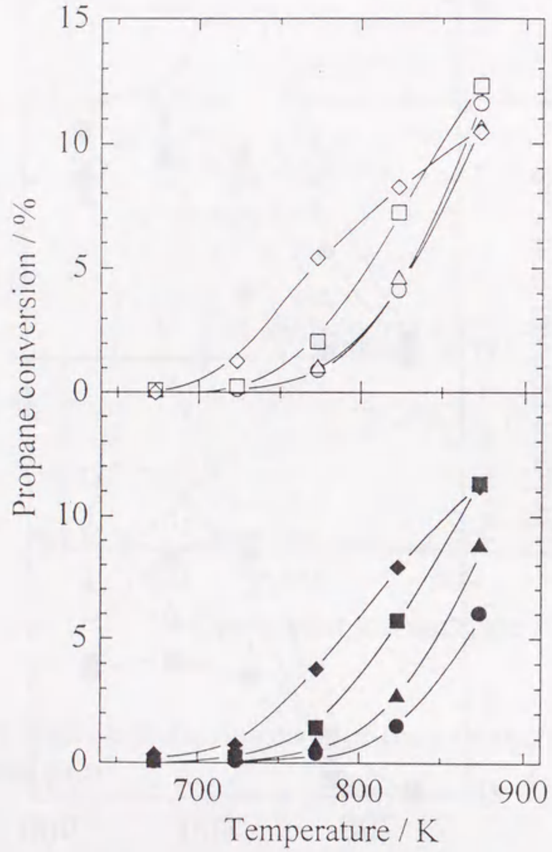

Fig. 9a Conversion in the reaction of propane dehydrogenation on supported Ga_2O_3 catalysts prepared by impregnation of SiO_2: (○) SI-1; (△) SI-2; (□) SI-3; (◇) SI-4.

Fig. 9b Conversion in the reaction of propane dehydrogenation on supported Ga_2O_3 catalysts prepared by impregnation of SiO_2-Al_2O_3: (●) SA-1; (▲) SA-2; (■) SA-3; (◆) SA-4.

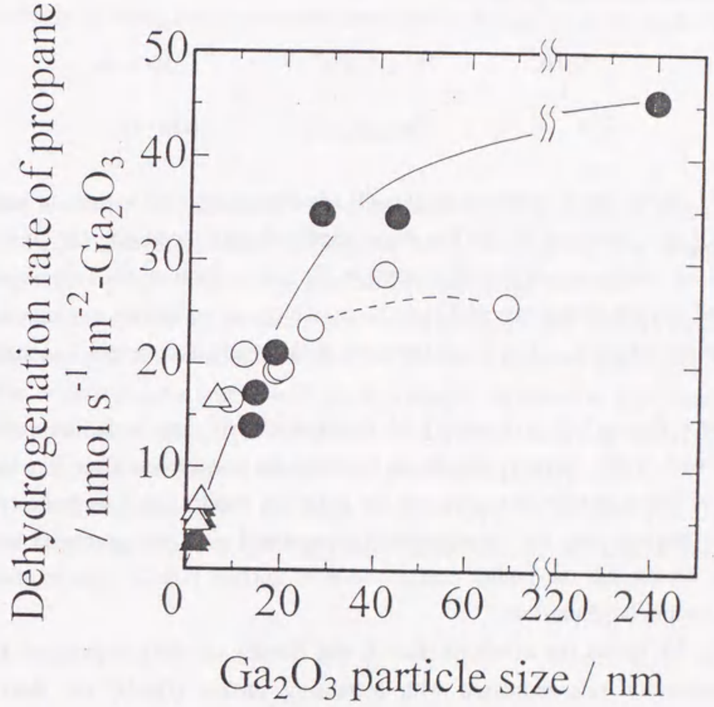

Fig. 10 Effect of Ga_2O_3 particle size on dehydrogenation of propane at 773 K: (○) unsupported Ga_2O_3 obtained from gallium hydroxide; (●) unsupported Ga_2O_3 obtained from gallium nitrate; (△) supported Ga_2O_3 on SiO_2; (▲) supported Ga_2O_3 on SiO_2-Al_2O_3.

The effect of [Ga-O] site density

Propane is said to be activated over Ga_2O_3 through the dissociative adsorption of propane with formation of gallium hydride and gallium alkoxide species, in which [Ga-O] site is regarded as active site [11].

$$\begin{array}{ccccccc} C_3H_8 & & H^- \quad C_3H_7^+ & & C_3H_6 + H_2 \\ \downarrow & \Rightarrow & | \quad\quad | & \Rightarrow & \uparrow \\ [Ga - O] & & [Ga - O] & & [Ga - O] \end{array}$$

Figure 11 shows the dependence of [Ga-O] site density on Ga_2O_3 particle size. The density of [Ga-O] site measured by BAT method increased with increasing Ga_2O_3 particle size. In general, the smaller oxide particles result in the larger fraction of coordinatively unsaturated metal and oxygen atoms exposed at surfaces, which are accessible to reactant molecules and available for catalysis. The result obtained in this study is therefore in conflict with general aspect.

Since the surface free energy of fine particles is very high, the surfaces should be covered with water, oxygen, *etc.* so as to minimize surface free energy. In contrast at the surface of larger particle, it seems that the adsorbed species, such as hydroxyls, are removed from the surfaces and the coordinatively unsaturated sites are generated with ease. As a result, it seems that the higher concentration of surface [Ga-O] sites is obtained in Ga_2O_3 catalyst having large particle.

Fig. 12 shows the effect of [Ga-O] site density on dehydrogenation rate of propane. Dehydrogenation rate increased with increasing surface [Ga-O] site density. The rate, however, varied from catalyst to catalyst. This result suggests that each surface [Ga-O] site exhibits different activity and whose activity is sensitive to local structure.

The effect of local structure of Ga_2O_3

Figure 13 shows dependence of turnover frequency of propane dehydrogenation, defined as the reaction rate per surface [Ga-O] site, on the local structure of Ga_2O_3 catalysts, reported by the ratio of Ga(tet)/Ga(oct) estimated on the basis of the deconvolution of XANES spectra. Ga_2O_3 catalysts having Ga(tet)/Ga(oct) ratio being close to unity, *i.e.*, Ga_2O_3 consisting of β-phase, exhibited higher turnover frequency.

From the result of IR (Fig. 5), it was confirmed that the Lewis acid sites exhibiting moderate strength exist on β-Ga_2O_3 (N-6) surface, and the supported catalyst has the strongest acid sites. The strong acid site could be related to the presence of a larger number of Ga ion in tetrahedral coordination, as reported in alumina samples [34, 35]. CO_2-TPD profiles in Fig. 6 show that the presence of the strong basic sites only on β-Ga_2O_3 catalyst. As described previously, propane undergoes heterolytically dissociative adsorption, thus

forming gallium hydride and gallium alkoxide intermediates. It is obvious that propyl carbenium cations could be formed on Lewis acid-base pair sites, via hydride ion abstraction. This suggests that the coexistence of tetrahedrally and octahedrally coordinated Ga ions in β-Ga_2O_3 provides both strong acidic sites and basic sites and contributes the higher activity.

Conclusion

In order to clarify the structure-activity relationship in propane dehydrogenation on Ga_2O_3 catalysts, the dehydrogenation of propane were investigated over unsupported and supported Ga_2O_3 catalysts having various particle sizes and local structures.

The reaction rate per surface area increased with increasing the Ga_2O_3 particle size up to 240 nm, indicating that this reaction is a structure sensitive reaction demanding large Ga_2O_3 particle. Higher activity of a large Ga_2O_3 particle can be attributed to high concentration of coordinatively unsaturated surface [Ga-O] sites. Ga_2O_3 catalysts having Ga(tet)/Ga(oct) ratio being close to unity exhibited higher reaction rate per surface [Ga-O] site.

It was concluded that both the high concentration of surface [Ga-O] sites and coexistence of tetrahedrally and octahedrally coordinated Ga ions are key factors controlling catalytic activity.

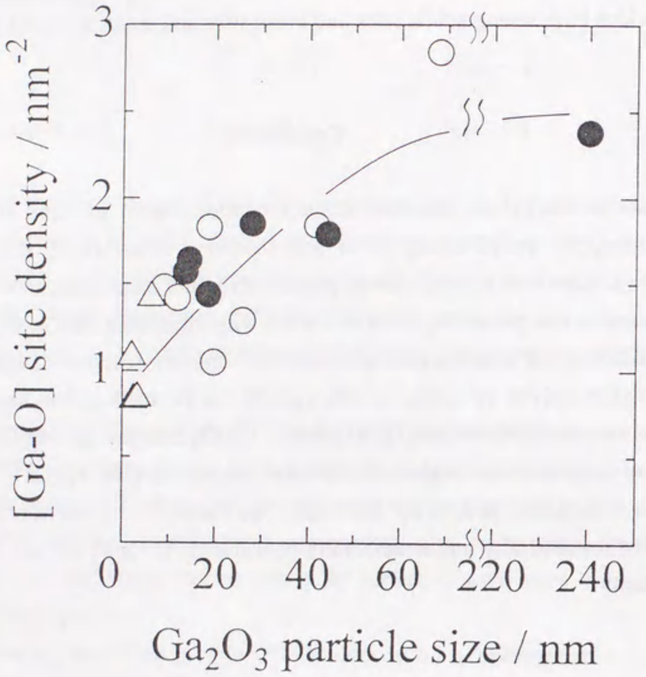

Fig. 11 Dependence of [Ga-O] site density on Ga_2O_3 particle size: (●) unsupported Ga_2O_3 obtained from gallium nitrate; (△) supported Ga_2O_3 on SiO_2.

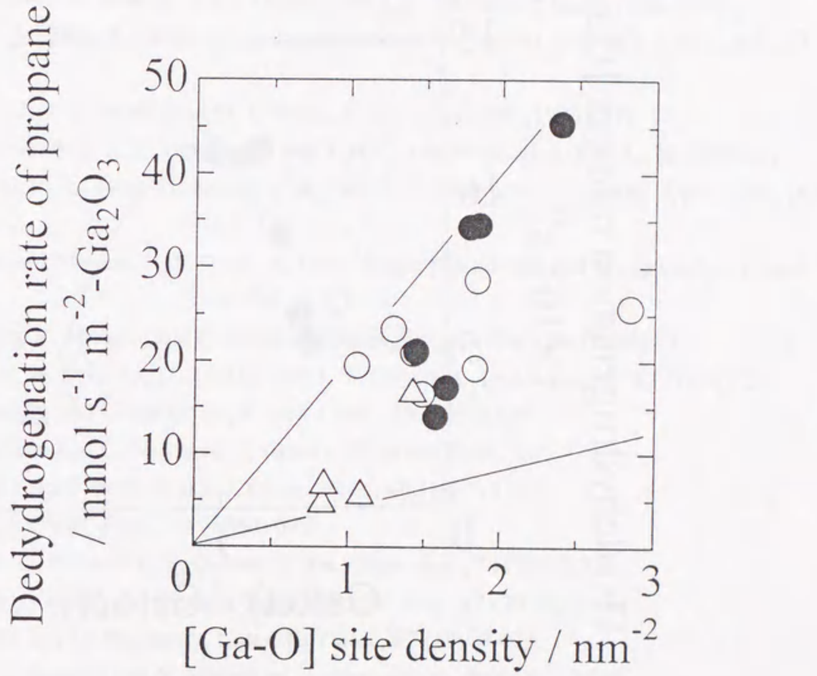

Fig. 12 Effect of [Ga-O] site density on dehydrogenation rate of propane: (●) unsupported Ga_2O_3 obtained from gallium nitrate; (△) supported Ga_2O_3 on SiO_2.

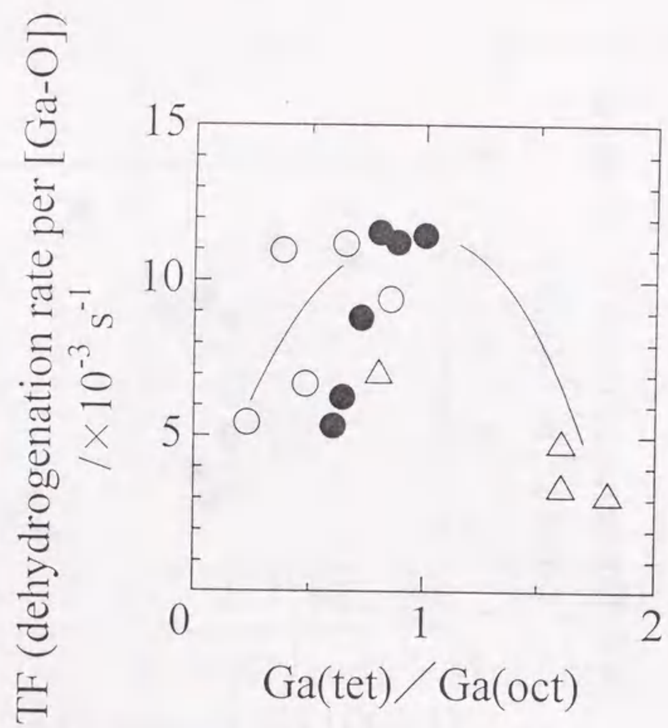

Fig. 13 Dependence of turnover frequency of propane dehydrogenation on the local structure of Ga_2O_3 catalysts: (●) unsupported Ga_2O_3 obtained from gallium nitrate; (△) supported Ga_2O_3 on SiO_2.

References

[1] M. Guisnet, N. S. Gnep and F. Alario, *Appl. Catal.*, **89** (1992) 1.

[2] Y. Ono, *Catal. Rev. Sci. Eng.*, **34** (1992) 179.

[3] D. K. Simmons, R. Szostak, P. K. Agrawal and T. L. Thomas, *J. Catal.*, **106** (1987) 287.

[4] T. Inui, Y. Makino, F. Okazumi, S. Nagano and A. Miyamoto, *Ind. Eng. Chem. Res.*, **26** (1987) 647.

[5] N. S. Gnep, J. Y. Doyemet and M. Guisnet, *J. Mol. Catal.*, **45** (1988) 281.

[6] C. R. Bayense, A. J. H. P. van der Pol and J. H. C. van Hoof, *Appl. Catal.*, **72** (1991) 81.

[7] H. D. Lanh, V. A. Tuan, H. Kosslick, B. Parlitz, R. Fricke and J. Völter, *Appl. Catal. A*, **103** (1993) 205.

[8] G. Gianetto, A. Montes, N. S. Gnep, A. Florentiono, P. Cartraud and M. Guisnet, *J. Catal.*, **145** (1993) 86.

[9] G. Giannetto, R. Monque and R. Galiasso, *Catal. Rev. Sci. Eng.*, **36** (1994) 271.

[10] M. Guisnet, N. S. Gnep, D. Aittaleb and J. Y. Doyemet, *Appl. Catal. A*, **87** (1992) 255.

[11] P. Meriaudeau and C. Naccache, *J. Mol. Catal.*, **59** (1990) L31.

[12] P. Mariaudeau and C. Naccache, *J. Catal.*, **157** (1995) 283.

[13] M. Marezio and J. P. Remeika, *J. Chem. Phys.*, **46** (1967) 1862.

[14] S. Geller, *J. Chem. Phys.*, **33** (1960) 676.

[15] R. Roy, V. G. Hill and E. F. Osborn, *J. Am. Chem. Soc.*, **74** (1952) 719.

[16] H. Knözinger and P. Ratnasamy, *Catal. Rev. Sci. Eng.*, **17** (1978) 31.

[17] C. Morterra and G. Magnacca, *Catalysis Today*, **27** (1996) 497.

[18] M. Niwa, S. Inagaki and Y. Murakami, *J. Phys. Chem.*, **89** (1985) 2550.

[19] M. Niwa, K. Suzuki, M. Kishida and Y. Murakami, *Appl. Catal.*, **67** (1991) 297.

[20] J. Wong, F. W. Lytle, R. P. Messmer and D. H. Maylotte, *Phys. Rev.B*, **30** (1984) 5596.

[21] T. Tanaka, H. Yamashita, R. Tsuchitani, T. Funabiki and S. Yoshida, *J. Chem. Soc. Faraday Trans. 1*, **84** (1989) 2987.

[22] F. Tourtin, P. Armand, A. Ibanez, G. Tourillon and E. Philippot, *J. Phys. IV France*, **7** (1997) C2-975.

[23] J. Wong, Z. U. Rek, M. Rowen, T. Tanaka, F. Schäfers, B. Müller, G. N. George, I. J. Pickering, G. Via, B. DeVries, G. E. Brown Jr. and M. Fröba, *Physica B*, **208&209** (1995) 220.

[24] T. Tanaka, T. Hanada, S. Yoshida, T. Baba and Y. Ono, *Jpn. J. Appl. Phys.*, **32-2** (1993) 481.

[25] C. H. Kline and J. Turkevich, *J. Chem. Phys.*, **12** (1944) 300.

[26] H. Knözinger, *Adv. Catal.*, **25** (1976) 184.

[27] H. Knözinger and C. P. Kaerlein, *J. Catal.*, **25** (1972) 436.

[28] V. A. Ivanov, A. Piéple, J. C. Lavalley and P. Nortier, *Appl. Catal. A*, **131** (1995) 323.

[29] M. Boudart, *Adv. Catal.*, **20** (1969) 153.
[30] M. Che and C. O. Bennett, *Adv. Catal.*, **36** (1989) 55.
[31] G. A. Somorjai, *Introduction to surface chemistry and catalysis*, Wiley, New York, 1994, p. 500.
[32] J. E. Germain, *Stud. Surf. Sci. Catal.*, **21** (1985) 355.
[33] J. C. Volta and J. L. Portefaix, *Appl. Catal.*, **18** (1985) 1.
[34] F. Abbattisa, S. Delmastro, G. Gozzelino, D. Mazza, M. Vallino, G. Busca, V. Lorenzelli and G. Ramis, *J. Catal.*, **117** (1989) 42.
[35] P. Nortier, P. Fourre, A. B. Mohammed Saad, O. Saur and J. C. Lavalley, *Appl. Catal.*, **61** (1990) 141.

Chapter 4

Local structure of gallium in Ga-MFI catalysts characterized by XAFS and microcalorimetry

Synopsis

In order to elucidate the catalytic activity for dehydrogenation of propane, the structural analysis of Ga-MFI catalysts calcined at various temperatures was carried out using Ga K-edge X-ray absorption spectroscopy and microcalorimetry. On the basis of the deconvolution of XANES spectra and EXAFS curve-fitting analyses, the fractions of tetrahedrally and octahedrally coordinated gallium species were evaluated. With an increase in calcination temperature, the number of tetrahedrally coordinated gallium species decreased and that of octahedrally coordinated gallium species increased. The microcalorimetry revealed that the fractions of framework and extraframework gallium species changed with Ga content and calcination temperature. Ga-MFI catalysts having large extraframework gallium species exhibited higher activity for dehydrogenation of propane. The higher activity was correlated with the ratio of tetrahedral gallium species to octahedral species.

Introduction

MFI-type gallosilicates (Ga-MFI) show high aromatization activity and selectivity in the conversion of light alkanes [1-12]. The high activity and selectivity of this zeolite are attributed to its high activity for the dehydrogenation of alkane and naphthene intermediates [3, 5, 9, 13]. It is suggested that the active gallium species for the dehydrogenation are not the framework Ga but the extraframework Ga species, formed during zeolite synthesis or calcination present in the zeolite [3, 4, 5, 8, 9, 14]. However, the state and quantity of framework and extraframework Ga species are not understood well. In the previous chapter, the catalytic properties of the framework and extraframework Ga species were investigated, and the change of catalytic activity with calcination temperature was attributed to the changes in acidity and particle size of Ga_2O_3 caused by extraction of framework Ga.

In the present chapter, the X-ray absorption spectroscopy (XANES and EXAFS) and microcalorimetry were applied for the characterization of Ga-MFI catalysts prepared by changing Ga content and calcination temperature. X-ray absorption spectroscopy has attained a growing importance in material science due to its ability to provide information on the local atomic structure in rather complex systems. Through the studies on supported and unsupported Ga_2O_3 samples, it was found in the previous chapter that Ga K-edge XANES provides the useful information about the local structure and the fraction of Ga atoms in different coordination state, *i.e.*, tetrahedral and octahedral coordination. Microcalorimetry is one of the most reliable method for the measurement of acid sites which are generally accepted to be responsible for transformations of various hydrocarbons in zeolites, and this technique is continuing to generate reliable data about the acid strength and number of the

sites in solid catalysts [15-19]. On the basis of these structural analyses, in this chapter, the factors generating and controlling the dehydrogenation activity were discussed.

Experimental

Catalyst Preparation

The gallosilicates having MFI structure were synthesized with different gallium contents according to the literature [8]. This includes the hydrothermal treatment of gels having the following composition 15 Na_2O·x Ga_2O_3·100 SiO_2·13 TPABr·4400 H_2O at 443 K under autogeneous pressure. The samples with different Si/Ga ratio (Si/Ga=12.5, 20, 40, 80) were prepared under the same conditions but the gallium content. The gels were prepared from sodium silicate (Kishida Chem.), gallium nitrate (Mitsuwa Chem.), sodium chloride, sulfuric acid, distilled water and tetrapropylammonium bromide (TPABr) used as template. The crystallization time was 48 h. The as-synthesized products were calcined for 8 h at 803 K, ion exchanged three times with a 1 M NH_4NO_3 solution a 353 K for 24 h, and calcined for 4 h at various temperatures (823, 923 and 993 K) under dry air flow.

X-ray absorption spectroscopy

Local structure of gallium was characterized by X-ray absorption spectroscopy. Ga K-edge XAFS were recorded at room temperature at BL-10B station in KEK-PF with a Si(311) two crystal monochromator (ring energy 2.5-3.0 GeV and store current 250-350 mA). XAFS measurements were carried out in a transmission mode. The intensities of the incident and transmitted X-ray were measured with a 17-cm ion chamber with a flowing gas mixture of N_2 (85%) and Ar (15%) and a 31-cm ion chamber with a flowing gas mixture of N_2 (75%) and Ar (25%), respectively. Energy calibration was carried out using a characteristic peak Cu K-edge at 8978.9 eV of Cu foil.

XANES (X-ray absorption near edge structure) analyses were carried out as described elsewhere [20, 21]. The normalized XANES spectrum was deconvoluted to two set of a post-edge peak with a continuum absorption curve [22-25]. The peaks at higher energy than the two peaks were not considered because the assignment is very difficult due to the influence of multiple scattering of photoelectrons.

Curve-fitting analysis of Fourier-filtered EXAFS was performed by using empirical parameters. Empirical backscattering amplitude and phase shift for Ga-O pair were extracted from the EXAFS spectrum of reference compound $Ga(acac)_3$ by assuming an average Ga-O distance of 1.952 Å.

Microcalorimetry

The differential heat of adsorption of ammonia was measured using a twin-conduction type microcalorimeter (Tokyo Riko Co., HTC-450) with a conventional vacuum system. About 0.5 g of the sample was weighed into the sample cell which was evacuated at 773 K under 10^{-2} Pa overnight and placed in the calorimeter. The heat of adsorption of ammonia was measured at 473 K in the same as described in a literature [26].

X-ray diffraction analysis

X-ray powder pattern was recorded by a Rigaku RINT 2500 equipment using Cu K α radiation. Unit cell parameters were obtained by a least-squares fit of the interplanar spacings of 9 strong reflections occurring in the 2 θ angular range 9-30 °. The selected reflections were recorded by step scanning procedure with step size of 0.02 °.

Temperature programmed desorption of ammonia (NH_3-TPD)

The acid amount and strength of zeolite samples were measured by temperature programmed desorption of ammonia (NH_3-TPD) in the same way as described previously [27-29].

Transmission electron microscopy

The Ga_2O_3 particle size on Ga-MFI catalysts was measured by transmission electron microscopy (TEM, HITACHI H-800), and exposed Ga_2O_3 surface area was calculated from the particle size.

Reaction of propane

The catalytic test was carried out by using a continuous flow reaction apparatus at atmospheric pressure. The catalyst (0.30 g) was placed in a quartz tube with an inner diameter of 10 mm. The catalyst was pretreated in flowing oxygen diluted with nitrogen (O_2/N_2=1/4) for 1 h at 823 K. Partial pressure of propane was 18 kPa with nitrogen balance, and total feed rate was 0.15 mol h^{-1}. The reaction temperature was raised every 50 K from 673 to 873 K, and was kept constant at each temperature for 30 min at the end of which reaction products were analyzed on line by gas chromatography. The yield and selectivity were expressed in C% on the basis of propane fed, and the selectivity was expressed in C% on the basis of total hydrocarbon products.

Results

X-ray absorption near edge structure (XANES) analysis

Absorption profile of the XANES spectra are caused by extraction of electrons from core levels to empty valence levels or continuum. Multiple scattering of the emitted photoelectrons leads to an intensive absorption structure, the white line, which depends on the local arrangement of neighboring atoms. Consequently, from the positions and relative intensities of absorption structures information can be drawn about *e.g.* effective charge of exited atom, coordination number and geometry of surrounding atoms. Due to the completely filled 3d-subshell in Ga(Ⅲ) systems, difficulties arise in the comparison of spectra with those of reference compounds due to the absence of pre-edge structures originating 1s → 3d transitions.

XANES spectra of the Ga-MFI catalysts are shown in Fig. 1. Every spectrum exhibited an intensive absorption maxima at 10376 eV, so called white line, with a discernible shoulder at higher energy side of the main absorption peak at about 10380 eV. Generally, the Ga ions incorporated into framework occupy tetrahedral framework sites in Ga-MFI. The spectrum of Ga-MFI sample with lower Ga content, in which all the Ga ions would occupy tetrahedral framework sites, is similar to that of Ga-MFI (Si/Ga=80) calcined at 823 K. On the other hand, the six oxygen atoms of the three ligands form a nearly ideal octahedron around the Ga atom in $Ga(acac)_3$. From a comparison with the spectra of reference samples, the prominent peak found at 10376 eV and the shoulder at 10380 eV can be assignable to Ga species having tetrahedral and octahedral oxygen coordination, respectively. This indicates that the sample contains at least two kinds of Ga species with different coordination and the fraction of such species varies with calcination temperature. It is found that the peak at 10380 eV appears in the spectrum with increasing intensity with calcination temperature, while the peak at 10376 eV remains or decreases. These results support that the framework Ga (referred to as Ga(FW)) species are extracted and the extraframework Ga (referred to as Ga(EFW)) species are formed by calcining at higher temperatures. Fig. 2 shows XANES spectra of Ga impregnated Ga-MFI and physical mixtures of β-Ga_2O_3 and Ga-MFI. It was clear that the formation of Ga(EFW) species causes an increase in peak intensity at 10380 eV. From a comparison with the spectra of Ga-promoted samples (Fig. 2) and calcined Ga-MFI catalysts (Fig. 1), the state of Ga(EFW) species in the latter could be different from that in the former.

To estimate the fraction of tetrahedrally and octahedrally coordinated Ga species, referred as to Ga(tet) and Ga(oct), respectively, a deconvolution analysis was carried out [22-25] as shown in Fig. 3 as an example. The positions of peaks A and B are found to be 10376 and 10380 eV, and did not change with Ga content and calcination temperature as shown in Fig. 3 and Table 1. These energies are characteristic for Ga(tet) and Ga(oct) species as

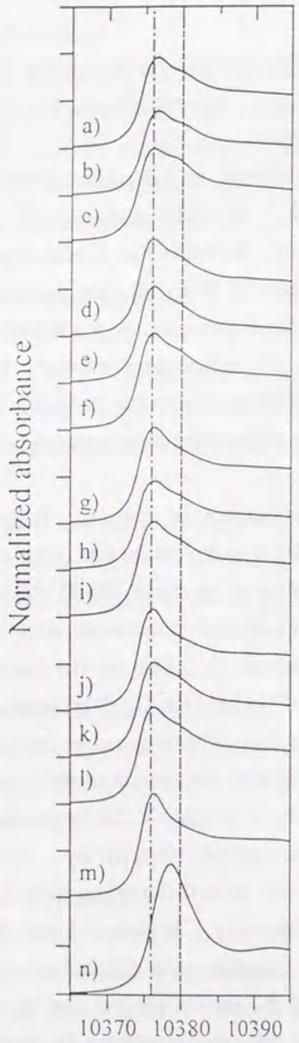

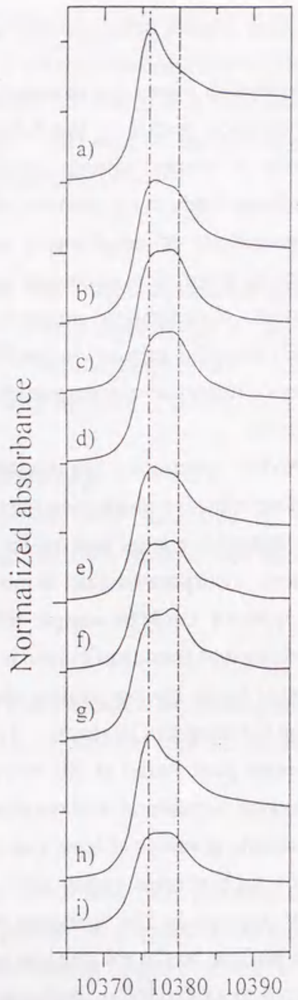

Fig. 1 (left) Ga K-edge XANES spectra of Ga-MFI catalysts: Si/Ga= (a)-(c) 12.5, (d)-(f) 20, (g)-(i) 40 and (j)-(l) 80; calcined at (a, d, g, j) 823, (b, e, h, k) 923 and (c, f, i, l) 993 K; (m) Ga-MFI (Si/Ga=120); (n) $Ga(acac)_3$

Fig. 2 (right) Ga K-edge XANES spectra of Ga-promoted zeolites: (a) Ga-MFI (Si/Ga=80, calcined at 823 K), Ga impregnated Ga-MFI; (b) 1 wt% Ga, (c) 3 wt% and (d) 5 wt%, physical mixtures of β-Ga_2O_3 and Ga-MFI; (e) 1 wt% Ga, (f) 3 wt% and (g) 5 wt%, Ga impregnated ZSM-5; (h) 3 wt% Ga and (i) 10 wt%

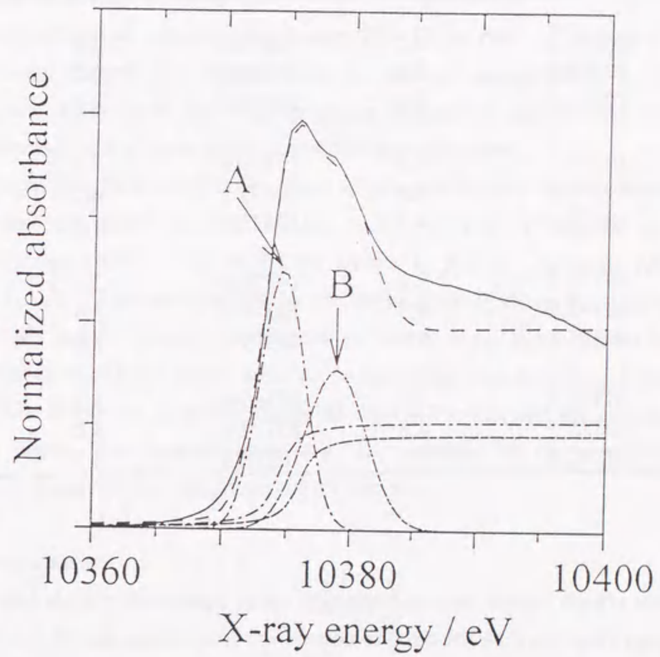

Fig. 3 Ga K-edge XANES and its deconvoluted spectrum of Ga-MFI (Si/Ga=12.5, calcined at 993 K)

Table 1 Positions and areas of post-edge peaks in Ga K-edge XANES spectra of Ga-MFI catalysts

catalyst	Ga(tet)		Ga(oct)		
calcin. temp.	position / eV	area / eV	position / eV	area / eV	A/B
Si/Ga=12.5					
823 K	10375.2	5.1	10379.4	3.9	1.3
923	10374.8	5.3	10379.0	3.7	1.4
993	10374.6	5.2	10378.8	4.5	1.1
Si/Ga=20					
823	10375.3	5.2	10379.6	3.9	1.3
923	10375.4	4.9	10379.5	4.1	1.2
993	10375.4	4.9	10379.5	4.2	1.2
Si/Ga=40					
823	10375.7	5.1	10379.9	3.3	1.6
923	10375.5	4.8	10379.9	3.3	1.5
993	10375.6	5.3	10379.9	3.6	1.5
Si/Ga=80					
823	10375.7	5.7	10380.0	3.1	1.8
923	10375.7	4.8	10379.8	4.0	1.2
993	10375.7	5.1	10379.8	3.7	1.4

reported in a literature [30]. Thus, the peaks A and B could be attributable to 1s→4p electron transitions of Ga(tet) and Ga(oct) species [31]. As shown in Table 1, the peak areas varied with Ga content and calcination temperature. The fraction of octahedrally coordinated Ga species increased with increasing Ga content and with increasing calcination temperature.

k^3-Weighted Ga K-edge EXAFS

Figure 4 shows k^3-weighted Ga K-edge EXAFS spectra. The each EXAFS spectrum is similar, and the maximum of the envelope is observed around 10 $Å^{-1}$. The position of the principal peak is the same for each spectrum, suggesting that the EXAFS signal for each sample comprises of the same kinds of sine wave components.

The local structures around Ga atoms of samples became visually clearer when a Fourier transform was performed on the EXAFS in the 4.0-15.0 $Å^{-1}$ region, to obtain the radial structure function (RSF). The RSFs are shown in Fig. 5. A single prominent peak was present at 1-2 Å. This peak is due to the backscattering from the adjacent oxygen atoms. The magnitude and the position of the peak appearing at 1-2 Å are almost constant, indicating that the number of oxygen atoms adjacent to Ga atoms and the distance between the oxygen atoms and Ga atoms are almost constant to the Ga content and the calcination temperature. Significant higher shell contributions, *e.g.*, the presence of the second-neighboring metal atoms (Ga or Si atoms), are not found for all samples.

Curve-fitting analysis

To make clearer the change of the coordination state around the Ga atoms in the samples, nonlinear curve-fitting analyses of the Fourier-filtered EXAFS of Ga-O shell were carried out by a least-squares method. The EXAFS oscillation for Ga-O peaks was fitted with two sine waves for Ga-MFI catalysts. To determine the structural parameters of the oxygen shell around gallium, a calculated x(k) function was fitted to the oxygen contribution to the experimental EXAFS signal filtered in the R-space (1 - 2 Å). For all samples, the fit was performed in 4.5 - 13.0 $Å^{-1}$ regions.

To verify the reliability of the amplitude and the phase shift extracted from $Ga(acac)_3$, the curve-fitting analysis of EXAFS of a reference sample, β-Ga_2O_3, was carried out. The results and crystallographic data [32] are summarized in Table 2. The curve-fitting results indicate coordination shells with 1.7 oxygen atoms at 1.86 Å and another 2.8 oxygen atoms at 2.00 Å. These results are in good agreement with the crystallographic data.

This method was applied to the samples, and the results are given Table 3. Fig. 6 shows the inversely transformed spectra for Ga-MFI catalysts and the best fits performed with two sets of Ga-O parameters shown in Table 3. The number of oxygen atoms neighboring Ga atoms in the first shell, in which the distance between Ga atoms and oxygen atoms were 1.81-1.84, changed with calcination temperature. As for the oxygen atoms neighboring Ga

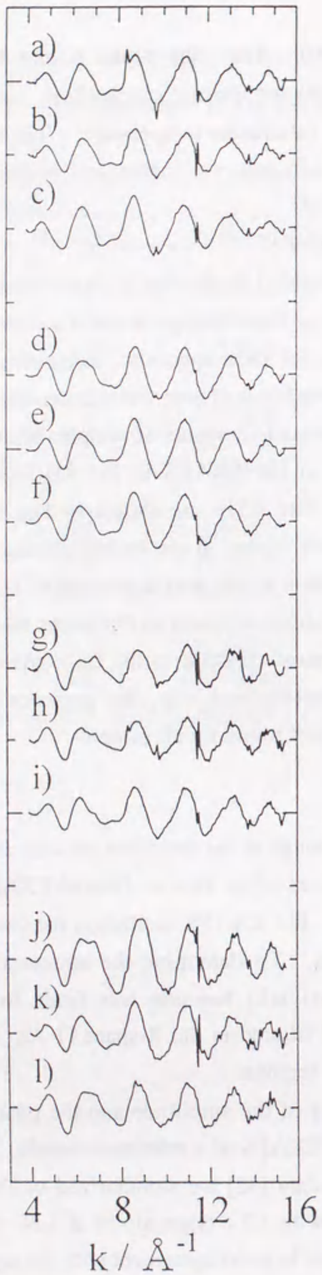

Fig. 4 k^3-weighted EXAFS spectra of Ga-MFI catalysts: Si/Ga= (a)-(c) 12.5, (d)-(f) 20, (g)-(i) 40 and (j)-(l) 80; calcined at (a, d, g, j) 823, (b, e, h, k) 923 and (c, f, i, l) 993 K

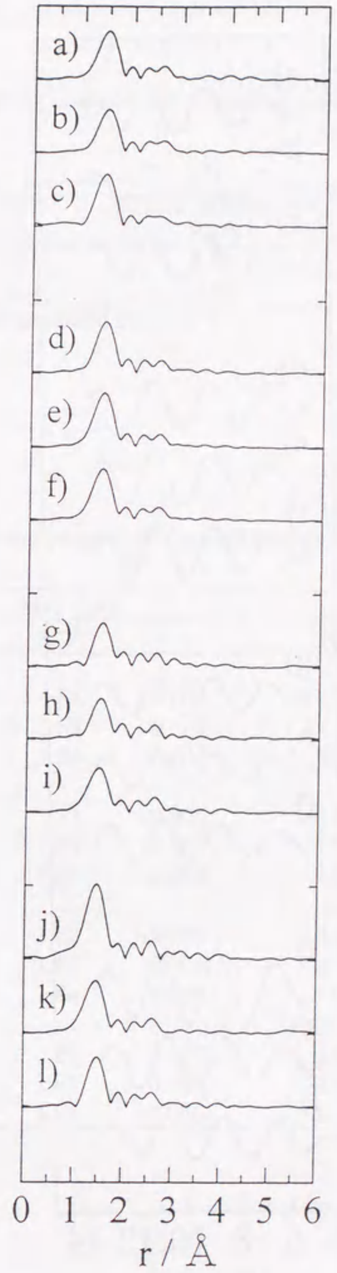

Fig. 5 Fourier transforms of Ga K-edge EXAFS spectra of Ga-MFI catalysts: Si/Ga= (a)-(c) 12.5, (d)-(f) 20, (g)-(i) 40 and (j)-(l) 80; calcined at (a, d, g, j) 823, (b, e, h, k) 923 and (c, f, i, l) 993 K

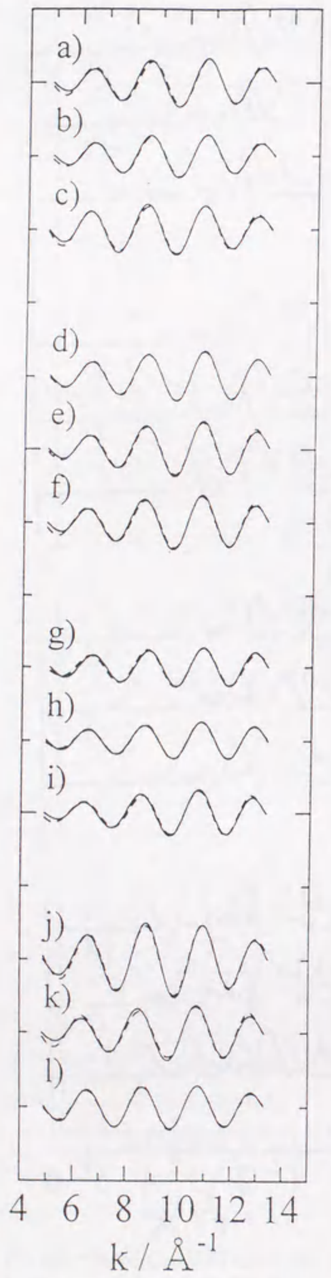

Fig. 6 Fourier filtered EXAFS functions (solid line) and resulting curve-fitting (dotted line) used to calculate structural parameters

Table 2 Results of curve-fitting analyses and crystallographic data of β-Ga_2O_3

	curve-fitting results		crystallographic data
shell	N	R / Å	R / Å
Ga-O (tet)	1.7	1.86	1.83
Ga-O (oct)	2.8	2.00	2.00

N: coordination number, R: interatomic distance

Table 3 Results of curve-fitting analyses of Ga-MFI catalysts

catalyst	Ga-O (tet)			Ga-O (oct)		
calcin. temp.	N	R / Å	$\Delta\sigma^2$	N	R / Å	$\Delta\sigma^2$
Si/Ga=12.5						
823 K	1.5	1.84	-0.005	0.9	2.00	0.007
923	1.7	1.83	-0.004	1.8	2.00	0.002
993	2.8	1.84	-0.002	3.0	2.00	0.009
Si/Ga=20						
823	1.4	1.83	-0.005	0.8	2.00	0.011
923	1.7	1.84	-0.005	1.8	2.00	0.010
993	1.9	1.83	-0.004	2.0	2.00	0.009
Si/Ga=40						
823	1.1	1.82	-0.005	0.4	2.00	0.015
923	1.1	1.83	-0.005	0.9	2.00	0.010
993	1.2	1.84	-0.006	1.0	2.00	0.006
Si/Ga=80						
823	2.6	1.81	-0.004	0.9	2.00	0.004
923	1.8	1.83	-0.004	0.7	2.00	0.015
993	1.8	1.84	-0.005	1.2	2.00	0.001

at 2.00 Å, the coordination number of Ga atom increased with an increase in the calcination temperature. By using the number of oxygen atoms, the fractions of Ga(tet) and Ga(oct) species in the samples were estimated. As shown in Table 3, the fraction of Ga(tet) species was higher when the Ga content and the calcination temperature were relatively high.

Acidic properties of Ga-MFI (microcalorimetry)

Figure 7 shows the differential heats of ammonia adsorption at 473 K as a function of the adsorption coverages. Figure 7a shows that Ga-MFI (Si/Ga=12.5) calcined at 823 K has a few sites which evolve high heats around 200 kJ mol^{-1} at low coverages. The curve then follows a nearly horizontal plateau extending over 0.3 mmol g^{-1} and situated at 130 kJ mol^{-1}, after which the curve drops sharply until new plateau is reached with heats of about 80 kJ mol^{-1}. The initial differential heat was increased with increasing calcination temperature for all Ga content. For all samples, on the other hand, a plateau was found at 130 kJ mol^{-1}, indicating that the presence of a large number of sites having similar acid strength. With an increase in the calcination temperature, the distribution around 130 kJ mol^{-1} of the heat of adsorption became markedly lower, while that above 130 kJ mol^{-1} increased slightly. This suggests that the acidity is also influenced by the calcination as well as the Ga content.

In the literature, it has been claimed by several authors that the sites with differential heats of ammonia adsorption of greater than 150 kJ mol^{-1}, *i.e.*, a plateau, in HZSM-5 zeolites are strong Lewis sites [15-19]. The sites evolving differential heats over 130 kJ mol^{-1} in this study are considered, therefore, to be strong Lewis acid sites. In the 80 kJ mol^{-1} region the heats that are evolved from HZSM-5 zeolites tend to be representative of physisorption and indicated the interaction of silanol groups and cations with ammonia [15-19]. It might be argued that the differential heats of adsorption ammonia of 130-80 kJ mol^{-1} can be ascribed to the adsorption on zeolitic Brønsted sites.

X-ray diffraction

X-ray diffraction patterns of all samples were similar to that of ZSM-5 zeolite. The unit cell parameters of Ga-MFI (Si/Ga=80) calcined at 823 K are listed in Table 4. It can be seen from the values reported in Table 4 that unit cell parameters of the sample are larger than those of silicalite [32]. This is consistent with the substitution of Ga in the SiO_2 framework and must be attributed to the larger tetrahedral Ga-O distance of 1.83 Å compared to the tetrahedral Si-O distance of 1.61 Å.

It was reported that the expected variation of unit cell volume, when replacing $(BO_2)^-$ tetrahedra in the SiO_2 framework, can be calculated, starting from the reasonable assumption that each tetrahedron contributes to the volume occupancy in the crystal proportionally to d_T^3, d_T being the related tetrahedral bond distance. For a mixed framework, characterized by a value x of the fraction nT/(nT+nSi), the unit cell volume V(x) is:

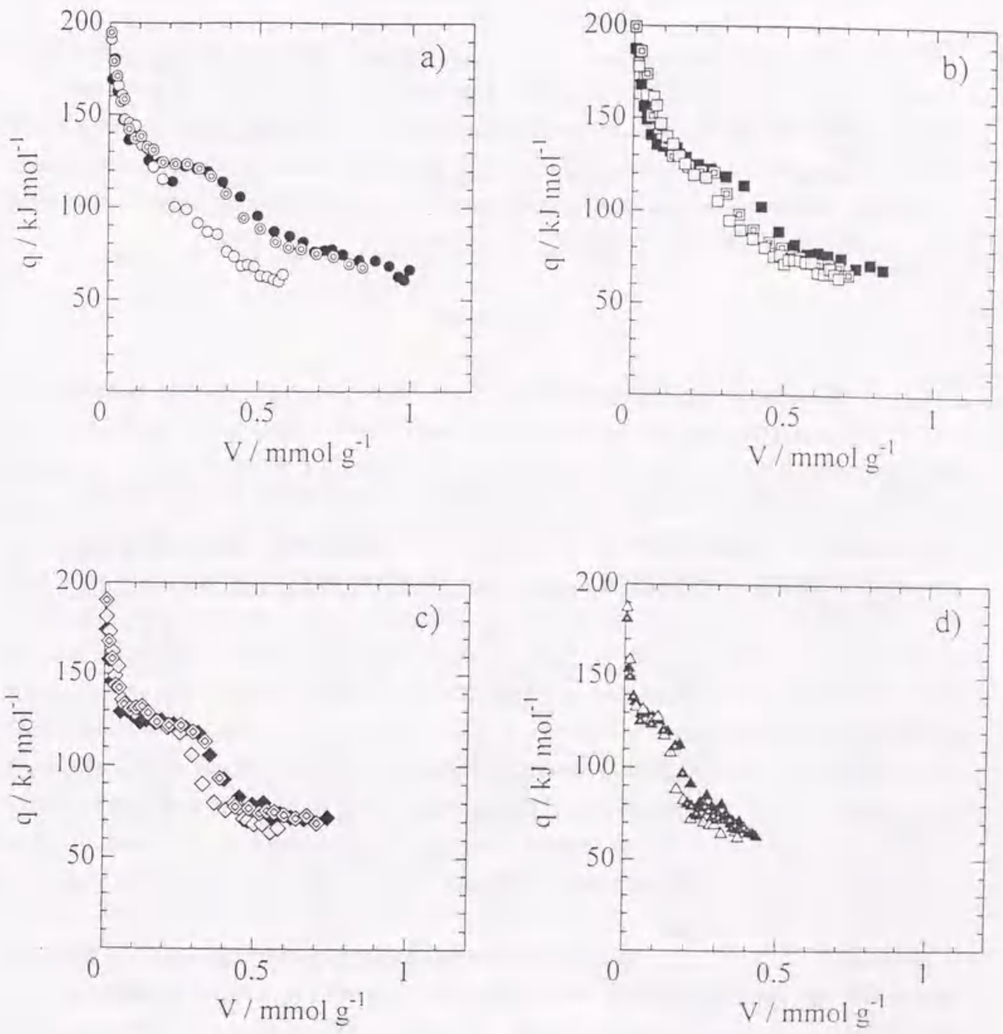

Fig. 7 Differential heats of ammonia adsorption on Ga-MFI catalysts at 473 K: Si/Ga= (a) 12.5, (b) 20, (c) 40 and (d) 80; calcined at (○△□◇) 823, (◎△□◇) 923 and (●▲■◆) 993 K

Table 4 Unit cell parameters of Ga-MFI catalyst (Si/Ga=80, calcined at 823 K)

a /Å	b /Å	c /Å	β / °	unit cell volume / Å^3
Silicalite[a)]				
19.874	20.117	13.371	90.62	5345.5
Ga-MFI				
19.919	20.123	13.387	90.46	5366.2

a) Ref. [31]

Table 5 Amount of Ga(FW) and Ga(EFW) species determined by microcalorimetry

catalyst calcin. temp.	Ga content[a)] mmol g^{-1}	Ga(FW) mmol g^{-1}	Ga(EFW) mmol g^{-1}	surface Ga(EFW) mmol g^{-1}
Si/Ga=12.5				
823 K	1.22	0.54	0.68	0.11
923	1.20	0.44	0.76	0.14
993	1.22	0.25	0.96	0.12
Si/Ga=20				
823	0.76	0.44	0.31	0.12
923	0.77	0.32	0.41	0.15
993	0.79	0.26	0.52	0.16
Si/Ga=40				
823	0.43	0.41	0.02	0.07
923	0.42	0.32	0.10	0.12
993	0.44	0.29	0.15	0.10
Si/Ga=80				
823	0.24	0.22	0.02	0.06
923	0.24	0.19	0.05	0.04
993	0.24	0.15	0.09	0.05

a) determined by ICP

$$V(x) = V_{Si} - V_{Si}\,[1-(d_T^3/d_{Si}^3)]x$$

and varies linearly as a function of x [32].

Based on this criterion, the composition in framework of Ga-MFI sample was evaluated. The amount of Ga in zeolite framework estimated on the basis of the result derived from chemical analysis and that from described above was 0.19 mmol g^{-1}. This result is in good agreement with the amount of zeolitic acid sites obtained from microcalorimetry.

Discussion

Coordination state of Ga species (tetrahedrally and octahedrally coordinated Ga)

According to the widely shared belief that Ga is isomorphously substituted for Si, it is presumed that Ga is sited in a tetrahedrally symmetric position in as-synthesized gallosilicate. As mentioned above, it was found that the calcining at higher temperatures causes the extraction of Ga species from zeolitic framework sites and the formation of extraframework Ga_2O_3 particles. From the deconvolution analyses of XANES spectra, the fraction of each Ga species changed with Ga content and calcination temperature as shown in Table 1. The fraction of Ga(oct) species increased with an increase in Ga content and calcination temperature. The changes in the fraction of each Ga species obtained by EXAFS curve-fitting analyses also showed same results. Fig. 8 shows coincidence between the fractions of Ga(tet) species in Ga-MFI catalysts obtained from deconvolution analyses of XANES spectra and those obtained from EXAFS curve-fitting analyses. The data fit well the straight line with a slope of unity. The substantial agreement between the results of XANES and EXAFS analyses could be a proof of the validity of the definition of coordination state of Ga species.

Location of Ga species (framework and extraframework Ga)

In order to estimate the fractions of Ga(FW) and Ga(EFW) species, the acidity was characterized by microcalorimetry. From the amount of zeolitic acid sites exhibited the differential heats of adsorption at the range of 130-80 kJ mol^{-1}, the number of Ga(FW) species was determined assuming that each framework gallium atom adsorbs one ammonia molecule, thus indicating one Brønsted site. Therefore, the difference from the total number of Ga gives the number of Ga(EFW). On the other hand, the amount of surface Ga cations on extraframework Ga_2O_3 species was determined from the number of the strong Lewis acid sites associated with differential heats of ammonia adsorption above 130 kJ mol^{-1} assuming that the Ga(EFW) species form the Ga_2O_3 particles providing the strong Lewis acid sites. Table 5 shows the estimated number of Ga(FW) species and exposed surface Ga(EFW) atoms in Ga-MFI catalysts. The number of Ga(FW) species varied greatly with the Ga content and the calcination temperature. The number of surface Ga(EFW) atoms, however, remained almost

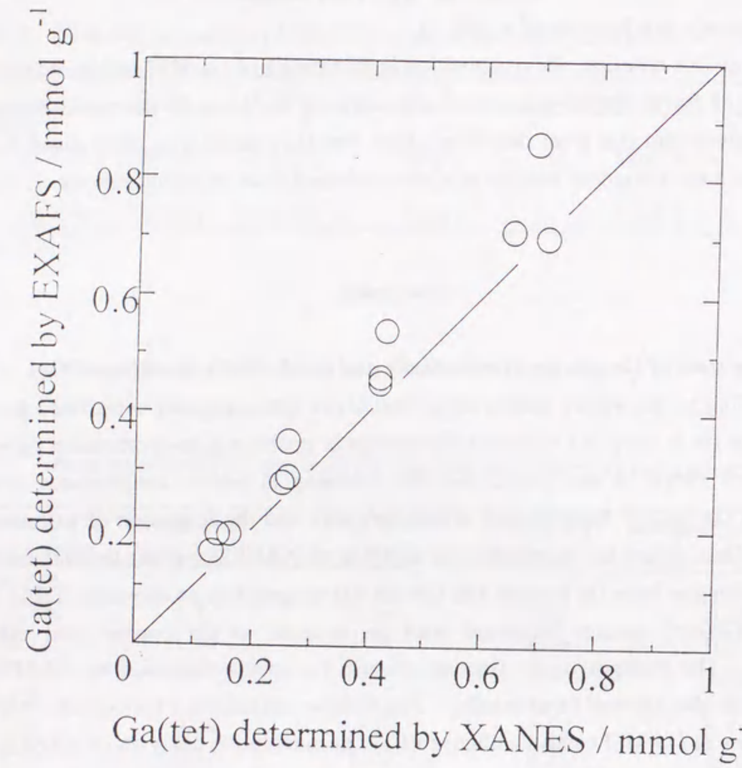

Fig. 8 Coincidence between the number of Ga(tet) species determined by XANES and EXAFS analyses

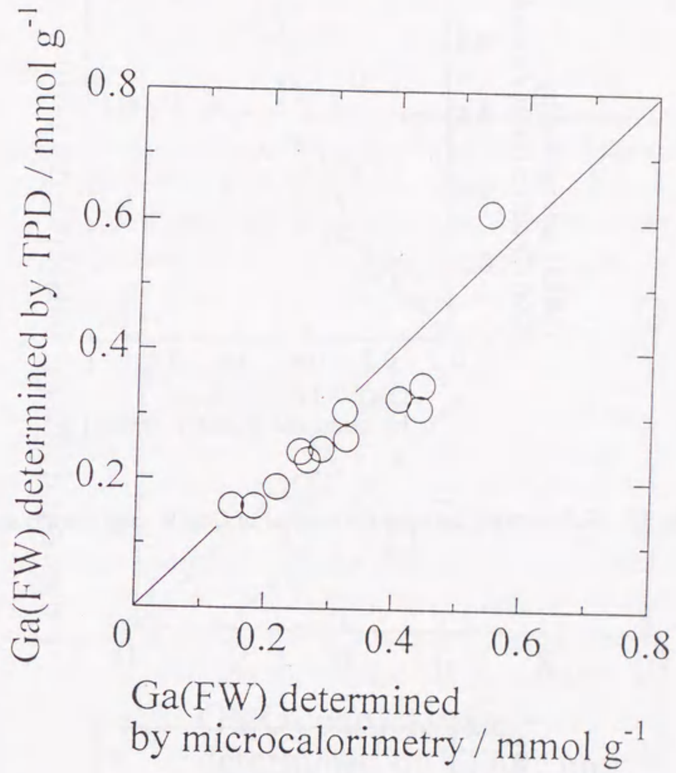

Fig. 9 Coincidence between the number of Ga(FW) species determined by microcalorimetry and TPD

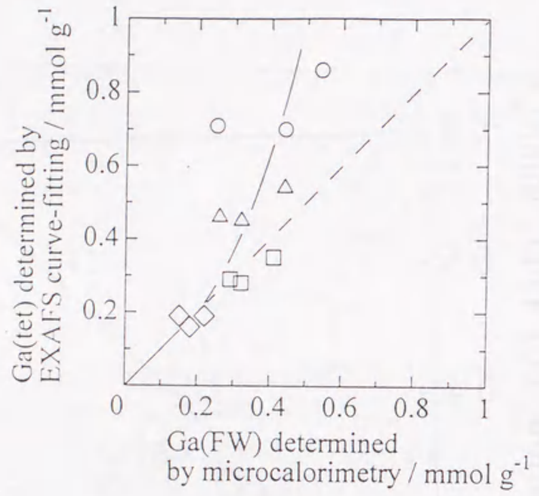

Fig. 10 Relationship between the number of Ga(FW) and Ga(tet) species

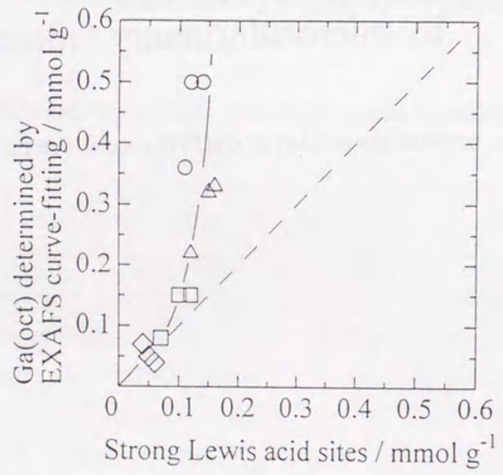

Fig. 11 Relationship between the number of strong Lewis acid sites and Ga(oct) species

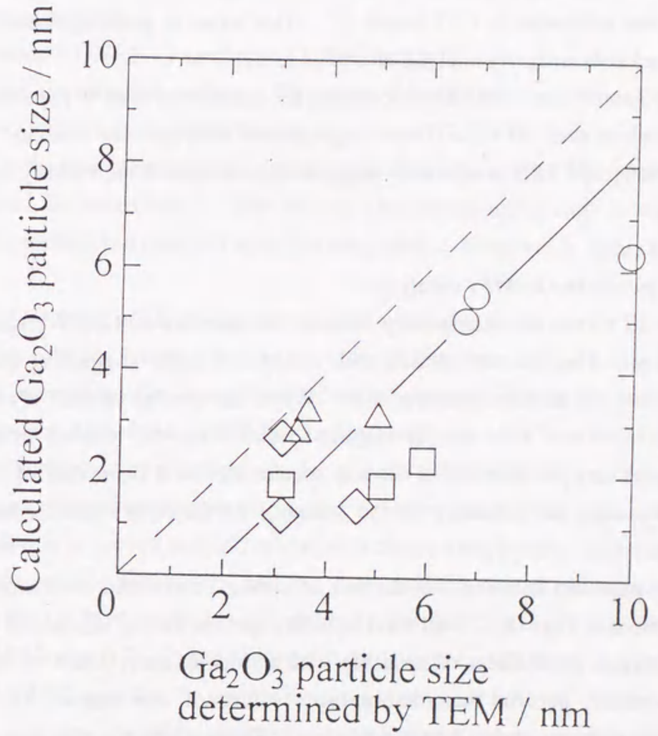

Fig. 12 Coincidence between Ga_2O_3 particle size calculated from EXAFS curve-fitting results and determined by TEM

constant with the Ga content and the calcination temperature.

The smallest number of Ga(EFW) species was attained on Ga-MFI (Si/Ga=80) calcined 823 K. The amount of Ga(FW) species in this sample, Ga-MFI (Si/Ga=80) calcined at 823 K, was estimated from the variation of unit cell volume as mentioned above. The framework Ga content was estimated as 0.19 mmol g^{-1}. This value is good agreement with the value obtained by microcalorimetry analysis as shown in Table 5.

Figure 9 shows the coincidence between the number of Ga(FW) species determined by microcalorimetry and TPD. Good agreement between the values determined by microcalorimetry and TPD is observed, suggesting that there is the validity in these estimated values.

State of Ga species in Ga-MFI catalysts

Figure 10 shows the relationship between the number of Ga(FW) species and that of Ga(tet) species. The line was drawn with a slope of unity, suggesting that each Ga(FW) species provides one zeolitic Brønsted site. When the number of Ga(FW) species was low, this value coincidence with that of Ga(tet) species. As the number of Ga(FW) species increased, however, the number of Ga(tet) species deviated from that of Ga(FW) species. This deviation may be indicative of the presence of Ga(EFW) species having tetrahedral coordination.

The relationship between the number of strong Lewis acid sites and that of Ga(oct) species is shown in Fig. 11. If all the Ga(EFW) species having octahedral coordination are highly dispersed, a good linear relationship with a slope of unity could be observed. These catalysts, however, showed remarkably lager values of the number of Ga(oct) species compared with those of strong Lewis acid sites. The deviation between two values became progressively greater as the number of Ga species increased. It is suggested that Ga(EFW) species generated by calcination are not highly dispersed but present as Ga_2O_3 particles.

On the basis of these results, the Ga_2O_3 particle size was calculated assuming that the number of strong Lewis acid sites obtained by microcalorimetry analysis correspond to that of exposed Ga atoms of extraframework Ga_2O_3 particles, as follows:

$$\text{Ga}_2\text{O}_3 \text{ particle size } (d) = 6\frac{V}{S} = \frac{6\, n_b\, \Gamma}{\rho\, n_s}$$

where n_b is the number of Ga(EFW) atoms, Γ is the density of surface Ga atoms on β-Ga_2O_3 obtained by benzaldehyde-ammonia titration method; 4.0×10^{-3} mmol m^{-2}, ρ is the density of β-Ga_2O_3; 3.1×10^{7} mmol m^{-3} and n_s is the number of surface Ga(EFW) atoms.

Figure 12 shows the validity in the Ga_2O_3 particle size estimated by X-ray absorption and microcalorimetry analyses. Fairly good agreement is observed, between the values

determined by X-ray absorption and microcalorimetry analyses and those determined by TPD and electron microscopy analyses described in preceding chapter. It is suggested that the fractions of Ga(FW) and Ga(EFW) species in Ga-MFI catalysts could be estimated by microcalorimetry analysis.

In conclusion, Ga(EFW) species in Ga-MFI catalysts were generated by calcination and were located on the external surface. The ratio of Ga(EFW)/Ga(FW) calculated using the data of microcalorimetry suggests that the fraction of Ga(EFW) species increases with Ga content and calcination temperature. It was proved that the Ga(EFW) species comprised of both Ga(tet) and Ga(oct) species. The ratio of Ga(tet)/Ga(oct) is high in Ga-MFI catalysts with higher Ga content and calcined at higher temperature, as shown in Table 6.

Dependence of the state of Ga on dehydrogenation activity

On the basis of the results revealed by X-ray absorption and microcalorimetry analyses, in this section, we discuss the dependence of the catalytic activity on the local structure such as coordination and state of Ga species for Ga-MFI catalysts.

Table 6 shows the structural parameters and the activity of propane dehydrogenation at 773 K. TF was defined as the rate of propane dehydrogenation per surface Ga(EFW). As mentioned above, it is proved that the calcining at higher temperature causes the extraction of Ga atoms from zeolitic framework and the formation of Ga_2O_3 particles on the external surface. For the Ga-MFI catalysts with higher Ga content (Si/Ga=12.5 and 20), the ratio of Ga(EFW)/Ga(FW) was 0.7-3.8, suggesting that the number of Ga(FW) species is higher than the that of Ga(EFW) species. And this ratio was increased with an increase in calcination temperature. On these catalysts, the catalytic activity was reduced with increasing the ratio. On the other hand, the catalytic activity was enhanced with increasing the fraction of Ga(EFW), on the catalysts having lower Ga(EFW)/Ga(FW) ratio, 0.1-0.6. This result indicates that the absolute amount of Ga(EFW) and the Ga(EFW)/Ga(FW) ratio may play a significant role in the enhancement of dehydrogenation activity.

As shown in Table 6, the change in the number of Ga(FW) species, *i.e.*, zeolitic acid sites, with calcination temperature was practically the same with the two series of Ga-MFI catalysts (Si/Ga=20 and 40). By comparing the dehydrogenation activity under the same number of zeolitic acid sites, TF was increased with the estimated Ga_2O_3 particle size. This result clearly shows that the dehydrogenation of propane is a demanding reaction when carried out over Ga-MFI catalysts. Through the investigation of coordination state of Ga species in Ga-MFI catalysts, higher activity of large Ga_2O_3 particles can be attributed to the fact that the large Ga_2O_3 particles have Ga(tet)/Ga(oct) ratio being close to unity. This result is good agreement with the result reported in the study on Ga_2O_3 model catalysts, in which Ga_2O_3 catalysts having Ga(tet)/Ga(oct) ratio being close to unity exhibited higher reaction rate per surface [Ga-O] site. It was concluded that the not only the ratio of Ga(EFW)/Ga(FW) but

Table 6 Structural parameters and propane dehydrogenation activity of Ga-MFI catalysts

catalyst calcin. temp.	zeolitic acid[a] mmol g^{-1}	strong Lewis acid[a] mmol g^{-1}	Ga(EFW)/Ga(FW)[a]	Ga(tet)/Ga(oct)[b]	Ga_2O_3 size[c] nm	conversion[d] %	TF[d] h^{-1}
Si/Ga=12.5							
823 K	0.54	0.11	1.2	2.4	5.0	30.2	249
923	0.44	0.14	1.7	1.4	5.5	19.2	123
993	0.25	0.12	3.8	1.4	6.3	9.5	70.1
Si/Ga=20							
823	0.44	0.12	0.70	2.5	2.8	22.1	170
923	0.32	0.15	1.4	1.4	3.2	15.3	93.1
993	0.26	0.52	2.0	1.4	3.1	14.0	79.3
Si/Ga=40							
823	0.41	0.07	0.05	4.4	1.8	8.5	114
923	0.32	0.12	0.32	1.9	1.8	6.9	50.6
993	0.29	0.10	0.53	1.9	2.3	10.9	99.5
Si/Ga=80							
823	0.22	0.06	0.09	4.3	1.2	1.8	27.3
923	0.18	0.04	0.29	4.1	1.7	5.0	110
993	0.15	0.05	0.60	2.3	2.2	5.5	97.5

a) determined by microcalorimetry, b) determined by EXAFS curve-fitting, c) calculated as shown in text,
d) reaction of propane at 773 K

also the ratio of Ga(tet)/Ga(oct) in extraframework Ga_2O_3 species are key factors controlling dehydrogenation activity over Ga-MFI catalysts.

Conclusion

In order to clarify the factors generating and controlling the dehydrogenation activity, the structural analyses such as X-ray absorption spectroscopy and microcalorimetry were carried out for Ga-MFI catalysts calcined at various temperatures.

From the analyses of X-ray absorption spectroscopy for Ga-MFI catalysts, it was found that the fraction of Ga(tet) was high when the Ga content and the calcination temperature were low. The ratio of Ga(EFW)/Ga(FW) calculated using the data of microcalorimetry increased with an increasing calcination temperature. This suggests that the calcining at higher temperatures causes the generation of Ga(EFW) species on the external surface of Ga-MFI catalysts. It was found that these Ga(EFW) species comprised of both Ga(tet) and Ga(oct) species, and that the ratio of Ga(tet)/Ga(oct) in Ga(EFW) is high when Ga-MFI catalysts are calcined at higher temperatures. Estimated Ga_2O_3 particle sizes increased with increases in Ga content and calcination temperature. This result was good agreement with that obtained by TEM analysis.

By comparing the dehydrogenation activity under the same number of zeolitic acid sites, the reaction rate per surface Ga(EFW) species was increased with the estimated Ga_2O_3 particle size. This suggests that the dehydrogenation of propane is a demanding reaction when carried out over Ga-MFI catalysts. Higher activity of large Ga_2O_3 particles can be attributed to the Ga(tet)/Ga(oct) ratio being close to unity.

References

[1] D. K. Simmons, R. Szostak, P. K. Agrawal and T. L. Thomas, *J. Catal.*, **106** (1987) 287.

[2] T. Inui, Y. Makino, F. Okazumi, S. Nagano and A. Miyamoto, *Ind. Eng. Chem. Res.*, **26** (1987) 647.

[3] M. Guisnet, N. S. Gnep and F. Alario, *Appl. Catal.*, **89** (1989) 1.

[4] I. Kanai and N. Kawata, *Appl. Catal.*, **55** (1989) 115.

[5] C. R. Bayense, A. J. H. P. van der Pol and J. H. C. van Hoof, *Appl. Catal.*, **72** (1991) 81.

[6] C. R. Bayense and J. H. C. van Hoof, *Appl. Catal. A*, **79** (1991) 127.

[7] Y. Ono, *Catal. Rev. Sci. Eng.*, **34** (1992) 189.

[8] H. D. Lanh, V. A. Tuan, H. Kosslick, B. Parlitz, R. Fricke and J. Völter, *Appl. Catal. A*, **103** (1993) 205.

[9] G. Giannetto, A. Montes, N. S. Gnep, A. Florentino, P. Cartrand and M. Guisnet, *J. Catal.*, **145** (1995) 86.

[10] V. R. Choudhary, C. Sivadinarayana, A. K. Kinage, P. Devadas and M. Guisnet, *Appl. Catal. A*, **136** (1996) 125.

[11] J. A. Biscardi and E. Iglesia, *Catal. Today*, **31** (1996) 207.

[12] G. Giannetto, G. León, J. Papa, R. Monque, R. Galiasso and Z. Gabelica, *Catal. Today*, **31** (1996) 317.

[13] J. Bandiera and Y. Ben Taarit, *Appl. Catal.*, **76** (1991) 199.

[14] A. Yu. Khodakov, L. M. Kustov, T. N. Bondarenko, A. Dergachev, V. B. Kazansky, Kh. M. Minachev, G. Borbely and H. K. Beyer, *Zeolites*, **10** (1990) 603.

[15] A. Auroux, J. C. Védrine, P. C. Gravelle, *Stud. Surf. Sci. Catal.*, **10** (1982) 305.

[16] A. L. Klyachko, G. I. Kapustin, T. R. Brueva and A. M. Rubinstein, *Zeolites*, **7** (1987) 119.

[17] D. J. Parrillo and R. J. Gorte, *J. Phys. Chem.*, **97** (1993) 8786.

[18] L. C. Jozefowicz, H. G. Karge and E. N. Coker, *J. Phys. Chem.*, **98** (1994) 8053.

[19] A. Aurox and A. Gervasini, *J. Phys. Chem.*, **94** (1990) 6371.

[20] J. Wong, F. W. Lytle, R. P. Messmer and D. H. Maylotte, *Phys. Rev.B*, **30** (1984) 5596.

[21] T. Tanaka, H. Yamashita, R. Tsuchitani, T. Funabiki and S. Yoshida, *J. Chem. Soc. Faraday Trans. 1*, **84** (1989) 2987.

[22] S. Yoshida, T. Tanaka, T. Hanada, T. Hiraiwa, H. Kanai and T. Funabiki, *Catal. Lett.*, **12** (1992) 277.

[23] T. Tanaka, T. Hanada, S. Yoshida, T. Baba and Y. Ono, *Jpn. J. Appl. Phys.*, **32-2** (1993) 481.

[24] H. Yoshida, T. Tanaka, T. Yoshida, T. Funabiki and S. Yoshida, *Physica B*, **208**&**209**, (1995) 681.

[25] H. Yoshida, T. Tanaka, T. Yoshida, T. Funabiki and S. Yoshida, *Catal. Today*, **28** (1996) 79.

[26] K. Tsutsumi, S. Hagiwara, Y. Mitani and H. Takahashi, *Bull. Chem. Soc. Jpn.*, **55** (1982) 2572.

[27] M. Niwa, M. Sawa and Y. Murakami, *Proc. 9th Intern. Cong. Catal.*, Chem. Inst. Canada, Ottawa, (1988) p. 380.

[28] M. Sawa, M. Niwa and Y. Murakami, *Appl. Catal.*, **53** (1989) 169.

[29] A. Satsuma, T. Ishikura, T. Shimizu, M. Niwa, T. Hattori and Y. Murakami, *Kagaku Kougaku Ronbubshu*, **21** (1995) 1120.

[30] F. Martin, Ph. Ildefonse, J. L. Hazemann, P. E. Mathe, Y. Noack, O. Grauby, D. Beziat and Ph. de Parseval, *J. Phys. IV France*, **7** (1997) C2-821.

[31] F. Tourtin, P. Armand, A. Ibanez, G. Tourillon and E. Philippot, *J. Phys. IV France*, **7** (1997) C2-975.

[32] S. Geller, *J. Chem. Phys.*, **33** (1960) 676.

[33] M. Taramasso, G. Perego and B. Notari, *Proc. 5th Int. Conf. on Zeolites*, Hyden, (1980) p. 40.

Chapter 5

Oxide-Zeolite Composite Catalysts for the Reduction of Carbon Dioxide with Simultaneous Aromatization

Synopsis

Oxide-zeolite composite catalysts were designed for the reduction of CO_2 with simultaneous aromatization of C_3H_8. Oxides of Fe and V were selected as the oxide components which are active for the reduction of CO_2 and inactive for the decomposition of C_3H_8, and Ga-loaded HZSM-5 was selected as the zeolite component selectively aromatizing C_3H_8. Composite catalysts containing these components were revealed to exhibit high activity for the reduction of CO_2 and high selectivity for the aromatization of C_3H_8.

Introduction

We proposed a novel method for the reduction of CO_2 by lower alkanes, concurrently producing more value-added products, such as alkenes [1] and aromatics [2-4], from alkanes as reducing agents. These reaction systems may enables us to use CO_2 as chemical feed stock in energetically and economically favorable situation. This is because the systems do not require the production of reducing agents which can usually be produced only through energy consuming processes, and because the reducing agents can be converted into more value-added products. Further, in the CO_2 reduction with simultaneous aromatization of C_3H_8 on Zn-loaded HZSM-5, CO_2 was found to suppress unfavorable side reactions such as the decomposition of olefinic species and the deposition of coke [3,4]. The problem in this reaction system, which is composed of the aromatization of C_3H_8 and the reduction of CO_2 with H_2 formed through alkane aromatization, is that the catalyst should be active for both of the reverse water gas shift (RWGS) reaction and the aromatization of alkanes. Zn-HZSM-5 exhibited moderately high activity for CO_2 reduction, but it had only moderate selectivity in aromatic formation. Ga-HZSM-5, on the other hand, exhibited high selectivity for aromatic formation, but only poor activity for CO_2 reduction.

This chapter aims at examining the possibility to improve the activity for CO_2 reduction by using a composite catalyst containing an oxide component for CO_2 reduction and Ga-HZSM-5 which is known to aromatize C_3H_8 selectively [5,6]

Experimental

Preparation of Catalyst

NH_4-ZSM-5 was prepared by ion-exchange of Na-ZSM-5 (SiO_2/Al_2O_3 molar ratio = 23.3, supplied from TOSOH Co.) with NH_4NO_3 followed by drying and calcination in flowing air at 823 K. Ga-loaded HZSM-5 catalyst was prepared by refluxing an aqueous solution of

$Ga(NO_3)_3$ containing NH_4-ZSM-5 powders for 24 h, followed by evaporation-to-dryness. Thus obtained materials were calcined in flowing air at 873 K. Ga content was 1 wt%. Commercially supplied oxides were used after pressed, crushed, sieved to 28-48 mesh, and calcined at 873 K. The catalyst was pretreated in flowing H_2/N_2 mixture at 823 K for 2 h immediately before the catalytic test.

Catalytic Test

The catalytic tests of the reverse water gas shift (RWGS) reaction and the conversion of C_3H_8 in CO_2 atmosphere on oxide catalysts, and the reduction of CO_2 with aromatization of C_3H_8 on composite catalysts were conducted by using a conventional flow reactor. The catalyst amount, the total flow rate, and the partial pressures in the catalytic test were 0.3 g, 60 cm^3 min^{-1}, and CO_2/H_2 = 18/36 kPa in the RWGS reaction; and 0.5g, 60 cm^3 min^{-1}, and C_3H_8/CO_2 = 18/18 kPa in the conversion of C_3H_8; and 0.3g of Ga-HZSM-5 and 0.3g of oxide, 60 cm^3 min^{-1}, and C_3H_8/CO_2 = 18/43 kPa in the reduction of CO_2 with C_3H_8. N_2 was used as a balance gas in all cases.

Characterization

XRD patterns of catalysts were measured with Cu-K_α radiation, and BET surface area was measured through the adsorption of N_2 at liquid nitrogen temperature.

Results and Discussion

Screening of Oxide Component

The RWGS reaction and the conversion of C_3H_8 under CO_2 atmosphere were conducted by using a series of oxide catalysts for the screening of an oxide component which should be active for the reduction of CO_2 and inactive for the side reactions of C_3H_8 such as the decomposition and the coke-formation.

In the RWGS reaction, most of the catalysts examined produced CO as a sole reaction product. On Fe, Co, and Ni catalysts, however, CH_4 was also produced at significant yield at moderately low temperature. The increase of the reaction temperature resulted in the decrease of CH_4 yield and the increase of CO yield. These catalysts seemed to be excessively reduced during the pretreatment to form metallic species which catalyze the methanation of CO_2. With increasing reaction temperature, the metallic species seemed to be oxidized by CO_2 resulting in the suppression of methanation. Among these catalysts, Fe catalyst exhibited the lowest activity for CH_4 formation and it did not produce CH_4 above 773K. As shown in Table 1 which summarizes the results at 823 K, V, Cr, Fe, Co, Ni, and Zn catalysts exhibited relatively high activity for CO formation, though Co and Ni catalysts

produced also a significant amount of CH_4 even at 823K.

The catalytic test of the decomposition of C_3H_8 was conducted in CO_2 atmosphere so as to make the oxidation state of catalysts close to that in the target reaction, i.e., the reduction of CO_2 with simultaneous aromatization of C_3H_8. CH_4, C_2H_6, C_2H_4, and C_3H_6 were observed as the products of the decomposition and dehydrogenation of C_3H_8. Among these products, CH_4 and C_2H_6 are unfavorable side products, because CH_4 and C_2H_6 are not readily converted into aromatics on Ga-HZSM-5.

As shown in Table 1, Cr and Ga catalysts exhibited high activity and V, Fe, and Zn catalysts exhibited moderate activity for the dehydrogenation of C_3H_8 forming C_3H_6. A significant amount of CH_4, on the other hand, was formed on Cr, Co, Ni, Zn and Ge catalysts. Especially, Ni catalyst produced extremely large amount of CH_4. A large amount of coke was also deposited on Ni catalyst at 823K, the catalyst bed was completely plugged by the deposited coke. The formation of CO was observed on V, Fe, Co, and Ni catalysts which exhibited also high activity for the RWGS reaction as mentioned above.

As a result of screening, oxides of Fe and V were selected as the oxide component, because these oxides belong to those having high activity for the RWGS reaction and to the group less active for the decomposition of C_3H_8. This can be confirmed through the ratio of CO formed in the RWGS reaction to CH_4 formed in the decomposition of C_3H_8 shown in the last column of Table 1. Oxide of Co which also had high ratio was not selected, because it produced significant amount of CH_4 in the RWGS reaction.

Performance of Oxide-Zeolite Composite Catalysts

The target reaction, *i.e.*, the reduction of CO_2 with simultaneous aromatization of C_3H_8, was conducted by using oxide-zeolite composite catalysts. Ga-HZSM-5 was used as a zeolite component, because Ga-HZSM-5 is known to produce selectively aromatics from lower alkanes [5,6]. Oxides of V and Fe were selected as the oxide component on the basis of the results of screening, as mentioned above. Zn oxide was also tested as the reference, because it was found in the previous study [3] that HZSM-5 containing excess Zn is effective for the reduction of CO_2 in the present reaction system, though the selectivity of aromatization is lower than that on Ga-HZSM-5.

Powder-mixed Composite Catalysts.

Figure 1 shows the results of catalytic tests of composite catalysts prepared through mixing fine powders of Ga-HZSM-5 and oxide in a mortar followed by pressing into pellets, crushing, and sieving. In the case of Ga-HZSM-5 alone, C_3H_8 converted into aromatics with high selectivity, but CO_2 was reduced only slightly. The additions of the oxides remarkably increased the yield of CO, indicating that the oxide components actually act as the active ingredient for the reduction of CO_2. The yield of aromatics, on the other hand, was

significantly decreased by the additions of the oxides. Especially, the addition of V_2O_5 greatly suppressed the formation of aromatics. The conversion of C_3H_8 was also decreased in the same extent as that of aromatics yield.

The decrease in aromatization activity by the additions of oxides may be possibly due to the destruction of zeolite crystal structure through solid-state reaction of zeolites with added oxides, because the deposition of V-compound is known to destroy the crystal structure of zeolites [7,8]. This possibility was confirmed by measuring XRD patterns of the composite catalyst containing V_2O_5 before and after the catalytic test. As shown in Fig. 2, XRD lines due to ZSM-5 were less intense after the catalytic test (b) than those before the test (a), when powders of ZSM-5 and V_2O_5 were mixed, indicating that the ZSM-5 framework in the composite catalyst was destroyed during the pretreatment and catalytic test and that the loss of zeolite component resulted in lower catalytic activity for the aromatization of C_3H_8.

Particle-mixed Composite Catalysts.

Particles of Ga-HZSM-5 and oxides were mildly mixed in the reactor and used as the catalyst so as to minimumize the solid-state reaction and the destruction of ZSM-5 framework. It was confirmed, as shown in Fig. 2, that XRD line intensities of the catalysts after the reaction was not significantly decreased.

As shown in Fig. 3, the addition of ZnO moderately increased the yield of CO, but it decreased to some extent the conversion of C_3H_8 and the yield of aromatics. This result was rather similar to that on HZSM-5 containing excess Zn [3]. Lowered activity for aromatic formation may suggest that the solid state ion exchange occurs even when Ga-HZSM-5 and ZnO were mixed in the form of particles. Another possibility is that the lowered activity is due to the activity of ZnO for the decomposition of C_3H_8 into CH_4 and C_2H_4 as shown in Table 1. The addition of Fe_2O_3 greatly improved the activity for the reduction of CO_2, but it slightly decreased the aromatization activity. The addition of V_2O_5, on the other hand, increased significantly the yield of CO, keeping aromatization activity and selectivity high.

These results strongly indicate the possibility of CO_2 reduction with simultaneous aromatization of C_3H_8 at high selectivity, if a proper oxide component is developed.

Table 1. Rate of product formation in the reverse water gas shift (RWGS) reaction and the decomposition of C_3H_8 on oxide components at 823K.

Catalyst	Surface Area m^2g^{-1}	RWGS Reaction		C_3H_8 Decomposition				CO/CH_4[a]
		CO[b]	CH_4[b]	CH_4[b]	C_2H_6[b]	C_2H_4[b]	C_3H_6[b]	
CaO	10.0	0.00	0.00	0.41	0.00	0.38	0.50	-
Sc_2O_3	18.5	0.01	0.00	0.21	0.02	0.20	0.27	0.05
TiO_2	42.3	0.01	0.00	0.20	0.00	0.12	3.26	0.05
V_2O_5	4.7	0.91	0.00	1.30	0.00	1.30	6.88	0.70
Cr_2O_3	2.4	1.54	0.00	7.60	0.00	3.82	64.4	0.20
MnO_2	5.1	0.27	0.00	0.58	0.00	0.50	0.51	0.47
Fe_2O_3	6.1	0.96	0.00	0.73	0.00	0.66	11.33	1.32
CoO	1.2	3.02	1.83	2.36	0.00	0.00	0.00	1.28
NiO	2.3	1.46	1.10	449[c]	2.25[c]	0.00[c]	2.39[c]	0.00[c]
ZnO	2.7	1.05	0.00	3.21	0.00	0.00	8.75	0.33
Ga_2O_3	4.6	0.34	0.00	1.02	0.14	1.04	33.1	0.33
GeO_2	3.3	0.26	0.00	3.37	0.00	0.39	0.89	0.08

[a] ratio of CO formation in RWGS reaction to CH_4 formation in C_3H_8 decomposition,
[b] rate of formation in mmol m^{-2} h^{-1}, [c] at 773K.

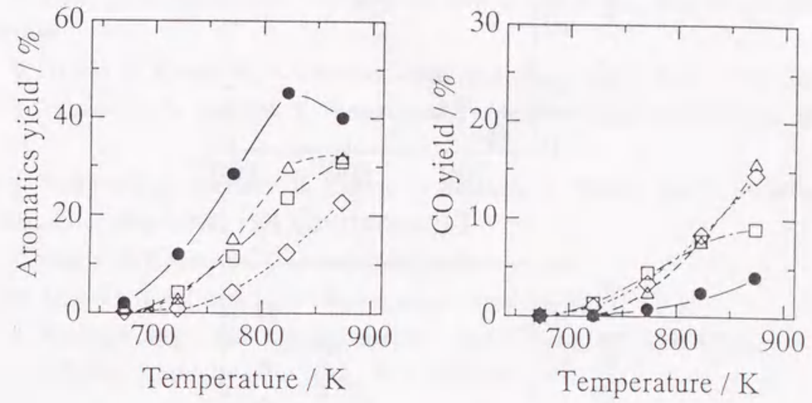

Fig. 1 Activities of powder-mixed composite catalysts for aromatic formation and CO_2 reduction; Ga-HZSM-5 (●), V_2O_5 + Ga-HZSM-5 (◇), Fe_2O_3 + Ga-HZSM-5 (□) and ZnO + Ga-HZSM-5 (△).

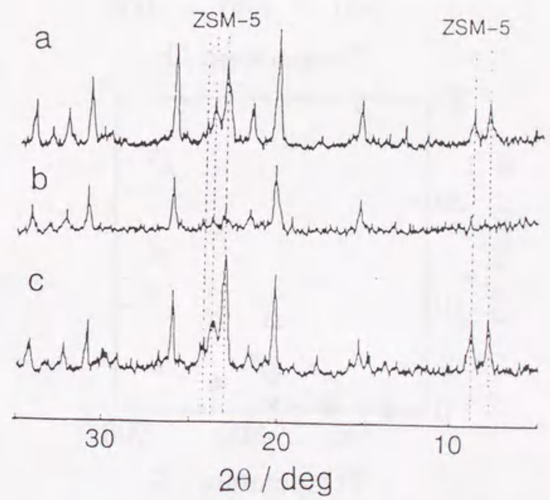

Fig. 2 XRD patterns of powder-mixed V_2O_5 + Ga-HZSM-5 catalyst before (a) and after (b) the catalytic test and particle-mixed catalyst after the test (c).

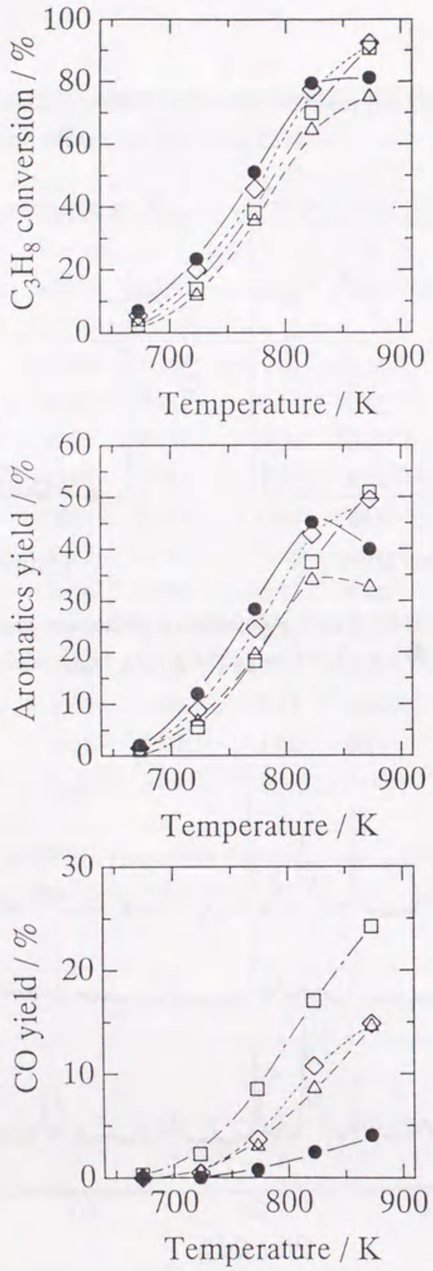

Fig. 3 Activities of particle-mixed composite catalysts for C_3H_8 conversion, aromatic formation, and CO_2 reduction; Ga-HZSM-5 (●), V_2O_5 + Ga-HZSM-5 (◇), Fe_2O_3 + Ga-HZSM-5 (□) and ZnO + Ga-HZSM-5 (△).

References

1. T. Hattori, M. Komatsuki, A. Satsuma, and Y. Murakami, *Nippon Kagaku Kaishi*, (1991) 648.
2. T. Hattori, S. Yamauchi, A. Satsuma, and Y. Murakami, *Chem. Lett.*, (1992) 629.
3. S. Yamauchi, A. Satsuma, T. Hattori, and Y. Murakami, *Sekiyu Gakkaishi*, **37**, (1994) 278.
4. S. Yamauchi, A. Satsuma, S. Komai, T. Asakawa, T. Hattori and Y. Murakami, *Stud. Surf. Sci. Catal.*, **84**, (1994) 1571.
5. Y. Ono, *Catal. Rev. -Sci. Eng.*, **34**, (1992) 179.
6. M. Guisnet, N.S. Gnep, and F. Alario, *Appl. Catal., A*, **89**, (1992) 1.
7. R. Pompe, S. Jaras, and N.-G. Vannerberg, *Appl. Catal.*, **13**, (1984) 171.
8. M. L. Occelli, *Catal. Rev. -Sci. Eng.*, **33**, (1991) 241.

Chapter 6

Effect of Carbon Dioxide on Aromatization of Ethane

Synopsis

For the purpose of examining the possibility of promotion of aromatization of ethane with carbon dioxide, the reaction of ethane and carbon dioxide on Ga-, Zn- and Pt-loaded HZSM-5 catalysts was conducted. The catalytic test on Ga-HZSM-5 revealed that the introduction of carbon dioxide improves the formation of aromatics, in particular, the aromatics formation from ethylene consisting of oligomerization of ethylene and dehydrocyclization of alkenes. The strength of adsorption of ethylene and carbon dioxide were approximately equal in magnitude on Ga_2O_3. On the other hand, carbon dioxide preferentially adsorbed on ZnO, and ethylene did on Pt/SiO_2, respectively. Although the hydrogen consumption through the reverse water-gas shift conversion was improved in the catalytic run on Ga-HZSM-5-V_2O_5 composite catalyst, the yield of aromatics and the selectivities of ethylene and aromatics remained essentially unchanged. These results indicate that the balance of adsorption strength of both substrates on metal species is significant in order to promote aromatization of ethane with carbon dioxide, and that promotion of aromatization by the introduction of carbon dioxide is not attributable to thermodynamic effect, but to kinetic effect.

Introduction

The aromatization of light alkane attracts much attention as a possible technology for the production of chemicals and fuels from less valuable light alkanes. However, the process seems to have some rooms for further improvement, such as by-production of methane and ethane through the hydrogenolysis of higher hydrocarbons and the hydrogenation of olefinic species. These side reactions may be suppressed, if hydrogen will be consumed. The consumption of hydrogen also might improve the conversion of alkanes into aromatics and hydrogen, because the reaction is thermodynamically restricted. In the present study, the aromatization of lower alkanes such as ethane and propane was conducted in an atmosphere of carbon dioxide which possibly consumes hydrogen through the reverse water-gas shift reaction. The present reaction is also attractive from the standpoint of the utilization of carbon dioxide, because carbon dioxide is expected to be reduced into carbon monoxide. It is frequently pointed out that carbon dioxide is quite stable and its reduction requires much energy. Utilization of hydrocarbons as a reducing regent might be one of the approach for the problem.

We reported a novel method for the reduction of carbon dioxide by lower alkanes, concurrently converting alkanes into more value-added products, such as alkenes [1] and aromatics [2]. In the latter reaction on Zn-HZSM-5, carbon dioxide was found to suppress

unfavorable side reactions such as the decomposition of olefinic species and the deposition of coke in propane aromatization. However, the promotion of aromatization with carbon dioxide was not clearly observed. This chapter aims to examine the possibility of promotion of aromatization of ethane, which is less active than propane, with carbon dioxide by using Ga-, Zn- and Pt-loaded HZSM-5 catalysts. These catalysts are known to aromatize ethane [3-8].

Experimental

Catalyst preparation

H-ZSM-5 was prepared by ion-exchange of Na-ZSM-5 (SiO_2/Al_2O_3=23.3, supplied from TOSOH Co.) with NH_4NO_3 aqueous solution at 353 K. After ion-exchange, the sample was calcined in flowing air for 4 h at 823 K. Metal-loaded HZSM-5 catalysts were prepared by refluxing aqueous solutions of $Ga(NO_3)_3$, $Zn(NO_3)_2$ and $Pt(NH_3)_4Cl_2 \cdot H_2O$ containing NH_4-ZSM-5 powders for 24 h, followed by evaporation-to-dryness. Metal content was 10 wt% for Ga and Zn and 1 wt% for Pt. Ga- and Zn-HZSM-5 thus obtained were calcined in flowing air for 4 h at 823 K. Pt-HZSM-5 was calcined in flowing air for 3 h at 773 K, followed by reduction in flowing hydrogen for 3 h at 773 K.

Zeolite-oxide composite catalysts were prepared through mixing powders of Ga-HZSM-5 and V_2O_5 in a mortar, and the powder were pressed into pellets, crushed and sieved.

Ethane conversion

The catalytic test was conducted by using a continuous flow reaction apparatus at atmospheric pressure. The catalyst (0.3-1.0 g) was placed in a quartz tube with an inner diameter of 10 mm. The catalyst, except Pt-HZSM-5, was pretreated in flowing oxygen diluted with nitrogen (O_2/N_2=1/4) for 1 h at 823 K. Hydrogen was used instead of oxygen-nitrogen mixture for the pretreatment of Pt-HZSM-5. Partial pressures of ethane and carbon dioxide were 21 and 42 kPa, respectively, with nitrogen balance, and that of ethane in the reaction of ethane alone was 21 kPa with nitrogen balance. Total feed rate was 0.15 mol h^{-1} in both cases. The reaction temperature was raised every 50 K from 673 to 873 K, and at each temperature the catalytic run was conducted for 45 min, at the end of which reaction products were analyzed with gas chromatography.

The yield of hydrocarbon was expressed in C% on the basis of ethane fed.

Ethylene conversion

Reaction of ethylene was carried out at the W/F of 1.2 g h mol^{-1}. Partial pressures of reactants were the same as those specified for the reaction of ethane.

Competitive hydrogenation of ethylene with carbon dioxide over metal oxide

Hydrogenation of ethylene in the presence of carbon dioxide was conducted by using the same apparatus as that describe above. At first the catalyst was exposed to a flow of carbon dioxide-hydrogen mixture with nitrogen as a diluent ($CO_2/H_2/N_2$=1/1/4), and then, ethylene (14 kPa) was added. W/F was 31 g h mol^{-1} for ZnO and Ga_2O_3 and 1.8 g h mol^{-1} for Pt/SiO_2, respectively.

Results

Aromatization of ethane with carbon dioxide

Ga-HZSM-5

In the reaction of ethane alone on Ga-HZSM-5, the conversion of ethane occurred above 773 K, as shown in Fig. 1. The reaction products were methane, ethylene, propane, propylene and aromatic hydrocarbons (mainly benzene, toluene and xylene). At lower temperatures, ethylene was the main product. The yield and selectivity of aromatics were lower than those reported in the literatures [4, 6, 7], which may be due to a lower value of W/F.

In the reaction of ethane and carbon dioxide, a noticeable amount of carbon monoxide was formed above 773 K. The introduction of carbon dioxide had some effect on the conversion of ethane and the yield of aromatics, as shown in Table 1. The conversion of ethane and yield of aromatics were higher and the yield of ethylene was lower than those without carbon dioxide above 823 K.

Zn-HZSM-5

Fig. 2 shows the results of the reaction on Zn-HZSM-5. In the reaction of ethane alone, the conversion of ethane occurred above 723 K. The conversion of ethane and yield of aromatics increased with a rise in reaction temperature. As shown in Table 1, the major products were ethylene and aromatics. The conversion of ethane and yield of aromatics were higher than those on Ga-HZSM-5. The addition of Zn is more effective than Ga in the reaction of ethane alone. These results are in good agreement with the reported results [7].

In the reaction of ethane and carbon dioxide, the yield of carbon monoxide was higher than that on Ga-HZSM-5 over the whole temperature range, as can be seen by comparing Fig. 2 with Fig. 1. The conversion of ethane was lower than that without carbon dioxide at lower temperatures, but higher above 823 K. The yield of methane remarkably increased by the introduction of carbon dioxide above 823 K (Table 1). However, the yield of aromatics was lower than that without carbon dioxide below 823 K. These results seem to indicate that the

cracking and/or the hydrogenolysis of ethane preferentially occur at higher temperatures.

A low hydrocarbon balance shown in Table 1 can be attributed to the significant deposition of coke. Actually, the catalyst appeared highly darkened after the catalytic run. On the other hand, the balance of carbon oxides exceeded 100% and the total carbon balance was close to 100%. These results confirm that carbon monoxide is formed not only through the reduction of carbon dioxide but also through the gasification of deposited coke by carbon dioxide.

Pt-HZSM-5

As shown in Fig. 3, Pt-HZSM-5 exhibited the highest activity for the conversion of ethane at lower temperatures among the catalysts examined in the present study. A further increase in the temperature, however, led to drop in conversion. As for product distribution, the selectivities to methane and propane were high in comparison with the results over Ga- and Zn-HZSM-5 (Table 1), as reported in literatures [3, 5, 8].

When carbon dioxide was introduced, a noticeable amount of carbon monoxide was formed at higher temperatures. The conversion of ethane and the yield of aromatics dropped seriously, by the introduction of carbon dioxide, especially at higher temperatures. This would lead to the supposition that carbon monoxide might suppress the conversion of ethane by covering metal site, because carbon monoxide is well known to adsorb strongly on the surface of Pt metal.

Reactions of ethane and carbon dioxide over Ga-HZSM-5

Fig. 4 shows the change in the conversion of ethane, the yields of ethylene and aromatics with W/F. The yield of ethylene passed through a maximum, and decreased with further increase in W/F. The yield of aromatics increased with W/F. These results show that ethylene is the primary product of ethane conversion, and undergoes secondary transformations leading to aromatics as reported in the literatures [6, 7].

The introduction of carbon dioxide increased the yield of aromatics and decreased the yield of ethylene over a whole range of W/F examined, while the conversion of ethane was increased only at a high W/F.

Reaction of ethane and carbon dioxide over zeolite-V_2O_5 composite catalyst

In order to confirm if the promotion of aromatization of ethane by the introduction of carbon dioxide is attributable to the hydrogen consumption through the reverse water-gas shift conversion, the reaction of ethane and carbon dioxide was carried out over Ga-HZSM-5 and Ga-HZSM-5-V_2O_5 composite catalyst. Vanadium oxide was selected as the oxide components which are active for the reduction of carbon dioxide and inactive for the decomposition of propane. We have reported that the zeolite-oxide composite catalysts were

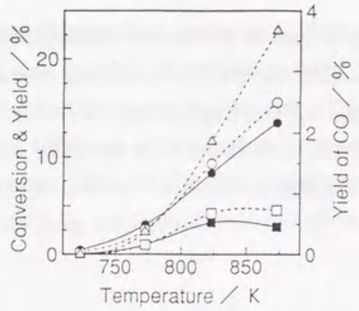

Fig.1 Conversion and yields in the reaction of ethane alone (●■) and in the reaction of ethane and carbon dioxide (○□△) on 10 wt%Ga-HZSM-5. Conversion of ethane (●○), yield of aromatics (■□), yield of carbon monoxide (△).

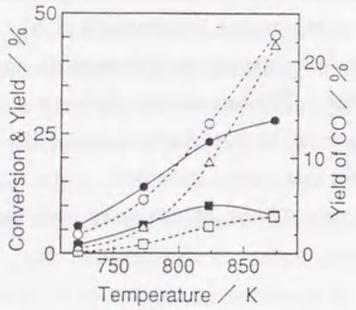

Fig.2 Conversion and yields in the reaction of ethane alone (●■) and in the reaction of ethane and carbon dioxide (○□△) on 10 wt%Zn-HZSM-5. (For the symbols, see Fig. 1.)

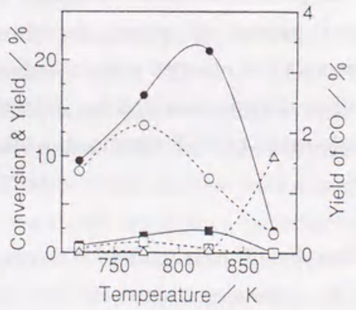

Fig.3 Conversion and yields in the reaction of ethane alone (●■) and in the reaction of ethane and carbon dioxide (○□△) on 1 wt%Pt-HZSM-5. (For the symbols, see Fig. 1.)

Table 1 Reactions of C_2H_6 alone and C_2H_6+CO_2 over metal-loaded HZSM-5

Catalysts	Ga-HZSM-5[a]		Zn-HZSM-5[a]		Pt-HZSM-5[b]	
Reaction	C_2H_6	C_2H_6+CO_2	C_2H_6	C_2H_6+CO_2	C_2H_6	C_2H_6+CO_2
Temperature / K	873	873	873	873	773	773
Conversion / %						
C_2H_6	13.6	15.6	27.9	45.5	16.4	13.3
CO_2	-	3.4	-	14.1	-	0.5
Yield / %						
CH_4	0.4	0.9	1.4	9.3	3.7	2.0
C_2H_4	7.9	6.2	14.2	17.0	8.6	8.0
C_3H_8	trace	0.1	0.1	0.2	0.7	0.3
C_3H_6	0.4	0.4	0.7	0.7	1.3	0.9
Aromatics	2.9	4.6	8.1	7.7	1.8	1.1
CO	-	3.7	-	21.6	-	0.0
Balance / %						
Hydrocarbon	98.0	96.6	96.5	89.3	99.8	98.9
CO_x	-	100.3	-	107.9	-	99.5
Total Carbon	98.0	98.4	96.5	98.2	99.8	99.2

[a] metal content, 10 wt%; [b] metal content, 1 wt%.

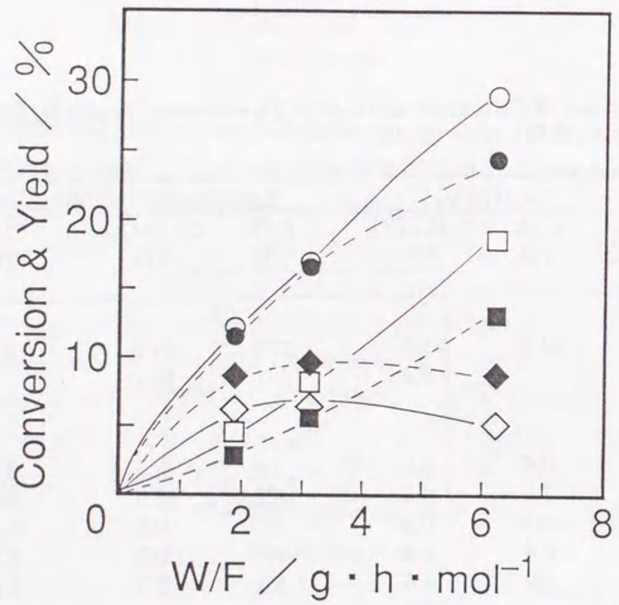

Fig.4 Conversion of ethane (●○), yield of ethylene (◆◇) and aromatics (■□) in the reaction of ethane alone (●◆■) and in the reaction of ethane and carbon dioxide (○◇□) over 10 wt%Ga-HZSM-5 at 873 K as a function of W/F.

Table 2 Reaction of C_2H_6+CO_2 over Ga-HZSM-5-V_2O_5 composite catalysts at 873 K

Catalyst	Ga-HZSM-5	Ga-HZSM-5-V_2O_5
Conversion / %		
C_2H_6	17.0	15.4
CO_2	4.4	9.1
H_2 Consumption / %	19.1	42.4
Yield / %		
CH_4	1.6	1.6
C_2H_4	6.5	5.4
C_3H_8	0.1	0.1
C_3H_6	0.5	0.4
Aromatics	8.3	7.9

Table 3 Effect of carbon dioxide on the reaction of C_2H_4 at 873 K

Reaction	C_2H_4	C_2H_4+CO_2
Conversion / %		
C_2H_4	57.4	73.1
CO_2	-	2.1
Yield / %		
CH_4	1.6	2.3
C_2H_6	7.3	8.1
C_3H_8	0.5	1.3
C_3H_6	3.7	3.8
C_{4+}	1.7	1.1
Aromatics	44.5	65.0

Table 4 Reactions of C_2H_4+CO_2+H_2 over metal and oxides at 873 K.

Catalyst	Ga_2O_3	ZnO	Pt/SiO_2
Conversion / %			
C_2H_4	5.0	2.1	13.6
CO_2	14.1	30.0	3.0
Relative Rates			
C_2H_4/CO_2	0.88	0.17	11.3

revealed to exhibit high activity for reduction of carbon dioxide and high selectivity for the aromatization of propane [9].

When vanadium oxide was mixed, the conversion of carbon dioxide and the rate of consumption of hydrogen were improved remarkably. The consumption of hydrogen is defined as the proportion of hydrogen consumed by the reverse water-gas shift conversion to that formed by ethane aromatization. This value increased from 19.1% on Ga-HZSM-5 to 42.4%, by factor of two on the average. However, the conversion of ethane and the product distribution remained essentially unchanged (Table 2).

Aromatization of ethylene with carbon dioxide

The results of the reaction of ethylene in the presence and absence of carbon dioxide on Ga-HZSM-5 at 873 K are shown in Table 3. In the reaction of ethylene alone, the conversion and the yield of aromatics were very high in comparison with the ethane aromatization. These results show that the formation of olefinic compounds from dehydrogenation of starting materials is the limiting step of ethane aromatization, as the case of propane [10].

When carbon dioxide was introduced, the conversion of ethylene and the yield of aromatics remarkably increased, although carbon dioxide was reduced slightly.

Competitive Hydrogenation of Ethylene and Carbon Dioxide over Metal Oxides

The competitive hydrogenation of ethylene and carbon dioxide was studied over metal oxides. The product mixture consisted of methane, ethane, propylene and also carbon monoxide. Table 4 shows the conversion and relative rate of hydrogenation of ethylene in comparison with that of carbon dioxide after 0.5 h on stream at 773 K. The relative rate can be a measure of relative strength of adsorption of ethylene in comparison with carbon dioxide. In the case of ZnO, the relative rate was very low, indicating that carbon dioxide is adsorbed in preference to ethylene. Pt/SiO_2 exhibited the highest activity for hydrogenation of ethylene, and the relative rate was very high, indicating that ethylene is adsorbed in preference to carbon dioxide. On the other hand, Ga_2O_3 gave a moderate relative rate, indicating that the strength of adsorption of ethylene is approximately equal to that of carbon dioxide.

Discussion

Effect of Metal Species on the Reaction of Ethane and Carbon Dioxide

It is well known that the aromatization of ethane on HZSM-5 can be accelerated by the incorporation of metal species [3-8]. In the present study, the effect of Ga, Zn and Pt on the aromatization of ethane with carbon dioxide was examined. As shown in Figs. 1-3 and

Table 1, the introduction of carbon dioxide had some effect on the conversion of ethane and the selectivities of hydrocarbon products. In the case of Ga-HZSM-5, the introduction of carbon dioxide promoted the formation of aromatics, while it suppressed in the cases of Zn-HZSM-5 and Pt-HZSM-5.

It has been widely accepted that the rate of aromatization may be determined by the formation rate of olefinic species on metal site, and in this step, Zn cation is expected to act as a hydride acceptor to form $[Zn\text{-}H]^+$ species [11]. Meriaudeau *et al.* suggested that two kind of sites are required for the dehydrogenation of propane: metal cation sites for accepting hydride ions and oxygen anion sites for propyl carbenium ions [12]. On the other hand, carbon dioxide is known to be adsorbed at oxygen vacancies on zinc oxide surface to formate species at elevated temperatures in hydrogen atmosphere [13]. As shown in Table 4, carbon dioxide adsorbed on ZnO surface in preference to ethylene. This would lead to the supposition that carbon dioxide covers the metal sites and suppressed the dehydrogenation of ethane. The decrease in the yield and selectivity of aromatics over Zn-HZSM-5 may be attributed to higher activity for the activation of carbon dioxide than that for the activation of hydrocarbons.

In the case of Pt-HZSM-5, the decrease in the yield and selectivity of aromatics may be due to higher activity for the hydrogenation and hydrogenolysis of hydrocarbons rather than that for the activation of carbon dioxide (Table 4). The strong adsorption of hydrocarbons inhibits the adsorption and the activation of carbon dioxide.

In contrast, carbon dioxide improved aromatization activity of Ga-HZSM-5. The strength of adsorption of both ethylene and carbon dioxide on Ga_2O_3, as shown in Table 4, were approximately equal in magnitude. Thus, these results show that in order to promote aromatization of ethane with the introduction of carbon dioxide, the balance of adsorption strength of both substrates is significant.

Effect of Carbon Dioxide on Aromatization of Ethane over Ga-HZSM-5

In the case of Ga-HZSM-5, the introduction of carbon dioxide increased aromatics yield and decreased ethylene yield (Table 1). In order to assess the contribution of carbon dioxide to aromatization of ethane, ethane aromatization was carried out in various W/F (Fig. 4). Fig. 4 shows that the introduction of carbon dioxide was clearly promoted dehydrogenation of ethane and aromatization of ethylene at a higher W/F. At a low W/F, although the dehydrogenation of ethane was not promoted, the aromatization of ethylene was clearly enhanced. It is interesting to see whether these observations were attributed to thermodynamic or kinetic effect.

Thermodynamic effect may be possible explanation, because the dehydrogenation of ethane ($C_2H_6 \rightarrow C_2H_4 + H_2$) is thermodynamically restricted under the present condition, and because hydrogen is consumed through the reverse water-gas shift conversion ($CO_2 + H_2 \rightarrow$

$CO + H_2O$). The partial pressure of ethylene at a outlet of catalyst bed, however, was less than the equilibrium pressures: the ratio of partial pressures, *i.e.*, $P(C_2H_4)\cdot P(H_2)/P(C_2H_6)$ was 0.001 and 0.004 at 823 and 873 K, respectively, in the presence of carbon dioxide, while the equilibrium constant, K_p, is 0.005 and 0.050 at 800 and 900 K, respectively.

The introduction of carbon dioxide increased aromatics yield and decreased ethylene yield, which suggests that carbon dioxide promotes the aromatization of ethylene consisting of oligomerization of ethylene and dehydrocyclization of alkenes. This was confirmed through the reaction of ethylene in the presence and absence of carbon dioxide. As shown in Table 3, although carbon dioxide was reduced only slightly, the conversion of ethylene and the yield of aromatics were remarkably increased.

From a thermodynamic point of view, because of the high thermodynamic barrier, the dehydrogenation of ethane into ethylene is unfavorable. However, aromatization of ethylene is favorable, because the free energy change ΔG_f is negative as shown in Fig. 5. The results of a catalytic run on Ga-HZSM-5-V_2O_5 composite catalyst shown in Table 2, also suggest that carbon dioxide kinetically promotes the aromatization of ethane. Although the consumption of hydrogen was much improved by the addition of V_2O_5, the yield of aromatics and the selectivities of ethylene and aromatics remained constant. It may therefore be concluded that the promotion of aromatization by the introduction of carbon dioxide is not attributable to thermodynamic effect through the consumption of hydrogen, but to kinetic effect.

Frilette *et al.* have shown that the introduction of carbon dioxide significantly enhances the catalytic activity for the dehydration for isopropyl alcohol in X zeolites [14]. Further, Minachev *et al.* reported that addition of carbon dioxide increased the catalytic activities of faujasite (Y) zeolites in the disproportionation of toluene [15] and for the alkylation of benzene with olefins [16]. They proposed that the active centers are formed as a result of chemisorption of carbon dioxide on the cations or on lattice defect, *e.g.*, the addition of carbon dioxide to the hydrated zeolites results in the production of Brønsted acid sites. Hall *et al.* have shown, by studying the adsorption of pyridine, that the proton acidity of Y zeolites was enhanced when carbon dioxide added to these systems [17]. The increase in acidity by carbon dioxide, reported in these literatures, seems to promote the aromatization of ethane in the present case.

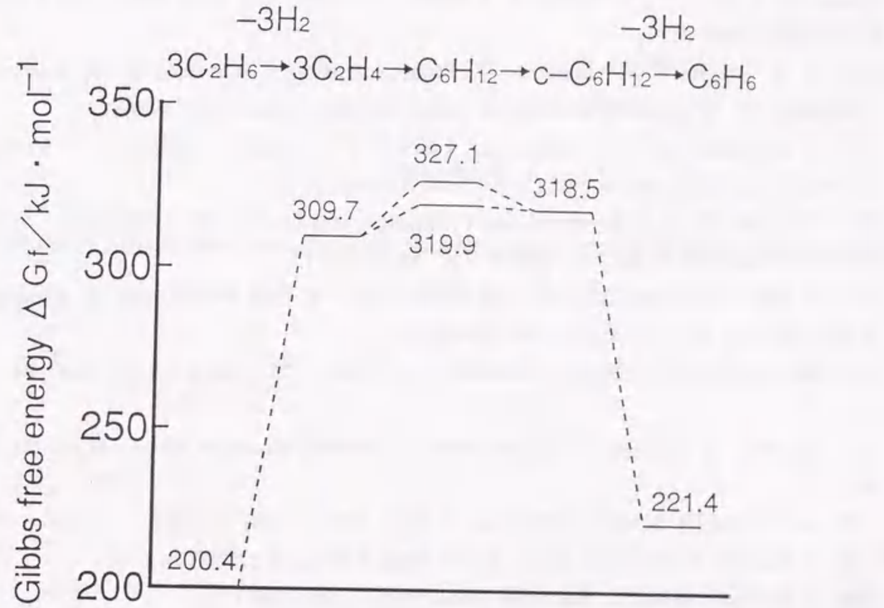

Fig.5 The free energy ΔG_f of aromatization of ethane.

References

[1] T. Hattori, M. Komatsuki, A. Satsuma and Y. Murakami, *Nippon Kagaku Kaishi*, (1991) 648.

[2] T. Hattori, S. Yamauchi, A. Satsuma and Y. Murakami, *Chem. Lett.*, (1992) 629; S. Yamauchi, A. Satsuma, T. Hattori and Y. Murakami, *Sekiyu Gakkaishi*, **37**, (1994) 278; S. Yamauchi, A. Satsuma, S. Komai, T. Asakawa, T. Hattori and Y. Murakami, *Stud. Surf. Sci. Catal.*, **84**, (1994) 1571.

[3] O. V. Bragin, E. S. Shpiro, A. V. Preobrazhensky, S. A. Isacov, T. V. Vasina, B. B. Dyusenbina, G. V. Antoshin and Kh. M. Minachev, *Appl. Catal.*, **27**, (1986) 219.

[4] V. I. Yankerson, T. V. Vasina, L. I. Lafer, V. P. Sytnyk, G. L. Dykh, A. V. Mokhov, O. V. Bragin and Kh. M. Minachev, *Catal. Lett.*, **3**, (1989) 339.

[5] K.-H. Steinberg, U. Mroczek, and F. Roessner, *Appl. Ctal.*, **66**, (1990) 37.

[6] P. Schulz and M. Baerns, *Appl. Catal.*, **78**, (1991) 15.

[7] Y. Ono, *Catal. Rev.-Sci. Eng.*, **34**, (1992) 179; Y. Ono, H. Nakatani, H. Kitagawa and E. Suzuki, *Stud. Surf. Sci. Catal.*, **44**, (1988) 279.

[8] A. Hagen and F. Roessner, *Stud. Surf. Sci. Catal.*, **75**, (1993) 1707; *ibid.*, **81**, (1993) 313.

[9] K. Nishi, A. Satsuma, T. Hattori and Y. Murakami, *Energy Convers. Mgmt*, **36**, (1995) 645.

[10] M. Guisnet, N. S. Gnep and F. Alario, *Appl. Catal. A*, **89**, (1992) 1.

[11] T. Mole, J. R. Anderson and G. Creer, *Appl. Catal.*, **17**, (1985) 141.

[12] P. Meriaudeau and C. Naccache, *J.Mol. Catal.*, **50**, (1989) L7.

[13] G. J. Millar, C. H. Rochester, S. Baily and K. C. Waugh, *J. Chem. Soc., Faraday Trans.*, **88**, (1992) 2085.

[14] V. J. Frilette and G. W. Muns, *J. Catal.*, **4**, (1965) 504.

[15] Kh. M. Minachev and Ya. I. Isacov, *Dokl. Acad. Nauk. SSSR*, **202**, (1972) 1341.

[16] Ya. I. Isacov, Kh. M. Minachev and V. P. Kalinin, *Izv. Akad. Nauk. SSSR, Ser. Khim.*, (1973) 1138 .

[17] B. V. Liengme, W. K. Hall, *Trans. Faraday Soc.*, **62**, (1966) 3229.

Chapter 7

Methanol Conversion into Branched-Aliphatics over Modified Mordenites

Synopsis

The influences of zeolite pore structure, dealumination and Na ion exchange on the product distribution were examined, in order to explore the possibility of selective formation of multi-branched-chain aliphatics, such as *iso*-octane, in methanol conversion. On H-form mordenite, the selectivity of multi-branched-chain aliphatics was higher than those on other type zeolites, such as ZSM-5 and Y zeolites. Modification of mordenite by both using Na ion exchange and dealumiation promoted the formation of multi-branched-chain aliphatics. The effect of the modifications in the formation of multi-branched-chain aliphatics is discussed in reference to methylation of 1-hexene with methanol.

Introduction

From a technological viewpoint, use of C_1 chemicals, such as methanol, is becoming more important for the supply of fuels and chemical feedstocks. Methanol conversion into hydrocarbons on zeolite catalysts has been extensively investigated since this reaction was announced as the MTG process by Mobil in 1976 [1]. This process make it possible to supply gasoline and chemical feedstocks from coal or natural gas instead of petroleum.

The growing concern about the environment has led to a drastic reduction of emissions from the transport sector. Although the improvements of engine management and emission control systems have contributed to lowering vehicle emissions, air quality is still not acceptable in many cities. Recently, attention is also being focused on how changes in the composition and properties of fuels can contribute. Therefore, changing the composition of the gasoline pool, *e.g.*, reduction of aromatic hydrocarbons, is required [2, 3]. In this sense, the methanol conversion into branched-chain aliphatics is attractive for compensating the decrease in the octane number of gasoline due to the decrease in aromatic content, *i.e.*, for synthesis of environmentally acceptable gasoline.

Since the high octane number of the product in MTG process using pentasil type zeolite is due to its high content of aromatic hydrocarbons, alternate zeolite catalysts must be used to synthesize a high octane number gasoline composed of branched-chain aliphatics. Large-pore zeolites, particularly mordenite and Y zeolites, would be more attractive in this reaction, because the multiple branched-chain alkanes are bulky. But, unfortunately, they are rapidly deactivated by coke deposition [4]. The present authors and co-workers have reported that dealumination and cation exchange decreased the coke deposition on mordenites and improved the catalyst life [5-8].

This chapter aims at examining possible factors controlling the formation of multi-branched-chain aliphatics, such as *iso*-octane, in methanol conversion; such factors include

dealumination and Na ion exchange.

Experimental

Catalyst preparation

H-mordenite (referred to as HM), H-ZSM-5 (HZ), and H-Y (HY) zeolites employed were the Reference Catalysts of the Catalysis Society of Japan, JRC-Z-HM15, JRC-Z5-25H, and JRC-Z-HY4.8, respectively [9]. Dealuminated mordenite (DM) was prepared by leaching HM in 8 mol dm^{-3} hydrochloric acid at 353 K for 24 h, followed by filtration and washing. Dealuminated mordenite thus obtained was dried overnight at 398 K. Dealuminated and Na ion-exchanged mordenite (NaDM) catalysts was prepared by ion exchange of DM with an aqueous solution of sodium acetate for 24 h at 353 K, followed by filtration, washing, and drying. Fully Na ion-exchanged mordenite (NaM) was prepared by applying the evaporation-to-dryness procedure instead of filtration and washing. The Na ion-exchanged zeolites were calcined at 673 K in an O_2 flow to remove further acetate ions. All zeolites were pelleted without binder, crushed and sized to 28-48 mesh.

Characterization

Al content and the degree of ion exchange were determined by inductively coupled plasma spectroscopy (ICP). The acid amount and strength of zeolite samples were measured by temperature programmed desorption of ammonia (NH_3-TPD) in the same way as described previously [6-8].

Methanol conversion

Methanol conversion was carried out using a conventional continuous flow reactor at atmospheric pressure in a similar way to that described previously [8]. Methanol (68.2 μ mol min^{-1}) in helium gas (40 ml min^{-1}) was fed over zeolite catalyst (0.05 g) at 623 K for ten minutes. Only a small amount of catalysts was used so as to obtain moderate conversion of methanol. Products eluted from the reactor were once collected in a trap cooled at 77 K, and then flushed into FID-GC through valves. Petrocol DH 150 fused silica capillary column was used at temperatures ranging at 308 K to 473 K. The amount of coke deposited during reaction was measured by thermogravimetry (TG). The yield was expressed in C% on the basis of methanol fed, and the selectivity was expressed in C% on the basis of total hydrocarbon products.

Methylation of 1-hexene with methanol

Methylation of 1-hexene with methanol was carried out using the same apparatus as that

described above. A mixture of 1-hexene (125 μ mol min^{-1}) and methanol (68.2 μ mol min^{-1}) in helium gas (40 ml min^{-1}) was fed over zeolite catalyst (0.05 g) at 623 K for five minutes. The analysis of products was carried out in the same manner as described above.

Results

The acidity of zeolite catalysts

Al content and degree of Na ion exchange are listed in Table 1. Fig. 1 shows the profiles of NH_3-TPD on H-form zeolites. The profile on HM zeolite showed two peaks (named *l*-peak and *h*-peak) at ca. 500 K and 770 K, respectively. It was reported that the amount of *l*-peak was affected by the experimental conditions of TPD [10], and that the *l*-peak sites are of little importance to the methanol conversion [11]. On the other hand, the *h*-peak was attributed to ammonia adsorbed on strong acid sites which were active for methanol conversion [10, 11]. Accordingly, the amount of strong acid sites was defined as the amount of ammonia desorbed above 573 K [11] and listed in Table 1. Similarly, HZ exhibited two peaks at ca. 500 and 650 K. HY showed broad unresolved spectrum. The *h*-peak was shown as an indistinguishable shoulder at higher temperature side of *l*-peak, as reported in literatures [12, 13]. Since the desorption temperature of ammonia must reflect the strength of acid sites, the order of the acid strength is HM>HZ≧HY. This order of acid strength agrees with that derived from NH_3-TPD [11, 12] and microcalorimetry [14] (the adsorption enthalpies for NH_3 were 160 kJ mol^{-1} for H-mordenite, 150 kJ mol^{-1} for H-ZSM-5 and 150-135 kJ mol^{-1} for H-Y). The order of the amount of strong acid sites is also HM≧HZ>HY, as shown in Table 1.

The profiles of NH_3-TPD on dealuminated and/or Na ion-exchanged mordenites are shown in Fig. 2. DM (dealuminated mordenite) exhibited two broad desorption peaks. The amount of ammonia desorbed in the *h*-peak and the temperature at peak maximum were much lower than those of HM, in line with previously reported results on moderately dealuminated mordenites [6-8]. NaDM (dealuminated and partially Na ion-exchanged mordenite) gave a TPD profile similar to that on DM, though the *l*-peak was slightly larger. The profile on NaM (fully Na ion-exchanged mordenite) showed only the large *l*-peak. The large *l*-peak strongly indicates that the sites adsorbing ammonia are formed by Na ion exchange. Fig. 3 shows IR spectra of adsorbed ammonia on partially Na ion-exchanged mordenite. Three

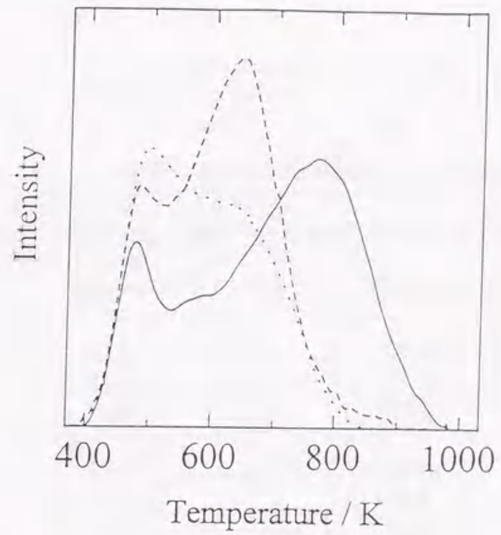

Fig. 1 (left) TPD profiles of NH_3 on H-form zeolites. HM(———), HZ(- - - -), and HY(·····).

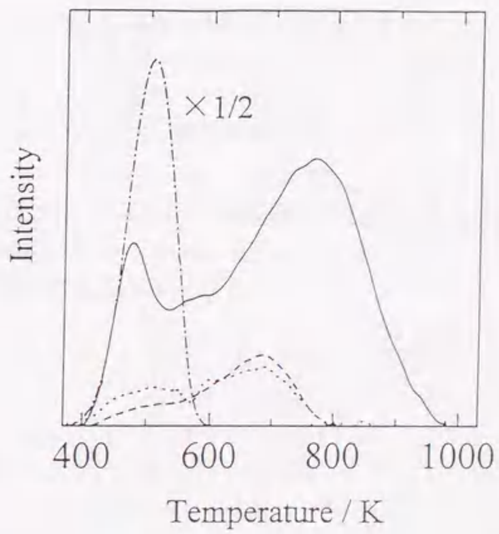

Fig. 2 (right) TPD profiles of NH_3 on dealuminated and/or Na ion-exchanged mordenites. HM(———), DM(- - - -), NaDM(·····), and NaM(-·-·-·).

Table 1 Al content and acidic property of zeolite catalysts.

catalyst	SiO_2/Al_2O_3	Al content	Na ion exchange	Amount of desorbed ammonia	
				total	strong acid sites*)
		(mmol/g)	(%)	(mmol/g)	(mmol/g)
HM	15	1.62	0	1.12	0.85
HZ	25	1.27	0	1.29	0.81
HY	4.8	2.91	0	0.99	0.51
HM	15	1.62	0	1.12	0.85
DM	164	0.20	0	0.17	0.13
NaDM	124	0.25	33	0.16	0.10
NaM	15	1.62	100	0.73	0.00

*) The amount of ammonia desorbed above 573 K.

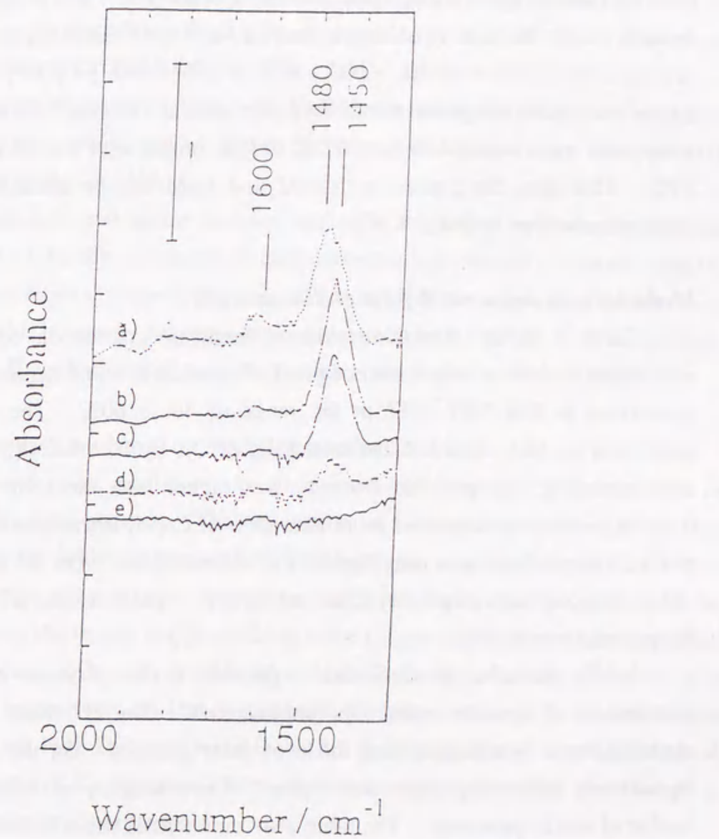

Fig. 3 IR spectra of NH_3 adsorbed on Na ion-exchanged mordenite, after adsorption of NH_3 for 0.5 h at room temperature followed by evacuation for 0.5 h at (1) room temperature, (b) 373 K, (c) 473 K, (d) 573 K, and (e) 673 K.

absorption bands were observed at 1600, 1480 and 1450 cm^{-1}. The bands at 1600 and 1450 cm^{-1} are attributed to ammonia which has interacted with Brønsted acid sites and Lewis acid sites, respectively. On the other hand, the band at 1480 cm^{-1} is not indicative of acid sites described above, but it is attributed to $-NH_2^-$ species [15]. It is thought that $-NH_2^-$ species are formed, due to dissociative chemisorption on Na^+ and O^{2-} sites, according to

$$NH_3 + Na^+ + O^{2-} \rightarrow [Na^+ - NH_2^-] + [OH^-]$$

As the evacuation temperature increased, the band at 1480 cm^{-1} decreased, and it disappeared completely by evacuation below 573 K. This agreed with the the results obtained by NH_3-TPD. Therefore, the *l*-peak on NaDM and NaM can be attributed to the desorption of ammonia adsorbed as $[NH_2^- + H^+]$.

Methanol conversion on H-form zeolite catalysts

Table 2 summarizes the results of methanol conversion on H-form zeolites. The conversion is defined as the sum of yield of hydrocarbon and deposited coke. The order of conversion is HM>HY>HZ in the range of 40 to 60%. The deposition of coke was significant on HM. On HZ, the selectivity of C_{5+} hydrocarbons (hydrocarbons with five or more carbons), *i.e.*, gasoline fraction, was higher than those on other zeolites. In this reaction, aromatics comprised more than 60% of C_{5+} hydrocarbons. On HM, the selectivity of C_{10+} hydrocarbons was only high in C_{5+} hydrocarbons. On the other hand, the formation of C_8, hydrocarbons was rarely observed on HY. These results are in good agreement with the reported results [16].

In C_6 products, all theoretically possible hexane isomers could be identified, and distribution of hexane isomer is summarized. On HZ and HY, the selectivity of methylpentanes was higher than those of other isomers. On the other hand, HM gave a significantly different product distribution. The selectivity of dimethylbutanes was as high as that of methylpentanes. The table also summarizes the selectivities of identified typical octane isomers in C_8 aliphatics, such as methylheptanes, dimethylhexanes, and trimethylpentanes. On HZ, observed octane isomers were methylheptanes and dimethylhexanes. On HY, while methylheptanes were observed, no dimethylhexanes and trimethylpentanes were. On the other hand, trimethylpentanes were observed only on HM.

Methanol conversion on modified mordenite catalysts

The results of methanol conversion on modified mordenites are summarized in Table 3. The conversion was decreased by dealumination and Na ion exchange. NaM did not exhibit any catalytic activity. Dealumination, however, remarkably improved catalyst life. HM was completely deactivated within 3 hours, but the conversion on DM decreased only slowly for the catalytic run of several hours, as reported previously [8]. The amounts of coke deposited on DM and NaDM were much less than that on HM, as shown in Table 3. This

result is in good agreement with the previously reported result that the coke deposition on mordenite can be suppressed by reducing the strong acid sites to less than 0.15 mmol g^{-1} [8].

Product distribution was also affected by dealumination and Na ion exchange. On DM, the selectivity of C_{1-3} hydrocarbons markedly decreased and that of C_{5+} hydrocarbons increased, in comparison with the result on HM. In C_{5+} hydrocarbons, the selectivity of aromatics was decreased by dealumination. On NaDM, the selectivity of C_{1-3} hydrocarbons and aromatics were lower, while that of C_{5+} hydrocarbons was higher than those on HM. This result was similar to that on DM.

Distribution in hexane and octane isomers were also influenced by dealumination and Na ion exchange. On DM, the selectivity of dimethylbutanes decreased in hexane isomers. Furthermore, the selectivities of dimethylhexanes and trimethylpentanes in C_8 aliphatics were also decreased. NaDM, however, produced multi-branched-chain alkanes, such as dimethyl- and trimethylalkanes. The selectivity of trimethylpentanes was higher than that on HM.

1-Hexene methylation with methanol on modified mordenite catalysts

Table 4 summarizes the results of the methylation of 1-hexene with methanol on unmodified and modified mordenites. The conversion of 1-hexene was very high on HM, but it was decreased by the dealumination and Na ion exchange. It should be noted, however, NaM, which was inactive for methanol conversion, exhibited some catalytic activity in this reaction. On all the catalysts, the major products were C_6 and C_7 hydrocarbons, especially branched-chain aliphatics. The selectivities of C_6 and C_7 branched-chain aliphatics were about 25% and 30%, respectively on HM. Although the selectivities of C_7 branched-chain aliphatics were lower on both DM and NaDM, that on NaDM decreased to a lower extent. On NaM, the selectivity of C_6 branched-chain aliphatics further decreased, but that of C_7 branched-chain aliphatics greatly increased.

Discussion

Influence of zeolite pore structure

As shown in Table 2, the product distribution, compared at a similar extent of reaction, is affected by the type of zeolites. In hexane isomers, HM exhibited the higher selectivity of dimethylbutanes than HZ, and the formation of trimethylpentanes was observed only on HM in octane isomers. This result would indicate that the shape selectivity of zeolites plays an important role in the formation of multi-branched-chain alkanes. Therefore, large-pore zeolites, such as mordenite, would be necessary to form these multi-branched-chain alkanes.

On HY, monomethylalkanes were predominant in C_6 and C_8 branched-chain alkanes and trimethylalkanes were not formed at all (Table 2), though the pore size of HY is larger than that of HM. This result indicates that the formation of multi-branched-chain alkanes is

affected not only by the pore size but rather by the other factors such as acid amount, acid strength and pore structure. The lower selectivities of multi-branched-chain aliphatics on HY, however, cannot be interpreted in terms of acidity: The formation of dimethyl- and trimethylalkanes was observed on DM, although the amount of strong acid sites was less than that of HY (Table 3). This result would indicate that lower selectivities of multi-branched-chain alkanes on HY are not caused by lower amounts of strong acid sites. On the other hand, the strength of acid sites of HY was similar to that of HZ (Fig. 1). Dimethylhexanes were observed on HZ, while they were not observed on HY (Table 2). These results would indicate that the strength of acid sites is not a key factor in formation of multi-branched-chain alkanes. Another possible factor would be the pore structure of zeolite catalysts. HM has a pseudo-unidimensional channel structure, while HY has three-dimensional openings. It seems that the progress of oligomerization and/or methylation is limited, because the diffusion of intermediate molecules to outer surface is easy on HY.

From the viewpoint of formation of multi-branched-chain alkanes, HM exhibited the most attractive shape selectivity among these three kinds of zeolites; this is attributed to its pore size and structure.

Effect of Na ion exchange on formation of branched-chain aliphatics

Although the acidity of NaDM was similar to DM (Table 1), NaDM exhibited the higher selectivity of trimethylpentanes than DM (Table 3). This result indicates that Na ion plays an important role, other than decreasing the density of strong acid sites, in the formation of multi-branched-chain alkanes.

In order to clarify the role of Na ion, the methylation of 1-hexene with methanol was carried out on Na ion-exchanged mordenite catalysts. As shown in Table 4, the formation of C_7 branched-chain aliphatics was promoted by Na ion exchange, although the formation of C_6 hydrocarbons, isomerization of 1-hexene, was depressed. On NaM, the selectivity of C_7 branched-chain aliphatics was higher than that on HM. And, all the C_7 hydrocarbons formed on NaM were branched-chain aliphatics. Furthermore, on NaDM, the selectivity of C_7 branched-chain aliphatics was higher than that on DM, even though the amount of strong acid sites and conversion were similar. These results indicate that the formation of side chains was promoted by Na ion exchange. It is widely accepted that the alkylation of alkenes proceeds through the carbenium ion intermediates on the acid catalysts, such as zeolites [17]. On the other hand, the base sites promote the proton abstraction from the α-carbon in alkenes to form a reactive carbanion intermediate [18-20], which is to be alkylated with methanol in side chain alkylation of toluene [19]. It was found that the base sites are generated by Na ion exchange in the IR spectra of adsorbed ammonia on Na ion-exchanged mordenite (Figure 3). In the present case, therefore, the basic oxygen sites generated by the introduction of Na ions would promote the proton abstraction and the alkylation at the α-

carbon of 1-hexene, as shown in Scheme 1. The formation of branched-chain aliphatics in methanol conversion on Na ion-exchanged mordenite would be accounted for by this reaction mechanism.

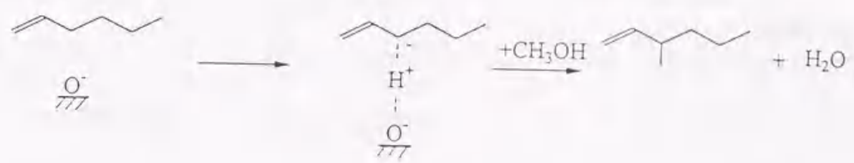

Scheme 1

Conclusions

The reactions of methanol on various H-form zeolite catalysts were carried out, and trimethylalkanes were formed only on HM zeolite. The formation of multi-branched-chain aliphatics was promoted by using dealuminated and partially Na ion exchanged mordenite. The dealumination of mordenite suppressed the formation of aromatics and coke by decreasing the density of strong acid sites. The base sites generated by Na ion exchange would promote the formation of side chains, which results in higher selectivity of multi-branched-chain aliphatics.

Table 2 Product distribution in methanol conversion on various zeolite catalysts.

	HZ	HM	HY
SiO_2/Al_2O_3	25	15	4.8
Na ion exchange (%)	0	0	0
Conversion (%)	40.3	62.3	54.6
Yield (%)			
Hydrocarbon	35.4	35.4	44.9
Coke	4.9	26.9	9.8
Selectivity (%)			
C_{1-3}	24.4	60.5	39.6
C_4	19.1	17.9	38.5
C_5	7.9	5.0	12.3
C_6	6.6	2.5	5.0
C_7	4.7	1.1	1.9
C_8	11.3	1.0	0.8
C_9	9.7	1.3	1.0
C_{10+}	16.5	10.7	1.1
gasoline (C_{5+})	56.6	21.6	21.9
Gasoline range distribution (%)			
aliphatics	34.3	36.1	84.6
naphthenes	0.1	0.0	0.4
aromatics	65.6	63.9	15.0
Distribution in hexane isomers (%)			
n-hexane	12.2	15.9	5.1
methylpentanes	80.9	47.8	94.1
dimethylbutanes	7.0	36.2	0.8
Branched-chain alkanes distribution in C_8 aliphatics (%)			
methylheptanes[a)]	16.0	22.1	31.4
dimethylhexanes[b)]	18.6	0.0	0.0
trimethylpentanes[c)]	0.0	16.3	0.0

a) 2-, 3-, and 4-methylheptane
b) 2, 5-dimethylhexane
c) 2, 2, 4-, and 2, 3, 4-trimethylpentane

Table 3 Product distribution in methanol conversion on dealuminated and/or Na ion exchanged mordenites.

	HM	DM	NaDM	NaM
SiO_2/Al_2O_3	15	164	124	15
Na ion exchange (%)	0	0	33	100
Conversion (%)	62.3	57.8	49.1	0.0
Yield (%)				
Hydrocarbon	35.4	56.6	46.7	0.0
Coke	26.9	1.2	2.5	0.0
Selectivity (%)				
C_{1-3}	60.5	36.8	33.0	0.0
C_4	17.9	32.3	41.5	0.0
C_5	5.0	7.7	7.7	0.0
C_6	2.5	6.1	6.2	0.0
C_7	1.1	3.5	2.9	0.0
C_8	1.0	1.6	1.4	0.0
C_9	1.3	0.9	1.4	0.0
C_{10+}	10.7	11.0	5.9	0.0
gasoline (C_{5+})	21.6	30.9	25.5	0.0
Gasoline range distribution (%)				
aliphatics	36.1	52.9	68.3	0.0
naphthenes	0.0	0.1	0.1	0.0
aromatics	63.9	47.0	31.6	0.0
Distribution in hexane isomers (%)				
n-hexane	15.9	38.7	15.2	0.0
methylpentanes	47.8	46.4	59.1	0.0
dimethylbutanes	36.2	14.9	31.6	0.0
Branched-chain alkanes distribution in C_8 aliphatics (%)				
methylheptanes[a)]	22.1	3.2	2.7	0.0
dimethylhexanes[b)]	0.0	1.7	0.0	0.0
trimethylpentanes[c)]	16.3	2.1	18.1	0.0

a) 2-, 3-, and 4-methylheptane
b) 2, 5-dimethylhexane
c) 2, 2, 4-, and 2, 3, 4-trimethylpentane

Table 4 1-Hexene methylation with methanol on dealuminated and/or Na ion exchanged mordenites.

	HM	DM	NaDM	NaM
SiO_2/Al_2O_3	15	164	124	15
Na ion exchange (%)	0	0	33	100
Conversion of 1-hexene (%)	93.9	32.4	30.9	2.4
Selectivity (%)				
C_{1-3}	7.1	10.9	10.0	0.5
C_4	9.4	20.0	16.6	20.7
C_5	6.4	11.9	9.8	4.2
C_6	40.0	24.6	27.9	20.7
	(24.6)*	(21.9)	(19.8)	(16.6)
C_7	30.7	21.7	25.6	54.0
	(29.8)*	(20.4)	(24.8)	(54.0)
C_8	2.7	4.2	4.7	0.0
C_9	2.0	2.8	2.4	0.0
C_{10+}	1.8	4.2	3.0	0.0

*) selectivity of branched-chain aliphatics is shown in parentheses

References

[1] S. L. Meisel, J. P. McCullough, C. H. Lechthaler and P. B. Weisz, *CHEMTECH*, **6**, (1976) 186.

[2] I. E. Maxwell, J. E. Naber and K. P. de Jong, *Appl. Catal. A*, **113**, (1994) 153.

[3] K. P. de Jong, W. Bosch and J. D. B. Morgan, *Stud. Surf. Sci. Catal.*, **96**, (1995) 15.

[4] B. E. Langner, *Appl. Catal.*, **2**, (1982) 289.

[5] H. Itoh, T. Hattori and Y. Murakami, *Appl. Catal.*, **2**, (1982) 19.

[6] M. Niwa, M. Sawa and Y. Murakami, *Proc. 9th Intern. Cong. Catal.*, Chem. Inst. Canada, Ottawa, 1988, p. 380.

[7] M. Sawa, M. Niwa and Y. Murakami, *Appl. Catal.*, **53**, (1989) 169.

[8] A. Satsuma, T. Ishikura, T. Shimizu, M. Niwa, T. Hattori and Y. Murakami, *Kagaku Kogaku Ronbunshu*, **21**, (1995) 1120.

[9] T. Uchijima, *Catalytic Science and Technology*, *Vol. 1*, Kodansha, VCH, Tokyo, Weinheim, 1991, p. 393.

[10] M. Niwa, M. Iwamoto and K. Segawa, *Bull. Chem. Soc. Jpn.*, **59**, (1986) 3735.

[11] H. Itoh, C. V. Hidalgo, T. Hattori, M. Niwa and Y. Murakami, *J. Catal.*, **85**, (1984) 521.

[12] C. V. Hidalgo, H. Itoh, T. Hattori, M. Niwa and Y. Murakami, *J. Catal.*, **85**, (1984) 362.

[13] J. Cattanach, E. L. Wu and P. B. Venuto, *J. Catal.*, **11**, (1968) 342.

[14] D. J. Pirrillo and R. J. Gorte, *J. Phys. Chem.*, **97**, (1993) 8786.

[15] H. Knozinger, *Adv. Catal.*, **25**, (1976) 184.

[16] M. L. Poustmsa, *Zeolite Chemistry and Catalysis*, ACS. monograph (7), American Chemical Society, Washington D. C., 1976, p. 473.

[17] E. G. Derouane, J. B. Nagy, P. Dejaifve, J. H. C. van Hooff, B. P. Spekman, J. C. Vedrine and C. Naccache, *J. Catal.*, **53**, (1978) 40.

[18] M. Huang, P. A. Zielinski, J. Moulod and S. Kaliaguine, *Appl. Catal. A*, **118**, (1994) 33.

[19] P. E. Hathaway and M. E. Davis, *J. Catal.*, **119**, (1989) 497.

[20] K. Tanabe, *Solid Acids and Bases*, Academic Press, New York, 1970, p. 137.

Chapter 8

Conclusions and Future Prospects

Summery of each chapter

This thesis aims at elucidating the structures of gallosilicate MFI-type zeolites by the physical and chemical characterization techniques and at clarifying the relationships among structural, chemical and catalytic properties. In addition, the possibility of the light alkane conversion into highly branched aliphatics has been examined.

Chapter 2 shows the influence of the structures of the framework and extraframework gallium species on the dehydrogenation activity. The calcination of gallosilicate MFI-type zeolite (Ga-MFI) at high temperature caused a partial extraction of gallium from the framework site and a decrease in its acidity. Further, the particle size of the extraframework Ga_2O_3 species increased with an increase in calcination temperature. The physicochemical properties of Ga-MFI varied in a same manner with calcination temperature, regardless of its Ga content. The change in catalytic activity with calcination temperature was, however, different according to Ga content. The catalytic activity of Ga-MFI with higher Ga content decreased by the calcination at higher temperature. The decrease in catalytic activity corresponded to the decrease in the zeolitic strong acid sites. Therefore, the amount of zeolitic acid sites seemed to be one of the key factor controlling the dehydrogenation activity. In the case of Ga-MFI with lower Ga content, the catalytic activity increased with calcination temperature. In this case, the activity would be affected not only by the acidity but by the extraframework Ga_2O_3 particle size. The reaction rate per exposed Ga_2O_3 surface area increased with an increase in Ga_2O_3 particle size, suggesting that dehydrogenation of propane and cyclohexane on Ga-MFI catalysts are structure sensitive reaction demanding large Ga_2O_3 particle.

In Chapter 3, the structure-activity relationship in propane dehydrogenation on Ga_2O_3 catalysts has been clarified. The dehydrogenation of propane was carried out over supported and unsupported Ga_2O_3, as model catalysts for extraframework gallium species on Ga-MFI, having various particle sizes and crystal phases. The catalytic activity was different according to the preparation procedure. The reaction rate per Ga_2O_3 surface area increased with increasing the Ga_2O_3 particle size up to 240 nm, indicating that this reaction is a structure sensitive reaction demanding large Ga_2O_3 particle. The atomic scale structures, *i.e.*, the coordination number around gallium atom and the surface density of coordinatively unsaturated [Ga-O] sites, were investigated through X-ray absorption spectroscopy (XAFS) and benzaldehyde-ammonia titration (BAT) method, respectively. Higher activity of a large Ga_2O_3 particle was attributable to high concentration of surface [Ga-O] sites. Ga_2O_3 catalysts having both tetrahedrally and octahedrally coordinated gallium species, such as β-Ga_2O_3, exhibited higher reaction rate per surface [Ga-O] site. It was revealed that both the high concentration of surface [Ga-O] sites and coexistence of tetrahedrally and octahedrally coordinated Ga ions are another key factors controlling dehydrogenation activity.

In Chapter 4, the quantitative structural analysis of Ga-MFI catalysts has been carried out using Ga K-edge XAFS and microcalorimetry, in order to elucidate the effect of the structures of gallium species on the catalytic activity for dehydrogenation of propane. By the deconvolution of XANES spectra and EXAFS curve-fitting analyses, it was revealed that the fraction of tetrahedral gallium species was high when the Ga content and the calcination temperature were low. On the basis of XAFS and microcalorimetry analyses, it was revealed that the generated extraframework Ga_2O_3 comprised of both tetrahedral and octahedral gallium species and that the fraction of tetrahedral gallium species in extraframework Ga_2O_3 is high when Ga-MFI are calcined at higher temperature. The Ga_2O_3 particle size estimated from the results of XAFS and microcalorimetry analyses was in good agreement with that obtained by TEM analysis. By comparing the propane dehydrogenation rate per surface extraframework gallium species under the same amount of zeolitic acid sites, the higher activity was attributed to the ratio of tetrahedral gallium species to octahedral species in extraframework Ga_2O_3 species being close to unity. Thus, it was revealed that not only the ratio of extraframework gallium species to framework species but also the ratio of tetrahedral gallium species to octahedral species in extraframework Ga_2O_3 are key factors controlling dehydrogenation activity over Ga-MFI catalysts.

In Chapters 5 and 6, in order to evaluate the possibility of the selective conversion of light alkanes into highly branched aliphatics, the promotion effect of carbon dioxide on light alkane conversion was investigated.

In Chapter 5, for the improvement of propane conversion with carbon dioxide reduction, metal oxide components were screened through catalytic tests of reverse water-gas shift reaction and cracking of propane in the presence of carbon dioxide. Oxide of Fe and V were selected as the oxide components which are active for the reduction of carbon dioxide and inactive for the decomposition of propane. As for zeolite component, Ga-HZSM-5 was selected, because it is known to be active and selective for aromatization of propane. Composite catalysts containing these components were revealed to exhibit high activity for the reduction of carbon dioxide keeping high activity and selectivity for the aromatization of propane.

In Chapter 6, it was examined if carbon dioxide improves aromatization activity of zeolite catalysts. The aromatization of ethane which is less active than propane was conducted in the presence and absence of carbon dioxide over Ga-, Zn- and Pt-HZSM-5 catalysts. The reaction on Ga-HZSM-5 revealed that the introduction of carbon dioxide improved the aromatization, in particular, the aromatization of ethylene consisting of oligomerization of ethylene and dehydrocyclization of alkenes. This was confirmed through the reaction of ethylene in the presence and absence of carbon dioxide. Although carbon dioxide was reduced only slightly, the conversion of ethylene and the yield of aromatics were remarkably increased. This indicated that the promotion of aromatization by introduction of

carbon dioxide is not attributed to thermodynamic effect, but to kinetic effect.

Chapter 7 dealt with the formation of highly branched aliphatics in methanol conversion over modified mordenites. In order to form a highly branched aliphatics, such as trimethylpentanes, selectively, large pore zeolites would be more attractive. On H-form mordenite, the selectivity of highly branched aliphatics was higher than those on other type zeolites, such as ZSM-5 and Y zeolites, and trimethylalkanes were formed only on mordenite. The formation of highly branched aliphatics was promoted by dealumination and Na ion exchange. The dealumination suppressed the formation of aromatics and coke by decreasing the density of strong acid sites. The formation of side chains was promoted by Na ion exchange, because the basic oxygen sites generated by the introduction of Na ions would promote the proton abstraction and the alkylation.

General conclusions

The dehydrogenation activity of MFI-type gallosilicate (Ga-MFI) catalysts depends on not only its acidity but also the structure of extraframework Ga_2O_3 species. Higher activity of a large Ga_2O_3 particle could be attributed to high concentration of coordinatively unsaturated surface [Ga-O] sites. Higher activity of Ga_2O_3 particle such as β-Ga_2O_3, having the ratio of tetrahedral gallium species to octahedral species being close to unity, could be attributed to providing both strong acid and basic sites.

Ga-loaded H-ZSM-5 catalyst could be revealed to promote the light alkane conversion in the presence of carbon dioxide. In the ethane aromatization over Ga-HZSM-5, the promotion is not attributed to thermodynamic effect, but to kinetic effect.

The highly branched aliphatics, such as trimethylpentanes, could be selectively formed over mordenite zeolites having large pseudo-unidimensional channels. The basic sites could promote the formation of side chains, resulting in higher selectivity of highly branched aliphatics.

Future prospects

Although numerous hydrocarbon reactions, like alkane hydrogenolysis and isomerization, over metal-loaded catalysts were studied in molecular order, the activity and selectivity on metal oxide catalysts have not been well clarified in terms of the structure of catalysts. In present thesis, the active structures of gallium species in MFI-type gallosilicate (Ga-MFI) catalysts were investigated by various physical and chemical analyses, and the relationship between the structure and catalysis were discussed. This approach must be

effective for the elucidation of the catalytic properties, and the findings from this approach will give a lot of scientific bases for the real oxide catalysts.

The present thesis described that the activity of MFI-type gallosilicate (Ga-MFI) catalysts for propane and cyclohexane dehydrogenation strongly depends on the local structures such as the coordination state around gallium atom and surface density of coordinatively unsaturated gallium atoms. From the viewpoints of utilization of light alkanes and emission control, the formation of highly branched aliphatics from light alkanes has attracted much attention. This reaction comprises numerous successive steps. For controlling the reaction it is necessary to know what are the steps involved in the pathway and how they occur. Gallium promoted zeolites are attractive because of their high activity for activation of light alkanes and it has been suggested that gallium species promote the initial activation step. The information about the active structures of gallium species clarified in the present thesis will be a great help for the design a functionalized catalysts.

The present thesis showed the possibility of the selective formation of highly branched aliphatics over the zeolite having large pore structure and basic sites. There are still some problems to utilize this process as follows: since light alkanes are thermodynamically stable and the activation of light alkanes requires much energy, the reactions take place usually at high temperatures. Under this condition, it is difficult to depress the formation of naphthenes and aromatics. In the future, if this disadvantages can be overcomed, this reaction process would be put into practical use.

List of publications

Location in this thesis

1. **Oxide-Zeolite Composite Catalysts for the Reduction of Carbon Dioxide with Simultaneous Aromatization of Propane** — Chapter 5
   K. Nishi, A. Satsuma, T. Hattori and Y. Murakami
   Enegy Convers. Mgmt., **36** (1995) 645.

2. **Effect of Carbon Dioxide on Aromatization of Ethane over Metal-loaded HZSM-5 Catalysts** — Chapter 6
   K. Nishi, M. Endo, A. Satsuma, T. Hattori and Y. Murakami
   Sekiyu Gakkaishi, **39** (1996) 260.

3. **Formation of Multi-Branched-Chain Aliphatics in Methanol Conversion over Modified Mordenites** — Chapter 7
   K. Nishi, T. Shimizu, H. Yoshida, A. Sastuma and T. Hattori
   Appl. Catal. A: General, in press.

Other publication

1. **Influence of Local Structure on the Catalytic Activity of Gallium Oxide for the Selective Reduction of NO by CH_4**
   K. Shimizu, M. Takamatsu, K. Nishi, H. Yoshida, A. Satsuma and T. Hattori
   Chem. Commun., (1996) 1827.